PhD degree in Molecular Medicine (curriculum in Computational Biology)

European School of Molecular Medicine (SEMM),

University of Milan and University of Naples "Federico II"

Settore disciplinare: Bio/11

Decoding Molecular and Phenotypic Properties of Proliferating Cells under constant Mitotic Checkpoint Activation

Andrea Corno

IFOM, Milan

Matricola n. R10758-R20

Supervisor: Dr. Andrea Ciliberto

IFOM, Milan

Added Supervisor: Dr. Marco Foiani

IFOM, Milan

Anno accademico 2016-2017

The study of cognition as a biological function may be unique in the life sciences in the extent to which findings ultimately are calibrated against a single species, Homo sapiens [...]. *The study of respiration and other biological functions, for example, are not so calibrated, although scientific investigation doubtless began with concern for the human case. (We stop breathing, we die – so what is breath?) Rather, evidence is followed wherever it leads, and it can lead to unexpected places.* [...] *Memory, needless to say, is critical to cognition. Without memory, present circumstances have no context; the detection of change is impossible. Without the ability to detect change, the decision to alter behavior can only be random, haphazard. Without memory, learning of any kind is impossible.*

— Pamela Lyon, *The cognitive cell: bacterial behavior reconsidered*, Front. Microbiol. 2015

Contents

List of Abbreviations

APC/C ..... Anaphase Promoting Complex or Cyclosome

BUB ..... Budding Unhinhibited by Benzimidazole

CDC ..... Cell Division Cycle

CDH1 ..... CDc20 Homolog 1

CDK ..... Cyclin-Dependent Kinase

CFIII ..... Chromosome Fragment III

CLB ..... CycLin B

DDR ..... DNA Damage Response

ESP1 ..... Extra Spindle Pole bodies 1

FDR ..... False Discovery Rate

GAL1pr ..... GALactokinase 1 promoter

GFP ..... Green Fluorescent Protein

GO ..... Gene Ontology

MAD ..... Mitotic Arrest Deficient

MND2 ..... Meiotic Nuclear Divisions 2

MCC ..... Mitotic Checkpoint Complex

MCM ..... MiniChromosome Maintenance

MEN ..... Mitotic Exit Network

MIH1 ..... Mitotic Inducer Homolog 1

MPS1 ..... MonoPolar Spindle 1

NFL ..... Negative Feedback Loop

PDS1 ..... Precocious Dissociation of Sister

PFL . . . . . Positive Feedback Loop

PP2A . . . . . Protein Phosphatase 2A

MPF . . . . . Mitotic Promoting Factor

MTOC . . . . . MicroTubules Organizing Center

NEBD . . . . . Nuclear Envelope BreakDown

SAC . . . . . Spindle Assembly Checkpoint

SIC1 . . . . . Substrate Inhibitor of Cyclin-dependent protein kinase 1

SPB . . . . . Spindle Pole Body

SSB1 . . . . . Stress-Seventy subfamily B 1

SWE1 . . . . . Saccharomyces WEe1

TUB1/2 . . . . . TUBulin 1/2

TPR . . . . . TetratricoPeptide Repeat

WT . . . . . Wild Type

YOX1 . . . . . Yeast homeobOX 1

List of Figures

List of Tables

Abstract

During mitosis, DNA material needs to be properly segregated. Chromosome segregation is triggered by the Anaphase Promoting Complex or Cyclosome (APC/C), an E3 ubiquitin ligase activated by its cofactor Cdc20. Activation of APC^{Cdc20} is conditioned by the presence of optimal conditions for a proper partition of sister chromatids. Without such conditions, activation of APC/C^{Cdc20} could lead to unequal chromosome segregation, by which an aneuploid progeny could arise. The Spindle Assembly Checkpoint (SAC) inhibits the activity of APC/C^{Cdc20}, blocking the progression through the cell cycle and thus preventing erroneous chromosome segregation.

When cells experience a prolonged SAC activation, they may die in mitosis by apoptosis, or overcome the arrest and progress into the cell cycle even when chromosome segregation is impaired. The second scenario is also known as adaptation to the SAC (or mitotic slippage). Once adapted, cell proliferation can still be blocked (via apoptosis or G1 arrest) or cells can resume cell division. The latter case may establish a progeny of cells in which aneuploidy and genomic instability introduce large genetic variability, with potentially irreversible and deleterious effect on the cell population.

Using *S. cerevisiae* as a model organism, we characterized a population of cells escaped from a prolonged mitotic arrest, which we called *adapted* cells. Proteomic analysis of these cells revealed large rewirings of biological processes and pathways, suggesting a pseudo "differentiated" state for adapted cells. The cell cycle of adapted cell is heavily modified, to account for the chronic inhibition of APC/C^{Cdc20}. On the one hand, APC/C^{Cdc20} itself become less responsive to the SAC, as observed in a population of cells where we uncoupled adaptation from missegregation. We showed that cellular size was not responsible for the partial recovery of APC/C^{Cdc20} activity in the presence of the SAC. Our data rather suggest a role for Cdc28-mediated phosphorylation. On the other hand, other activators of APC/C like Cdh1 become essential, unlike what observed in a regular cell cycle. The synthetic lethality of adapted cells with mitotic exit genes suggests potential molecular targets for specific inhibition of adapted cells.

1 Introduction

1.1 General Principles of Mitosis

One of the key aspects of the Cell Theory concerns the origin of each cell. In 1855, Robert Remak and Rudolf Virchow were the first scientists to monitor cellular proliferation, observing that each cell gives rise to two cells. From additional discoveries in the last century, we know that every cell originates from a division of pre-existing cells, herediting the genetic information encoded in the DNA. This process is accomplished by the Cell Cycle (Figure 1.1), which allows every (mother) cell to produce two (daughter) cells with identical DNA content.

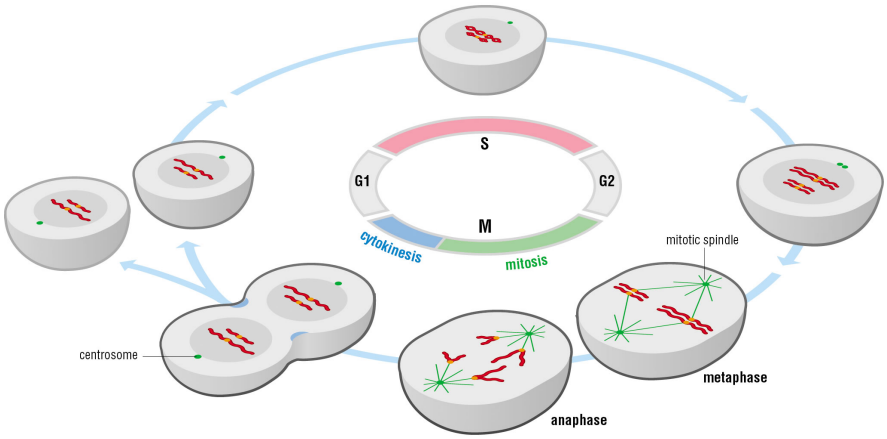

Figure 1.1: **The Eukaryotic Cell Cycle is composed by subsequent phases** - Schematic representation of the eukaryotic cell cycle. DNA is duplicated in S phase and organized in sister chromatids, which are properly segregated in M phase. After segregation, mother cells physically divide into two daughter cells by cytokinesis. Both S and M phase are preceded by Gap phases: G1 for S-phase, while G2 for M-phase. Source: (Morgan 1999-2007)

At the beginning of the cell cycle, S-phase takes place. Here, DNA is unwounded from heterochromatin to euchromatin, allowing replication origin firing and duplication of DNA. At the end of replication, the two DNA molecules produced by DNA replication stick together. They are known as *sister chromatids*. Then, cells proceed to M-phase, which is composed by mitosis and cytokinesis. During mitosis, sister chromatids attach to the mitotic spindle, a dynamic structure made of micro-

tubules that allows segregation of each pair of sister chromatids. Eventually, daughter cells separate at cytokinesis. Between S and M phase, Gap phases (G1 and G2) ensure a proper transition between one phase and the next, giving time to the cell to activate specific regulatory pathways and to grow properly. Phases G1, S and G2 form a major phase of the cell cycle called *interphase*. While interphase takes a large part of the cell cycle time, mitosis lasts for a shorter amount of time.

In this study, we investigate mitosis in *Saccharomyces cerevisiae* cells, whose main features are introduced in the following subsections.

1.1.1 Sister chromatids segregate during mitosis

At the end of interphase, DNA is organized in sister chromatids, held together by cohesin rings (Nasmyth & Haering 2009). Then, cells undergo mitosis through a series of events that can be organized in different subphases (Alberts *et al.* 2002-2008):

1. **Prophase**

   In this phase, each couple of sister chromatids becomes more condensed. In particular, a heterochromatic region called *centromere* is defined for both sister chromatids. For each centromeric region of each chromosome, a protein complex called *kinetochore* is assembled. Meanwhile, the mitotic spindle is polymerized from the two opposite poles, called MicroTubules Organizing Centers (MTOCs). In the open mitosis of mammalian cells, these poles are provided by centrosomes, which are located in the cytosol (Figure 1.2, 1).

2. **Prometaphase**

   The mitotic spindle starts to attach sister chromatids, by physically interacting with kinetochores. In mammalian cells, where MTOCs are outside the nucleus, the Nuclear Envelope BreakDown (NEBD) takes place to allow formation of the mitotic spindle (Figure 1.2, 2).

3. **Metaphase**

   At this stage, all kinetochores of the sister chromatids are attached to the opposite poles of the mitotic spindle and chromosomes are aligned on the *metaphase plate*, the equator of the mitotic spindle (Figure 1.2, 3).

4. **Anaphase**

   Cohesin rings are cleaved, and sister chromatids are separated due to the physical tension exerted by kinetochores-microtubules attachment. MTOCs pull away from each other, allowing chromosome segregation (Figure 1.2, 4).

At the end of mitosis, the two sets of chromosomes get closer to their MTOC. Then, telophase and cytokinesis ensure a proper division of the mother cell into two daughter cells. In mammalian cells,

nuclear envelope is reassembled and cytokinesis creates a cleavage furrow on the plasma membrane (Figure 1.2, 5-6).

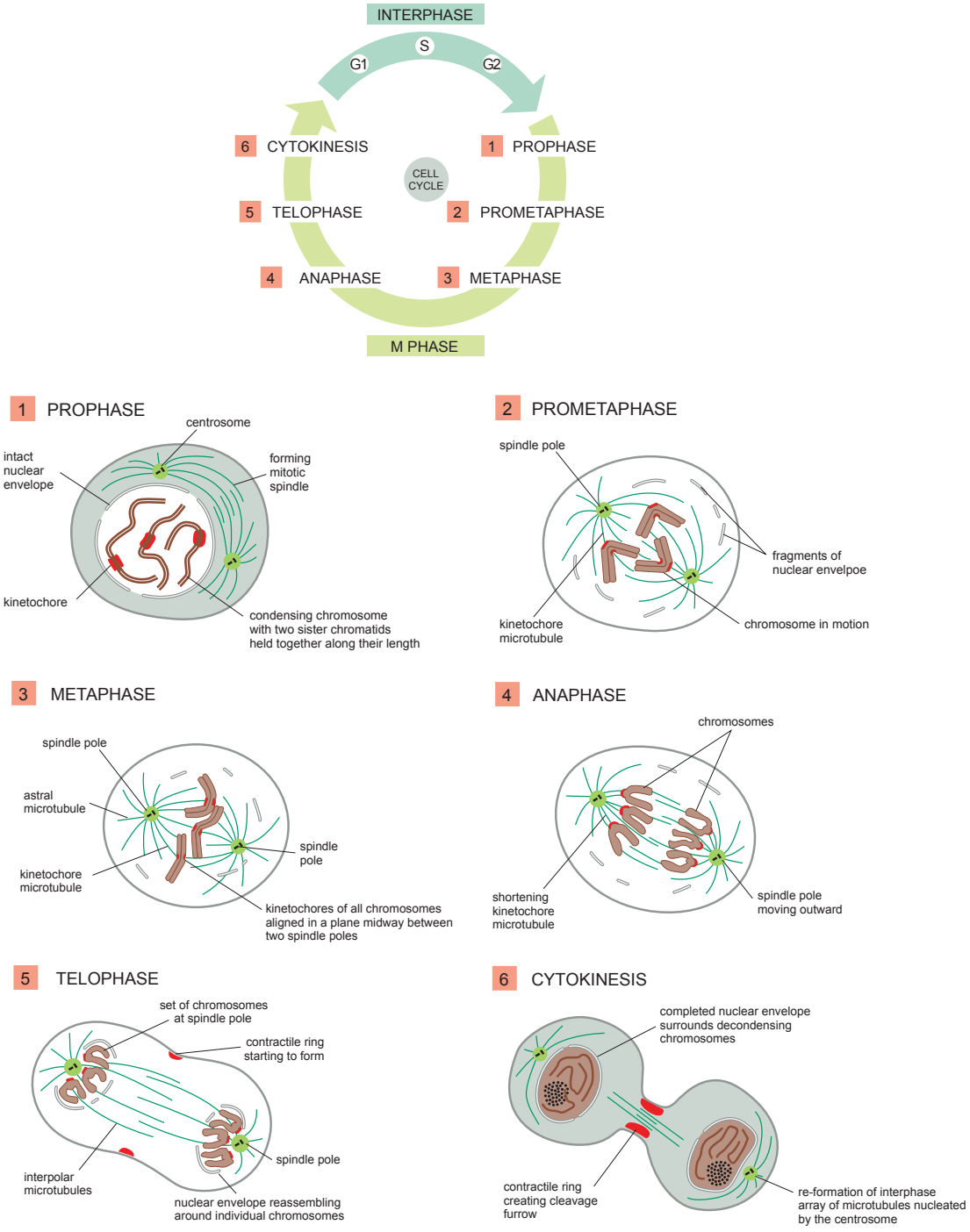

Figure 1.2: **Mitotic Phases ensure correct chromosomes segregation** - During mitosis, sister chromatids are segregated through several stages. A schematic representation of these stages is reported in this figure. Source (Alberts *et al.* 2010)

1.1.1.1 Budding yeast performs a closed mitosis

So far, we described an *open mitosis*, in which disassembly of the nuclear envelope allows the interaction of the mitotic spindle with chromosomes. This phenomenon occurs in human and mammalian

cell lines. Organisms like budding yeast, instead, undergo through the same mitotic phases, but with different cytological structures. First, budding yeast cells form a bud (Figure 1.3a). This bud will inherit half of the replicated DNA content, giving rise to a daughter cell. The cytoplasmic region between mother cell and bud is called *budneck*, and it provides a site for cleavage furrow.

Differently from mammalian cells, NEBD does not take place in budding yeast, which performs a *closed mitosis*. Here, the role of MTOCs is covered by Spindle Pole Bodies (SPBs), protein complexes that are located within the nuclear envelope. From these poles, both nuclear and cytoplasmic microtubules are assembled (Figure 1.3a). While nuclear microtubules ensure attachment to sister chromatids, cytoplasmic ones give a correct orientation of the metaphase plate: the axis of mitotic spindle has to be perpendicular to the budneck, with one SPB in the mother cell and the other one in the bud. Once anaphase is concluded, cytokinesis takes place, cleaving both plasma membrane and nuclear envelope (Figure 1.3b, c).

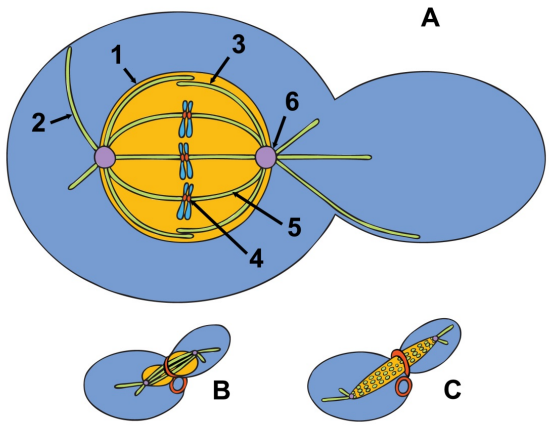

Figure 1.3: **Mitosis in budding yeast** - Schematic representation of mitotic spindle and MTOCs during mitosis of budding yeast, in particular during (A) G2-M phase, (B) anaphase and (C) early telophase. 1: nuclear membrane; 2: cytoplasmic microtubules; 3: interpolar microtubules; 4: kinetochore; 5: kinetochore microtubules; 6: spindle pole body (SPB). Source: (Vági *et al.* 2012)

1.1.2 Cyclin-dependent kinase 1 promotes mitotic onset and progression

From the description given above, it emerges that subcellular organelles and macromolecular structures undergo several reorganizations in mitosis (Morgan 1999-2007). Most of these rearrangements rely on the activity of Cyclin-dependent kinases (Cdks), which phosphorylate specific substrates on serine/threonine residues. Action range and phosphorylation activity of Cdks are determined by their binding with Cyclins, whose levels oscillate during the cell cycle and reach their maximum expression during specific cell cycle phases. These fluctuations allow selectivity of Cdks activity (Morgan 1999-2007).

Cyclin-dependent kinase 1 Cdk1 (Cdc28 in budding yeast) is the main mitotic kinase. It binds

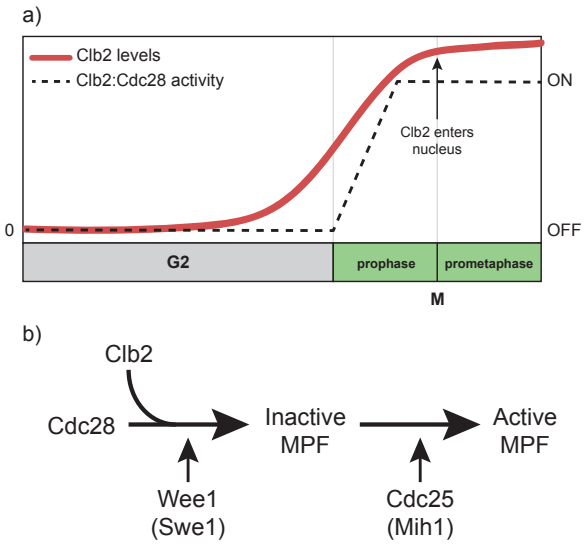

Figure 1.4: **Activation of Clb2:Cdc28 during mitotic onset** - (a) During G2/M phase, Clb2 synthesis starts. This cyclin B interacts with Cdc28 and enters in nucleus during prometaphase. Clb2:Cdc28 activity increases in prophase. (b) Activation of the MPF Clb2:Cdc28. Upon binding with Clb2, Cdc28 is inhibited by Wee1 (Swe1). A subsequent dephosphorylation performed by Cdc25 (Mih1) establishes an active MPF. Figure inspired from (Morgan 1999-2007)

mitotic Cyclins B, forming a complex - called Mitosis Promoting Factor (MPF) - that promotes progression through mitosis (Rahal & Amon 2008). In budding yeast, there are four cyclin B: Clb1, Clb2, Clb3 and Clb4. Their overall mitotic activity is redundant, even if deletion of Clb2 has the most severe effect on cellular viability and mitotic progression (Fitch *et al.* 1992), suggesting that the main MPF in budding yeast is represented by Clb2:Cdc28 complex.

Precisely, MPF activity rises upon Clbs synthesis (Figure 1.4a). While Clb1,2 start to be synthetized at the G2/M transition, mRNA of Clb3,4 accumulates at early stages of S-phase (Fitch *et al.* 1992). Once assembled, MPF complex is inactive, due to the inhibitory phosphorylation performed by Wee1 kinase (Swe1 in budding yeast) on the ATP-binding site of Cdk1. A counteracting activity of Cdc25 phosphatase (Mih1 in budding yeast) removes this inhibition (Figure 1.4b) and activates MPF. During mitotic onset, Clb2 localizes to the nucleus (Hood *et al.* 2001), ensuring an active MPF in the nuclear compartment until metaphase. In conjunction with chromosomes segregation, Clb2:Cdc28 activity decreases, due to the inhibition of both Clb2 and Cdc28, allowing mitotic exit. In the next subsections, we further describe the molecular mechanisms underlying the decline of Clb2:Cdc28 MPF activity during the metaphase-to-anaphase transition and after anaphase.

1.1.3 Metaphase-to-Anaphase Transition

As already mentioned in Subsection 1.1.1, sister chromatids segregation occurs during anaphase. This transition is not only driven by the mitotic spindle, but rather by several biochemical reactions, most of which involve an E3-ubiquitin ligase, called Anaphase Promoting Complex or Cyclosome (APC/C). This complex ubiquitinates specific substrates, which are then degraded by the 26S proteasome. Func-

tionality of APC/C relies on its structure and regulatory mechanisms, which we report in the next subsections.

1.1.3.1 Structure of the APC/C

The structure of the APC/C complex has been widely studied in budding yeast, human and animal models (Zhang *et al.* 2016; Qiao *et al.* 2016; Alfieri *et al.* 2017; Sivakumar & Gorbsky 2015; Thornton *et al.* 2006) and it is still under investigation. 14 different protein subunits (13 in yeast) are organized in three subcomplexes (Figure 1.5): a catalytic module, a scaffolding module platform and a TPR lobe (Alfieri *et al.* 2017; Sivakumar & Gorbsky 2015). The catalytic module is a flexible structure that mediates ubiquitination of APC/C substrates, cooperating with a ubiquitin-conjugating enzyme (E2). The TPR lobe consists of homodimeric proteins with multiple tetratricopeptide repeats. This subcomplex assumes an "arc lamp" shape and it mediates the binding with substrates and co-activators of APC/C. Both catalytic and TPR modules are anchored to the scaffolding platform, which stabilizes the overall structure of APC/C and supports its functionality.

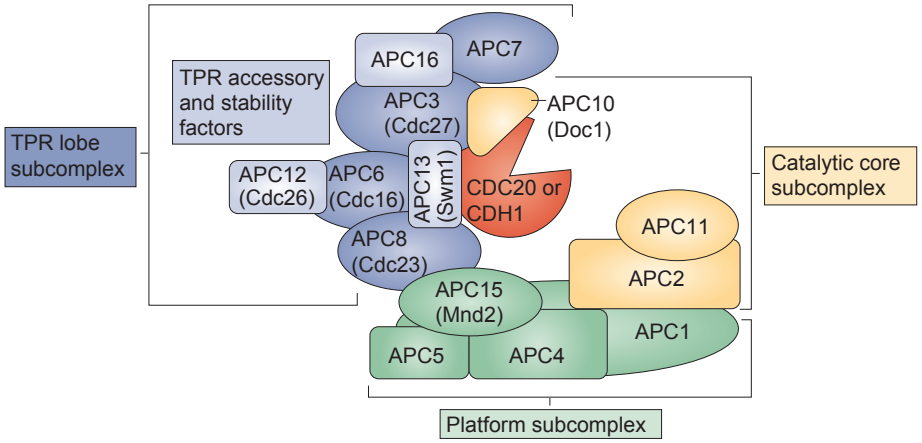

Figure 1.5: **Schematic representation of APC/C structure** - Representation of the three modules: platform subcomplex, catalytic core subcomplex and TRP lobe subcomplex. Each protein is reported with the mammals nomenclature in capital letters, and yeast nomenclature in parentheses. Source: (Sivakumar & Gorbsky 2015)

1.1.3.2 Cdc20 and Cdh1 are essential co-activators of APC/C

The described complex per se is inactive. In order to ubiquitinate its substrates, APC/C has to be activated by two co-factors: Cdc20 and Cdh1. Cdc20 activates APC/C during metaphase, while Cdh1 from the anaphase onset to the subsequent G1. Both co-activators possess a short N-terminal motif called C-box (Schwab *et al.* 2001) and a dipeptide C-terminal domain called IR (Vodermaier *et al.* 2003), which allow binding with the TPR lobe of APC/C. Once bound, each co-activator exposes its C-terminal domain, which contains WD40 repeats that allow binding of substrates. Only substrates with

degron sites are recognized by Cdc20 and/or Cdh1. D-box (or destruction box) RxxLx[D/E][Ø]xN[N/S], KEN box [DNE]KENxxP and ABBA motif Fx[ILV][FY]x[DE] represent the known canonical degron sites (Alfieri *et al.* 2017), and their recognition by APC/C co-activators depends on intrinsic factors encoded in protein sequence, or cell-state dependent, extrinsic factors (Davey & Morgan 2016).

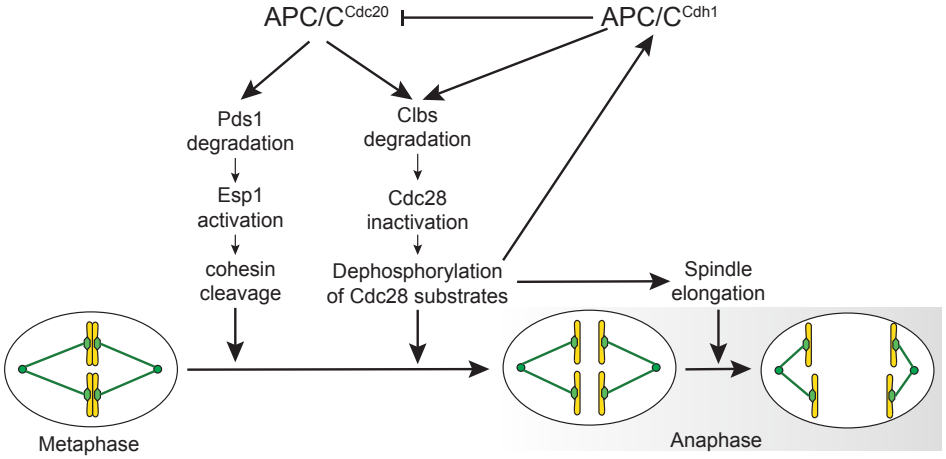

Figure 1.6: **APC/C promotes completion of mitosis** - Subsequent activation of APC/C^{Cdc20} and APC/C^{Cdh1} allows sister chromatids segregation and inhibition of Cdc28 kinase activity. Figure inspired from (Morgan 1999-2007)

APC/C^{Cdc20} activity Cdc20 activity is essential for anaphase onset, and yeast conditional mutants for this gene arrest in metaphase with undivided nuclei and stable securine levels (Shirayama *et al.* 1998; Yamamoto *et al.* 1996). A tight regulated balance between Cdc20 synthesis and degradation occurs through mitosis. Synthesis of Cdc20 starts in G2/M and it is mediated by mitotic Cdc28 activity in yeast, presumably by repressing the transcriptional inhibitor Yox1 via phosphorylation (Liang *et al.* 2012). Cdc20 degradation is APC/C-dependent and occurs in *cis*, via D- and KEN degron boxes located in Cdc20 protein sequence (Foe *et al.* 2011). A member of APC/C called Mnd2 covers an important role in Cdc20 degradation (Foster & Morgan 2012).

APC/C^{Cdc20} is assembled during prophase/prometaphase, reaching its high activity at the end of metaphase. When all sister chromatids are properly attached to the mitotic spindle, APC/C^{Cdc20} ubiquitinates Clb2 and securine (Pds1 in yeast). While degradation of Clb2 leads to the reduction of Cdc28 kinase activity, Pds1 degradation activates separase (Eps1 in yeast), which in turns cleaves the cohesin rings that helds sister-chromatids together. Finally, phosphorylation of Cdc28 substrates decreases, promoting chromosome movement to the MTOCs and spindle elongation (Morgan 1999-2007) (Figure 1.6). Among the Cdc28 substrates, Yox1 phosphorylation is reverted: Cdc20 synthesis is repressed, and Cdc20 degradation prevails.

APC/C^{Cdh1} activity In most higher eukaryotes, APC/C^{Cdc20} activity is sufficient for triggering a chain of events which revert phosphorylation of Cdk1-substrates. Budding yeast, instead, needs

additional mechanisms. Here, Cdh1 plays an important role. APC/C^{Cdh1} activity follows that of APC/C^{Cdc20} in early anaphase, and it mediates the complete degradation of mitotic cyclins. Cdh1 localizes to the nucleus in G1 (Höckner *et al.* 2016); once cells proceed in S and G2/M phases, the APC/C co-activator diffuses to the cytoplasm: this is due to the increased Cdc28 mitotic activity that phosphorylates Cdh1, inhibiting its ability to localize to the nucleus and to bind APC/C (Höckner *et al.* 2016). During anaphase onset, Clb2:Cdc28 is partially inhibited by APC/C^{Cdc20}, leading to the dephosphorylation of Cdh1 that enters in the nucleus and binds APC/C. The resulting APC/C^{Cdh1} complex induces degradation of mitotic cyclins and Cdc20, allowing exit from mitosis (Figure 1.6).

1.1.3.3 Regulation of APC/C activity by phosphorylation

As just described, Cdc28 kinase negatively regulates APC/C^{Cdh1}. In general, phosphorylation of APC/C and/or its co-activators provides several regulatory mechanisms (Figure 1.8).

Phosphorylation of TPR lobe promotes APC/C^{Cdc20} activity Binding affinity between APC/C and Cdc20 increases in the presence of phosphorylated TPR lobe (Cdc16, Cdc27, Cdc23), causing an increase of APC/C^{Cdc20} activity. (Rudner & Murray 2000; Qiao *et al.* 2016; Zhang *et al.* 2016; Cross 2003). In *Xenopus* egg extracts, phospho-mimicking mutants of Apc3 (Cdc27), Apc6 (Cdc16) or Apc8 (Cdc23) are able to ubiquitinate Cyclin B in vitro, in the presence of Cdc20 (Qiao *et al.* 2016). In budding yeast, nonphosphorylatable mutants of Cdc16 and Cdc27 impair APC/C^{Cdc20} function in vivo (Rudner & Murray 2000; Vernieri *et al.* 2013).

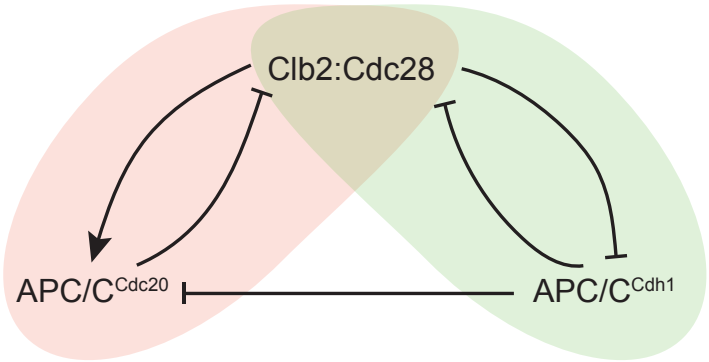

Figure 1.7: **Two oscillators regulate mitotic APC/C activity** - Representation of APC/C regulation discussed above. (Red) Clb2:Cdc28 stimulates APC/C^{Cdc20} via phosphorylating APC/C and promoting Cdc20 synthesis. During anaphase onset, active APC/C^{Cdc20} induces Clb2 degradation, resulting in a decreased Cdc28 activity. (Green) Clb2:Cdc28 inhibits APC/C^{Cdh1} via preventing binding of Cdh1 with APC/C. When activated, APC/C^{Cdh1} induces degradation of Clb2 and Cdc20. Figure inspired from (Cross 2003)

Phosphorylation of the TPR lobe is mainly Cdc28-dependent (Rudner & Murray 2000). Cdc28 activity on APC/C^{Cdc20} and Cdh1 draws the attention on two feedback loops (Figure 1.7). While Cdc28 establishes a negative feedback loop with APC/C^{Cdc20}, it interacts with APC/C^{Cdh1} in a positive

feedback loop. Combination of these two oscillatory mechanisms provides a circuit that is responsible for controlling Cdc28 mitotic kinase levels (Cross 2003).

Apc1 subunit inhibits Cdc20 binding with APC/C Recently, it has been proposed a role of phosphorylated Apc1 in promoting APC/C^{Cdc20} assembly (Qiao *et al.* 2016; Zhang *et al.* 2016). Apc1 belongs to the APC/C platform subcomplex (Figure 1.5), and it has a N-terminal Auto-Inhibitory (AI) segment that prevents Cdc20 binding with Apc3 (Cdc27). Several phosphosites were identified in AI loop in HeLa cells (Qiao *et al.* 2016; Zhang *et al.* 2016), and a phospho-mimicking mutant of AI segment was able to ubiquitinate Cyclin B in vitro (Qiao *et al.* 2016). Indeed, phosphorylation of this region removes Apc1 inhibitory effects, allowing binding of Cdc20 with APC/C (Qiao *et al.* 2016; Zhang *et al.* 2016). This phosphorylation could be mediated by recruitment of CyclinB-Cdk1 complex by Apc3 (Zhang *et al.* 2016), which may displace active Cdk1 to the N-terminal loop of Apc1 (Zhang *et al.* 2016), allowing phosphorylation of the AI segment. At the moment, there is no evidence about Apc1 inhibitory function in budding yeast.

Inhibition of Cdc20 by phosphorylation It has been found that Cdc20 is phosphorylated in vivo by CyclinA2-Cdk2 during interphase in HeLa cells (Hein & Nilsson 2016). CyclinB1-Cdk1 also contributes to this phosphorylation in early mitosis, targeting 3 threonine sites and reducing the activity of APC/C^{Cdc20} (Hein *et al.* 2017). In mammals, this phosphorylation is reverted by the phosphatase PP2A, which preferentially targets phosphothreonines rather than phosphoserines (Hein & Nilsson 2016; Hein *et al.* 2017). PP2A predominantly affects the phosphorylation state of Cdc20 and not that of Apc1, which is required for an active APC/C^{Cdc20} - as described in the subsection above. This is due to the presence of phosphoserine sites on Apc1, which are unlikely to be target of PP2A (Hein *et al.* 2017).

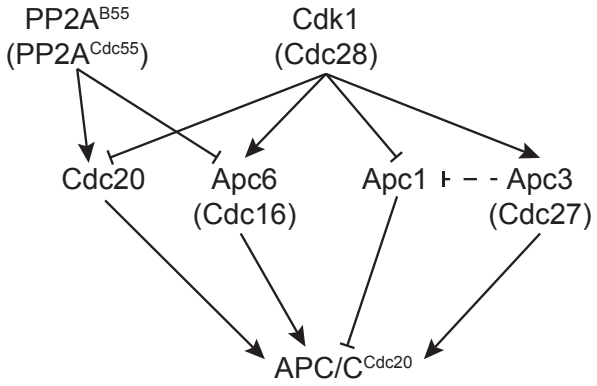

Figure 1.8: **Phosphorylation mechanisms regulate APC/C^{Cdc20} activity** - Schematic representation of the (de)phosphorylation reactions that has been proposed to regulate APC/C^{Cdc20} activity. Cdk1 activity phosphorylates Apc6 and Apc3, enhancing binding affinity between Cdc20 and APC/C (Rudner & Murray 2000; Qiao *et al.* 2016; Zhang *et al.* 2016; Cross 2003; Vernieri *et al.* 2013). This binding is improved when Apc1 is phosphorylated (Qiao *et al.* 2016; Zhang *et al.* 2016). On the other hand, PP2A activity has been proposed to have an active role in promoting Cdc20 (Hein & Nilsson 2016; Hein *et al.* 2017), while inhibiting Cdc16 phosphorylation (Vernieri *et al.* 2013).

1.1.4 Reversing Cdc28 activity: Cdc14 triggers mitotic exit

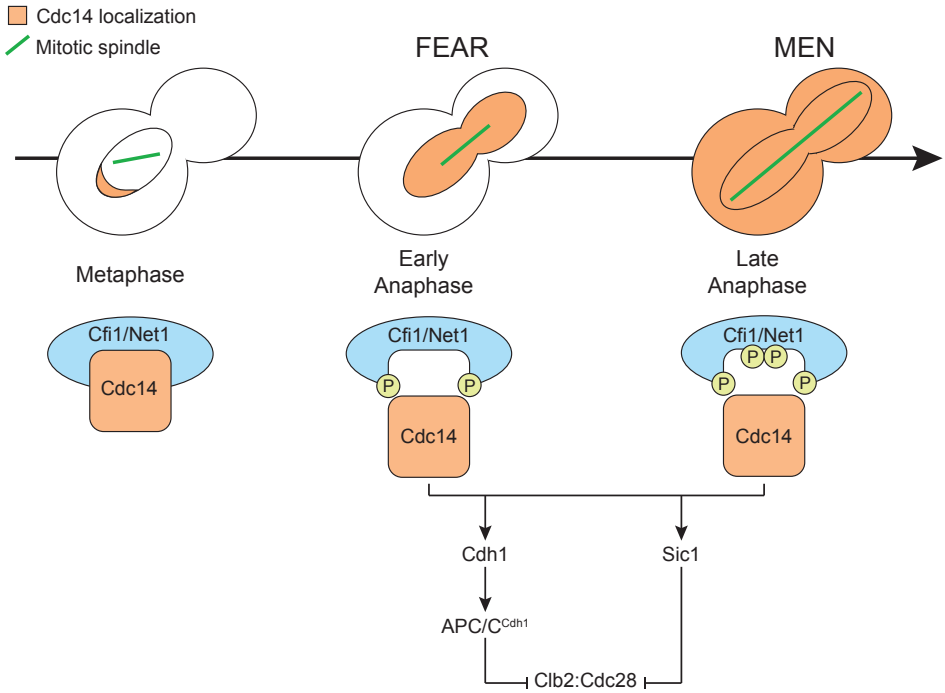

Figure 1.9: **Release of Cdc14 allows exit from mitosis** - Cdc14 localizes to the nucleolus, until anaphase. During early anaphase, a first pool of Cdc14 is released in the nucleus via FEAR pathway (Stegmeier *et al.* 2002). In late anaphase, Cdc14 is also released in the cytoplasm via MEN. Localization to the nucleolus is mediated by Cfi1/Net1 inhibitor. During anaphase, phosphorylation of Cfi1/Net1 weakens the bound with Cdc14, allowing its release. Among Cdc14 substrates, reversal of Cdh1 and Sic1 phosphorylation allows inhibition of residual Cdc28 kinase activity.

As described in the previous subsection, APC/C triggers the reversal of Cdc28 mitotic activity. In yeast, the phosphatase primarily involved is Cdc14. During interphase, Cdc14 is localized to the nucleolus and it is inactive, due to its binding with the inhibitor Cfi1/Net1; this conformation is maintained until metaphase (Figure 1.9). When cells undergo anaphase, a first pool of Cdc14 is released

to the nuclear compartment. This phenomenon is known as Cdc Fourteen Early Anaphase Release (FEAR), and it is mediated by phosphorylation of Cfi1/Net1 Figure 1.9). In late anaphase, Cfi1/Net1 is further phosphorylated, allowing the full release of Cdc14 in cytoplasm: at this stage of the cell cycle, Mitotic Exit Network (MEN) takes place (Figure 1.9).

Once released in the nuclear and/or cytoplasmic compartment, Cdc14 reverses the phosphorylation of several Cdc28 substrates. Among them, Cdh1 and Sic1 cover an important role in mitotic exit (Visintin *et al.* 1998): they are inhibited by Cdc28-mediated phosphorylation, and activated upon release of Cdc14. Dephosphorylation of Cdh1 promotes APC/C^{Cdh1} activity, as discussed in Subsection 1.1.3. Cdc14 dephosphorylation also activates Sic1, a stoichiometric inhibitor of Cdc28. (Visintin *et al.* 1998; Cross 2003).

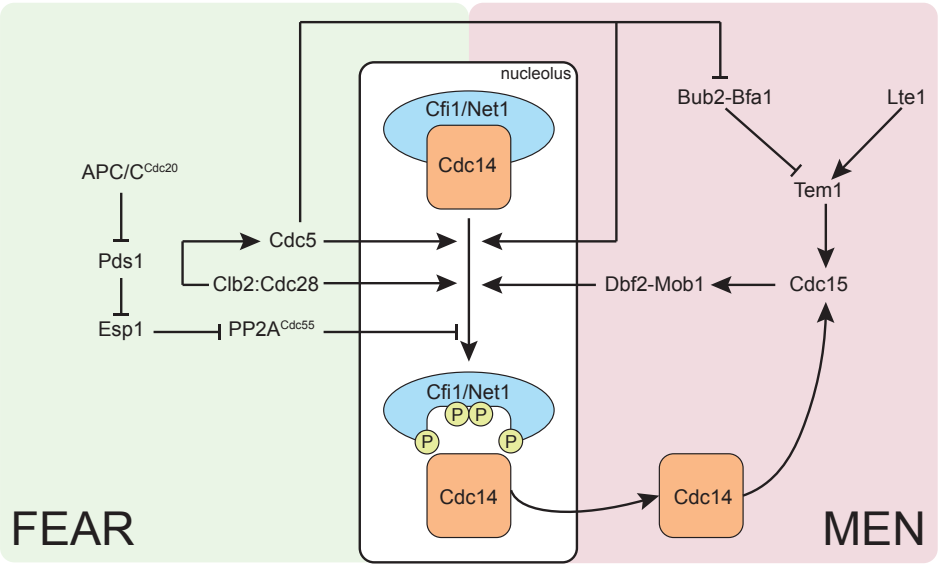

Figure 1.10: **FEAR and MEN regulate release of Cdc14** - Schematic representation of FEAR and MEN pathway. Both of them are responsible for release of Cdc14 from the nucleolus, therefore activating an efficient reversal of Cdc28 activity.

1.1.4.1 FEAR

This pathway allows the release of Cdc14 during early anaphase (Stegmeier *et al.* 2002) of yeast cells. It is not essential for cellular viability, but it is required for a correct timing of mitotic exit. Several components of FEAR trigger Cdc14 release via phosphorylation of Cfi1/Net1 inhibitor (Figure 1.10). One of them is Clb2:Cdc28 complex (Azzam *et al.* 2004; Queralt *et al.* 2006), which phosphorylates Cfi1/Net1 before being inactivated by APC/C^{Cdc20} during anaphase onset (Queralt *et al.* 2006).

Polo like kinase Cdc5 covers an important role in promoting FEAR: overexpression of Cdc5 anticipates Cdc14 release in metaphase, phosphorylating Cfi1/Net1 and Cdc14 in vivo (Visintin *et al.* 2003). Cdc5-dependent phosphorylation sites of Cfi1/Net1 differ from that of Cdc28-dependent, suggesting a non-redundant mechanism of Cfi1/Net1 inhibition (Rodriguez-Rodriguez *et al.* 2016). Moreover, Cdc28 phosphorylates Cdc5 on T242 site, mediating the Polo like kinase activity towards Cfi1/Net1

(Rodriguez-Rodriguez *et al.* 2016).

Phosphorylation of Cfi1/Net1 is reversed by $PP2A^{Cdc55}$, which localizes to the nucleolus during metaphase, in order to prevent premature release of Cdc14 (Queralt *et al.* 2006). In vivo, $PP2A^{Cdc55}$ activity is inhibited by separase Esp1, which physically interacts with Cdc55 (Queralt *et al.* 2006) and promote FEAR (Stegmeier *et al.* 2002).

1.1.4.2 MEN

The major release of Cdc14 takes place during late anaphase/telophase (Figure 1.9) of yeast cells. Here, the main kinase that phosphorylates Cfi1/Net1 is Dbf2 (Figure 1.10). Together with its coactivator Mob1, Dbf2 localizes to the SPBs in late anaphase, its kinase activity being complemented by the kinase Cdc15 (Visintin & Amon 2001). Colocalization of Cdc15 and Dbf2 is regulated by GTP-binding protein Tem1, whose levels increase during anaphase/telophase and localize to the SPB that is close to the bud (Bardin *et al.* 2000). Tem1 is further activated by the GDP/GTP exchange factor Lte1, which localizes to the plasma membrane of the bud (Bardin *et al.* 2000) and promotes Cdc15 localization to the SPB (Visintin & Amon 2001). The GTPase Bub2-Bfa1, instead, negatively regulates Tem1 activity.

Cdc5 also plays a role in MEN, phosphorylating the Bub2-Bfa1 complex and preventing its inhibitory effect on Cdc14 release (Hu & Elledge 2002; Hu *et al.* 2001). Cdc5 kinase activity depends on T70 phosphorylation site, which is Cdc28-regulated. Indeed, Cdc5 T70-phosphomutant delays mitotic progression and releases a poor pool of Cdc14 in late anaphase (Rodriguez-Rodriguez *et al.* 2016). Nevertheless, inhibition of Dbf2 in T70-phosphomutant does not completely abolish Cdc14 release, suggesting a MEN-independent mechanism of Cfi1/Net1 phosphorylation by Cdc5 (Visintin *et al.* 2003; Rodriguez-Rodriguez *et al.* 2016).

1.2 The Mitotic Guardian: Spindle Assembly Checkpoint

During anaphase onset, APC/C^{Cdc20} promotes sister chromatids segregation. In order to propagate identical copies of the DNA to the cellular progeny, each cell must segregate chromosomes evenly. In physiological conditions, APC/C^{Cdc20} promotes anaphase onset when all sister chromatids are properly attached to the mitotic spindle. Activation of APC/C^{Cdc20} in the presence of one or more unattached sister chromatids will cause missegregations, establishing two daughter cells with an unequal DNA content. This condition is known as *aneuploidy*, and it may cause deleterious and irreversible effects on the two daughter cells (Santaguida & Amon 2015). To prevent any erroneous chromosome segregation, each eukaryotic cell activates the Spindle Assembly Checkpoint (SAC) - or Mitotic Checkpoint - during prometaphase. This checkpoint provides a signaling pathway that prevents activation of APC/C^{Cdc20}, blocking cellular proliferation in prometaphase. When all sister chromatids are attached to the mitotic spindle, the SAC is inactivated and APC/C^{Cdc20} promotes anaphase onset. In this section we provide molecular details about this pathway.

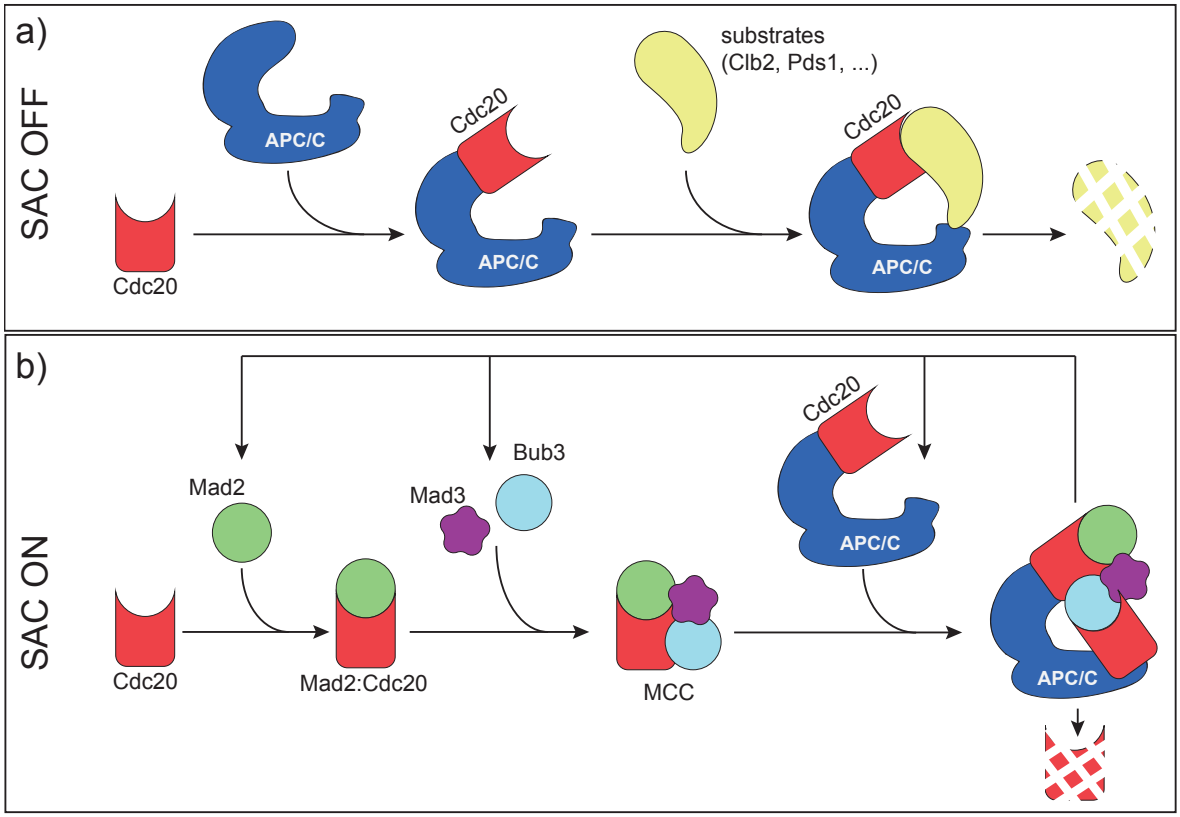

Figure 1.11: **MCC inhibits APC/C^{Cdc20} activity** - (a) Without SAC activity, Cdc20 binds APC/C and allows recognition of specific substrates, as discussed in Section 1.1. In this way, substrates are then ubiquitinated and degraded. (b) In the presence of SAC activity, Cdc20 is sequestered by an active Mad2. Then, the complex is stabilized by Mad3 and Bub1, forming the MCC. Finally MCC binds APC/C^{Cdc20}, which in turn promotes Cdc20 ubiquitination and degradation. In this way, APC/C^{Cdc20} substrates are not targeted for degradation by 26S proteasome.

1.2.1 Molecular network of the SAC

1.2.1.1 Inhibition of APC/C^{Cdc20}: the role of MCC

The mitotic checkpoint prevents APC/C^{Cdc20} activity by inhibiting Cdc20 from recognizing APC/C substrates (Figure 1.11, (a) vs (b)). The repression occurs via stoichiometric binding of Cdc20 with several proteins of the SAC: Mad2, Mad3 (BubR1 in mammals) and Bub3. Expression of these proteins is constant through the cell cycle, but they specifically interact with Cdc20 when the SAC is active. As expected, *mad*2Δ, *mad*3Δ and *bub*3Δ cells missegregate with a higher frequency than wild-type cells (Hoyt *et al.* 1991).

During early stages of Cdc20 inhibition, Mad2 undergoes a conformational switch that increases its binding affinity with Cdc20 (see Subsection 1.2.1.2 for details) . Then, Bub3 and Mad3 stabilize the Mad2:Cdc20 complex, forming the Mitotic Checkpoint Complex (MCC) (Figure 1.11b). Recently, it has been discovered the presence of 2 molecules of Cdc20 in MCC (Izawa & Pines 2015; May *et al.* 2017; Sewart & Hauf 2017). When in MCC, Cdc20 binds APC/C without promoting ubiquitination of any substrates. Indeed, Cdc20 itself is ubiquitinated and targeted for degradation (Foe *et al.* 2011) (Figure 1.11b). Finally, when MCC is disassembled both SAC proteins and APC/C are released.

1.2.1.2 Unattached kinetochores catalyze Mad2 conformational switch

The rate-limiting step of MCC assembly is Cdc20 sequestration by Mad2 (Faesen *et al.* 2017). In an unperturbed cell cycle, spontaneous binding between Mad2 and Cdc20 is slow, due to the inactive conformation of cytoplasmic Mad2 (open conformation, O-Mad2) (Simonetta *et al.* 2009). The SAC stimulates the Mad2 conformational switch to an active form (closed conformation, C-Mad2), which then binds with high efficiency Cdc20. In this context, unattached kinetochores serve as platforms for protein recruitment and catalysis of Mad2 conformational switch. This catalytic reaction does not occur spontaneously in the cytoplasm, but the requirement of unattached kinetochores is overrode by the ectopic overexpression of O-Mad2, or the ectopic expression of C-Mad2 (Mariani *et al.* 2012).

In physiological conditions, the reaction is catalysed by the checkpoint protein Mad1. Mad1 localization at the kinetochore requires several reaction to occur. In the presence of unattached kinetochores, one of the outer kinetochore proteins - Spc105, or Knl1 in mammals - is phosphorylated by the Mps1 kinase in multiple Met-Glu-Leu-Thr (MELT) motifs. Phosphorylated MELT motifs allow then to recruit Bub3 (Primorac *et al.* 2013), together with Bub1 (Primorac *et al.* 2013; London & Biggins 2014) (Figure 1.12). Then, Mps1 phosphorylates Bub1, which recruits a tetrameric complex composed by Mad1 and C-Mad2 (London & Biggins 2014). Localization of Mad1:C-Mad2 at the unattached kinetochore induces O-Mad2 conformational switch (De Antoni *et al.* 2005) (Figure

1.12), therefore allowing cytoplasmic MCC assembly. Hence, localization of Mad2 to the unattached kinetochore is a marker for SAC activity (Bonaiuti *et al.* 2017). The inhibitory strength of the SAC correlates with the number of unattached kinetochores, and already one kinetochore is sufficient for SAC signaling (Dick & Gerlich 2013).

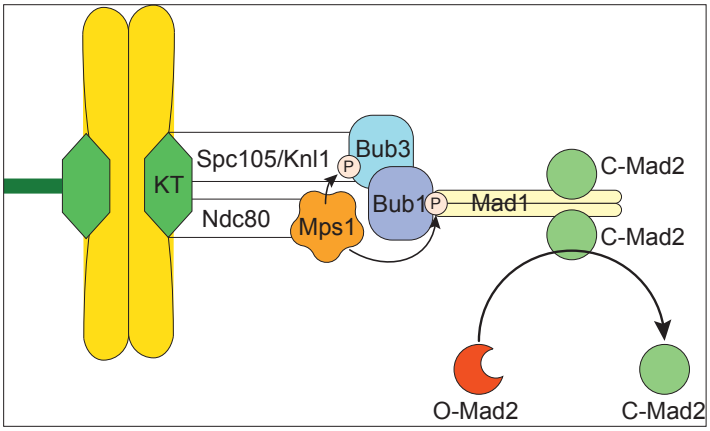

Figure 1.12: **Unattached kinetochore catalyzes conformational switch from open to closed Mad2** - During the checkpoint activity, several proteins are recruited to the unattached kinetochores (KT). Mainly via Mps1 activity, phosphorylation of Spc105 (Knl1 in mammals) allows recruitment of Bub3/Bub1, which in turns mediates localization of tetrameric complex Mad1-Mad2. For any molecule of Mad2 with an open conformation (O-Mad2) that localizes to the unattached kinetochore, a shift to closed conformation takes place (C-Mad2).

1.2.1.3 The unclear role of Cdk1 in SAC

Assembly of kinetochores and localization of checkpoint proteins is a process that requires energy and involves several kinases, as reported above. In the last years, it has been proposed a role of the Cdk1 kinase in supporting SAC signaling from unattached kinetochores. For instance, inhibition of Cdk1 in nocodazole-arrested HeLa cells overrides the checkpoint-dependent arrest (Vincenzo *et al.* 2003) and delocalizes Mad2 from the unattached kinetochores (Vázquez-Novelle *et al.* 2014). Moreover, a non-degradable cyclin B supports a constant Cdk1 activity that destabilizes kinetochore-microtubules attachment, leading to SAC activation (Vázquez-Novelle *et al.* 2014).

Experimental data on budding yeast, however, suggest the opposite scenario. Here, inhibition of Cdc28 (via analog-sensitive mutant or ectopic overexpression of Sic1 inhibitor) leads to a persistent arrest in nocodazole-treated cells, with stable levels of Clb2 and Pds1 and decreasing levels of Cdc20 (Vernieri *et al.* 2013). The inability to enter anaphase is not due the decreased Cdc20 levels, since deletion of the transcriptional repressor Yox1 recapitulates the same mitotic arrest (Vernieri *et al.* 2013), despite stable levels of Cdc20. These results suggest that in yeast inhibition of Cdc28 during a mitotic arrest alters primarily the APC/C^{Cdc20} activity. Most likely, Cdk1 has opposite effects on the SAC, and the prevailing of one over the other is species-specific.

Taken together, these experimental data propose a dual role of Cdk1 in regulating APC/C^{Cdc20}

(Figure 1.13). While Cdk1 promotes APC/C^{Cdc20} activity - as reported in Section 1.1 - it has also an inhibitory effect by promoting SAC activity.

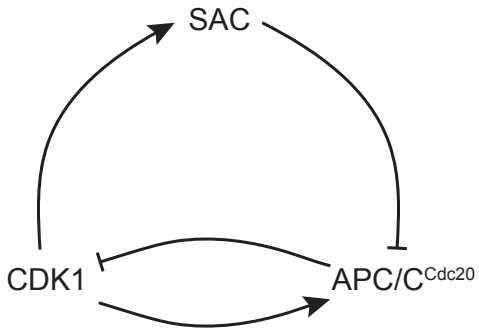

Figure 1.13: **Paradoxical regulation of APC/C^{Cdc20} by Cdk1** - Basing on experimental evidence, Cdk1 both promotes and inhibits APC/C^{Cdc20}. Inhibition is mediated by SAC activation.

1.2.2 Induction of SAC in budding yeast

In mammalian cells, the SAC is activated at each cell cycle. Indeed, knockout of SAC-related genes strongly affects cellular viability, suggesting that the mitotic checkpoint covers an essential role. On the other hand, budding yeast cells that lack SAC-related genes are still viable, suggesting that the SAC is not strongly activated at every cell cycle.

In this section, we provide an overview of the methods we used for engaging the SAC in budding yeast.

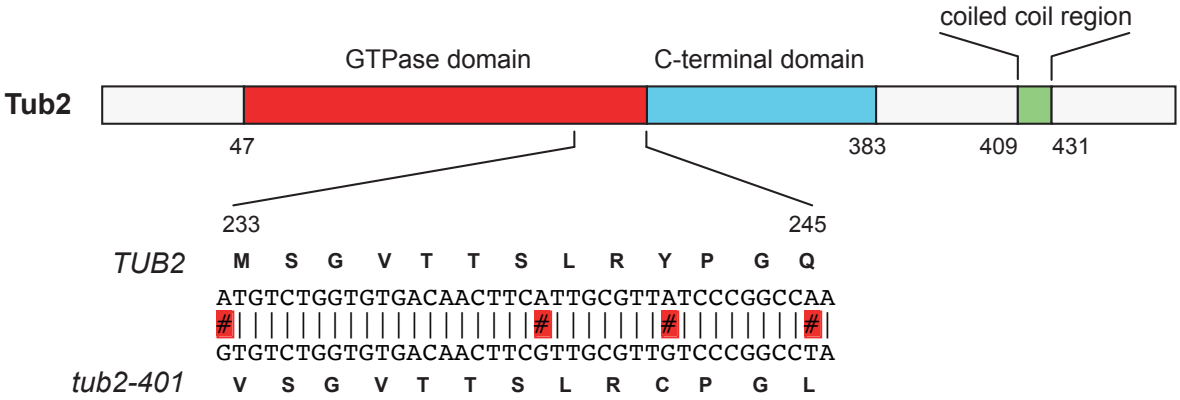

Figure 1.14: **Nucleotides and amino acid sequence of *TUB2* and *tub2-401*** - Schematic representation of Tub2 protein domains. The 3 mutated residues of *tub2-401* belong to the C-terminal portion of the GTPase domain.

1.2.2.1 Depolymerization of microtubules

As described in Subsection 1.2.1, the SAC signal generates from unattached kinetochores, which are not able to attach to the mitotic spindle. They can be created by inhibiting polymerization of microtubules, e.g., with antimitotic drugs such as nocodazole and benomyl. Nocodazole-arrested cells

exhibit Mad2 localization to the unattached kinetochores (Vernieri *et al.* 2013) - together with Bub3 checkpoint protein (Bonaiuti *et al.* 2017) - which activate the SAC signaling cascade. However, the effects of nocodazole starts to decrease after 5-6h of administration, and ad-hoc readditions have to be performed in order to maintain the mitotic arrest (data not shown).

Another way to induce a constant microtubules depolymerization relies on *TUB2* cold-sensitive mutants (Huffaker *et al.* 1988). Here, polymerization of microtubules is inhibited when cells grow at low temperatures. In this thesis we focus on *tub2-401* mutant, which has 4 point mutations in the *TUB2* ORF, but only 3 out of 4 introduce alterations in the sequence of the GTPase domain of the protein (Figure 1.14). When *tub2-401* cells are grown at the restrictive temperatures, cells arrest in mitosis and no nuclear and cytoplasmic microtubules are detectable (Huffaker *et al.* 1988), mimicking the effect due to nocodazole.

1.2.2.2 Ectopic overexpression of SAC proteins

Another way to induce the checkpoint is the overexpression of SAC molecular players. This method does not cause unattached kinetochores. For instance, overexpression of Mps1 under a galactose-inducible promoter *GAL1pr* ectopically induces a metaphase arrest, without altering mitotic spindle structure (K. Hardwick *et al.* 1996), in a Mad1-independent fashion.

In this thesis, we used overexpression of Mad2 (*GAL1-MAD2(3x)*, (Rossio *et al.* 2010b)). When these cells grow in galactose-containing medium, they arrest with metaphase spindles and stable levels of nuclear Pds1 (Rossio *et al.* 2010b). Despite the inactive conformation of the overexpressed Mad2 (O-Mad2, (Simonetta *et al.* 2009; De Antoni *et al.* 2005)), the expression of about 60 times the endogenous Mad2 levels induces a bona-fide SAC arrest: MCC assembly of these cells is similar to that of nocodazole-arrested cells, independently from Mad1 localization to the kinetochores (Mariani *et al.* 2012).

1.3 Adaptation to the Mitotic Checkpoint

THe mitotic checkpoint is invoked during specific cancer chemotherapy treatments. In particular, antimitotic drugs activate the SAC, causing a prolonged mitotic arrest; among them, taxanes are widely used for solid tumor treatment. They enhance microtubule assembly, causing a stabilization of the mitotic spindle and inhibition of chromosome segregation (Chabner & Longo 2014). Vinca alkaloids are another class of antimitotic drugs which destabilize microtubules, giving rise to unattached kinetochores and a SAC response. These drugs are mainly used for treatment of lymphomas, testicular cancer, breast and lung cancer (Chabner & Longo 2014).

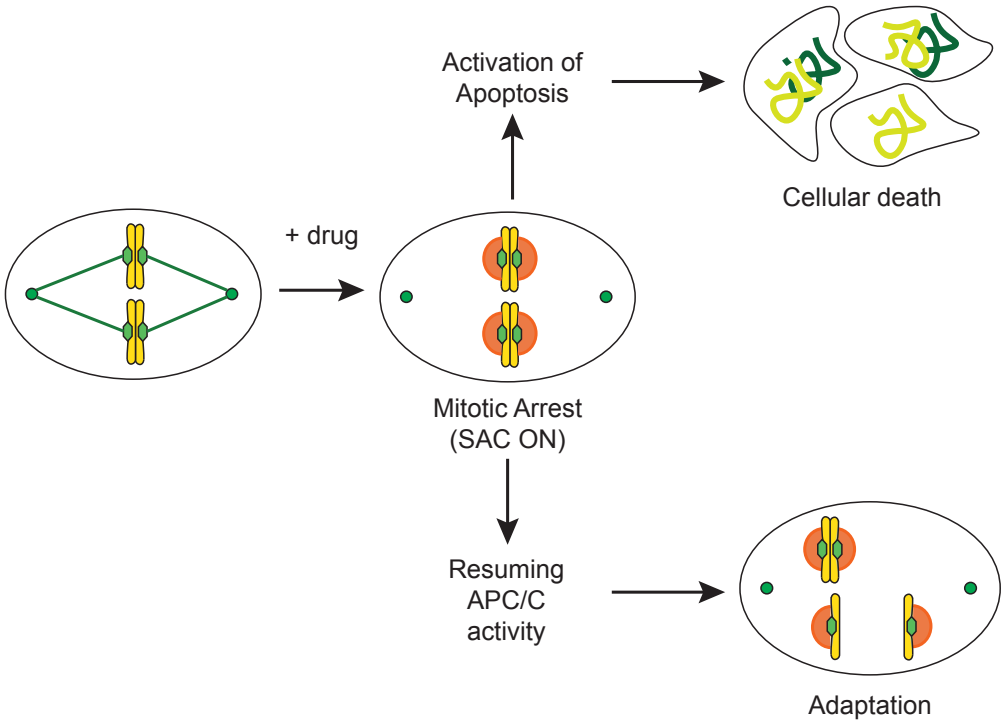

Figure 1.15: **Upon a prolonged mitotic arrest, cells eventually die or adapt to the SAC** - In the case of cells without drug resistance, administration of antimitotic drugs introduces a prolonged mitotic arrest via SAC activity. Then, cells undergo two possible outcomes: cellular death via apoptosis, or adaptation to the SAC by resuming an active APC/C.

If malignant cells acquire resistance to these drugs, they will not arrest in mitosis; otherwise, cells undergo a prolonged mitotic arrest. In such case, two outcomes are possible (Figure 1.15). Antimitotic drug promotes the death of treated cells, via triggering apoptotic pathways (Chabner & Longo 2014; Topham & Taylor 2013) (Figure 1.15). A second option is that cells resume an active APC/C^{Cdc20} despite continuous SAC activity, therefore adapting to the mitotic checkpoint (Figure 1.15). The ability to overcome the SAC and resume a metaphase-to-anaphase transition is also known as adaptation to the SAC, or *mitotic slippage*.

In this section, we report properties and different models of adapting cells, describing also the consequences of adaptation to the SAC.

1.3.1 Properties of adaptation to the SAC

One of the first examples of adaptation to the SAC was provided in PtK1 and RPE1 cells treated with different doses of nocodazole (Brito & C. L. Rieder 2006). In these vertebrate cells, a slow and progressive reduction of CyclinB levels took place during an active SAC arrest (Brito & C. L. Rieder 2006). These first studies put in evidence two properties of adapting cells:

- **Mitotic slippage is not a consequence of a weakened SAC signal**

  Adapting vertebrate cells exhibit localization of Mad1, Mad2 and BubR1 to the unattached kinetochores, even after CyclinB degradation (Brito & C. L. Rieder 2006). This result is in accordance with a recent study in our lab (Bonaiuti *et al.* 2017), in which we showed that the vast majority of the monitored yeast cells arrested in nocodazole degrades Clb2 in the presence of Mad2 localization.

- **Degradation of CyclinB requires APC/C activity**

  Inhibition of proteasome in nocodazole-arrested cells causes a stabilization of CyclinB levels and blocks mitotic slippage, suggesting that CyclinB is degraded by the proteasome. This active degradation is mediated by APC/C, since the combined knockdown of Cdc20 and Cdh1 co-activators prevents degradation of substrates during mitotic slippage (Lee *et al.* 2010). Interestingly, while vertebrate adapting cells exhibit a slow decay of mitotic cyclin levels during adaptation (Brito & C. L. Rieder 2006), budding yeast cells show an abrupt decay of Clb2 (Bonaiuti *et al.* 2017; Vernieri *et al.* 2013). This discrepancy may reflect the different weight of SAC and APC/C regulations operated by CylinB:Cdk1 in mammals as opposed to yeast, as mentioned above.

1.3.2 Adaptation requires Cdc20, but not Cdh1

Adapting cells undergo anaphase in the presence of SAC signal. In this transition, APC/C activity is expected to be sustained by its co-activators Cdc20 and/or Cdh1. Cdh1 is dispensable but not essential for promoting adaptation, since wild-type and *cdh1*Δ cells undergo anaphase with similar kinetics (Vernieri *et al.* 2013). Hence, there might exist a small fraction of free APC/C bound to Cdc20, capable to promote anaphase onset despite SAC signaling. In this respect, it has been proposed in budding yeast that the small number of APC/C, Cdc20 and Mads molecules can introduce fluctuations in the APC/C^{Cdc20} levels (Bonaiuti *et al.* 2017). During a mitotic arrest, these levels reach a steady-state, which is under a critical anaphase threshold. Fluctuations around the steady state allow APC/C^{Cdc20} to hit the threshold, reaching the required amount of APC/C^{Cdc20} for anaphase onset (Figure 1.16a).

According to this model, the distance between the anaphase threshold and APC/C^{Cdc20} levels

defines the ability of cells to adapt. In this scenario, the key molecular species is phosphorylated APC/C bound to Cdc20. For this reason, the amount of phosphorylated APC/C is critical to understand the adaptation process, and so are the mechanisms that control APC/C phosphorylation. As described in Section 1.1, phosphorylation of the Cdc16 and Cdc27 subunits of APC/C increases the binding affinity between APC/C and Cdc20. The latter covers an important role in adaptation to the SAC, since phosphomutants of Cdc16 and Cdc27 do not perform mitotic slippage (Rudner & Murray 2000; Vernieri *et al.* 2013). The phosphatase counteracting Clb2:Cdc28 on the phosphorylation state of APC/C is PP2A^{Cdc55} (Vernieri *et al.* 2013) (Figure 1.16b).

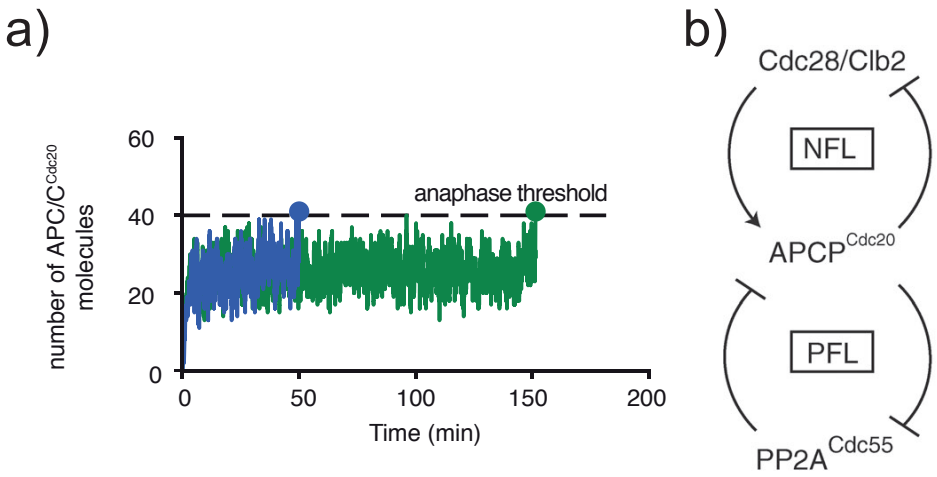

Figure 1.16: **APC/C^{Cdc20} is activated by stochastic fluctuations and phosphorylation in budding yeast** - (a) Stochastic simulation of APC/C^{Cdc20} levels during a mitotic arrest. Two trajectories assuming the same steady-state level are represented in time. Due to stochastic fluctuations, they hit the anaphase threshold in different times. Source: (Bonaiuti *et al.* 2017). (b) APC/C^{Cdc20} is activated by phosphorylation. A negative feedback loop (NFL) with Cdc28 kinase stimulates phosphorylation of Cdc16 and Cdc27 subunits, while PP2A^{Cdc55} phosphatases dephosphorylates Cdc16 in a positive feedback loop (PFL). Source (Vernieri *et al.* 2013).

As mentioned, Cdh1 is not required for adaptation. In special cases, however, adaptation can be driven by Cdh1 too. Deletion of the MEN inhibitor Bub2 anticipates mitotic slippage in nocodazole-arrested cells, due to a hyperactive MEN that activates Cdh1 (Toda *et al.* 2012).

These results are in accordance with what was observed in budding yeast cells arrested upon Mad2 overexpression (Rossio *et al.* 2010b). Here, deletion of Bub2 anticipates colony growth, while phospho-mimicking mutant of Net1 exhibits a delay, due to a reduced release of Cdc14. In this context, an additional role of RSC chromatin remodeling complex has been proposed (Rossio *et al.* 2010b).

1.3.3 Cellular fate after mitotic slippage: death or survival?

When cells adapt to the SAC, missegregation events are likely to occur (C. Rieder & Maiato 2004), due to an APC/C-dependent anaphase onset in the presence of antimitotic stimuli that alter mitotic spindle structure. In this event, each adapting cell will produce two aneuploid daughter cells, which

may undergo different fates (C. Rieder & Maiato 2004; Rossio *et al.* 2010a) (Figure 1.17). Daughter cells could undergo cellular senescence, due to the activation of p53 that leads to a prolonged G1 arrest (C. Rieder & Maiato 2004) (Figure 1.17). This tumor suppressor is induced by DNA damage, dosage compensation or metabolic alterations (Santaguida & Amon 2015; Santaguida *et al.* 2017; C. Rieder & Maiato 2004). Otherwise, cells can resume proliferation after adaptation (Figure 1.17). They may experience replication stress (Santaguida *et al.* 2017), after which they may perform several cell cycles with a slight or no activation of p53 (C. Rieder & Maiato 2004; Santaguida *et al.* 2017). During proliferation, cells have to deal with a persistent antimitotic drug and several stresses coming from their aneuploid state, for instance: proteotoxicity, genome instability, upregulation of factors involved in oxidative stress or amino acid biosynthesis/cellular bioenergetics (Santaguida & Amon 2015).

The combination of the reported features influences the viability of proliferating cells after adaptation. Furthermore, tumorigenicity of adapted cells may influence the cellular viability. As a matter of fact, many cancer cells would die, while normal cells would recover a proliferative status (C. Rieder & Maiato 2004). On the other hand, we cannot exclude that adapted cancer cells may acquire an increased efflux pump activity, mutations in taxanes/vinca alkaloids binding sites, or increased apoptotic inhibitors (Chabner & Longo 2014). The latter might promote proliferative status of cancer cells upon a prolonged SAC activity.

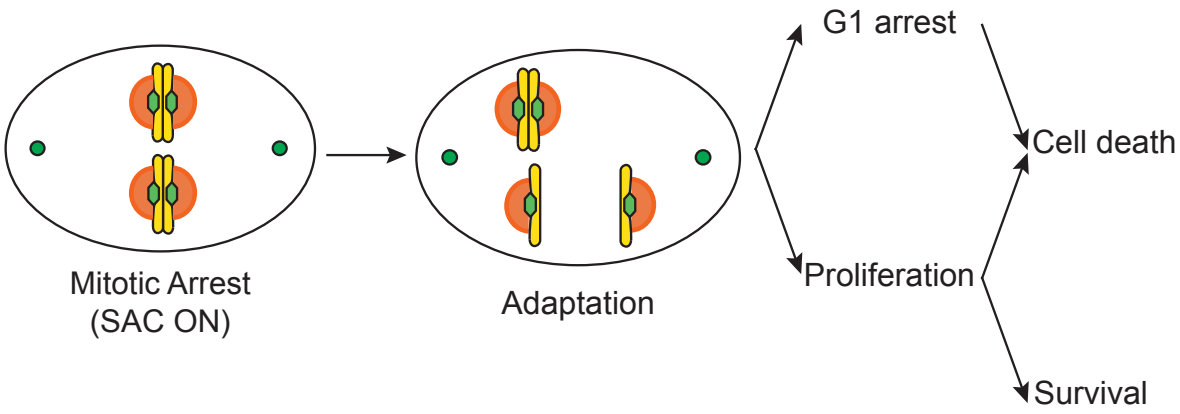

Figure 1.17: **Adapted cells undergo cell death or survival** - Upon mitotic arrest induced by antimitotic drug, adapting cells to the SAC missegregate and enter in the subsequent G1. In this phase, activation of p53 can introduce cellular senescence, which in turn leads cell death. On the other hand, cells can undergo proliferation, in which the survival rate depends on the deleterious effects acquired during adaptation and during proliferation after adaptation.

1.4 Cell Size Regulation

One of the important aspects that influences cellular proliferation is cell size, as cells have to properly couple cell growth with cell division, in order to ensure the correct cellular volume for biochemical reactions. Here, we present properties of cell size control in budding yeast cells.

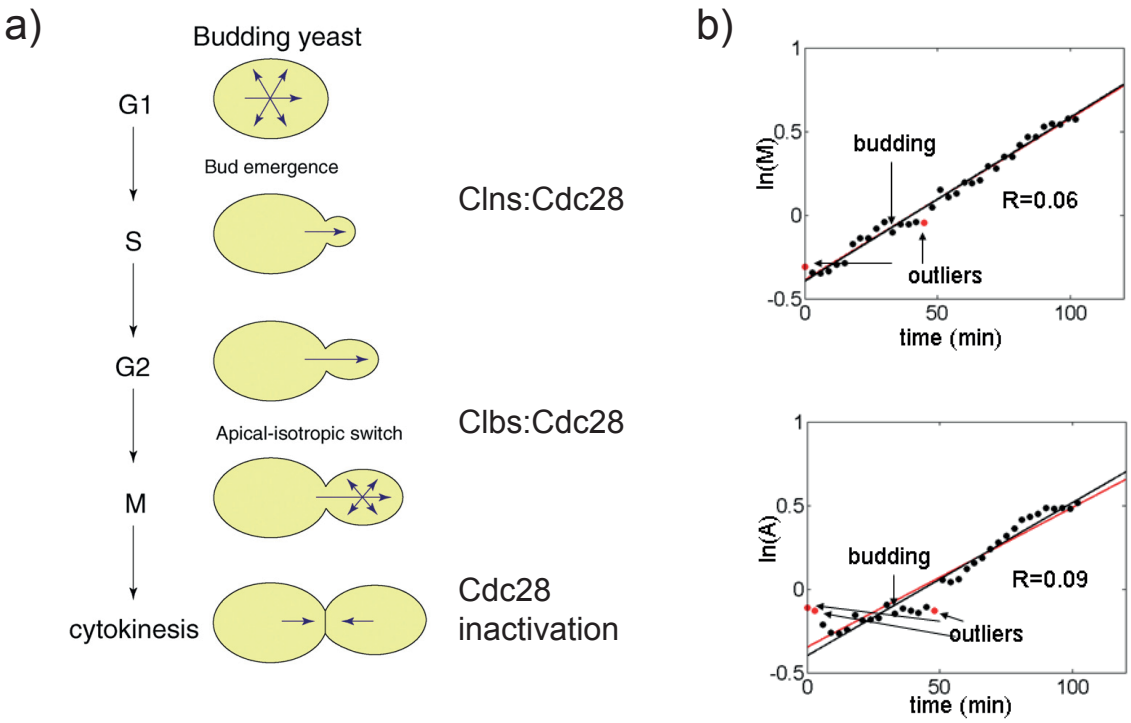

Figure 1.18: **General properties of budding yeast cell growth** - (a) Regulation of apical and isotropical growth is mediated by Cdc28. Clns:Cdc28 triggers apical growth, while Clbs:Cdc28 is responsible for isotropic growth during mitosis. Figure arranged from (Moseley & Nurse 2009). (b) Example of two cells, in which the logarithm of total amount of a cytoplasmic red fluorescent protein (top) or cell area (bottom) was measured in time, during an entire cell cycle. Both measurements fit an exponential law. Source: (Di Talia *et al.* 2007)

1.4.1 Morphology of budding yeast

As reported in Section 1.1, *Saccharomyces cerevisiae* cells proliferate by budding, which requires a polarized secretion in a restricted portion of the plasma membrane. In particular, bud dynamics is regulated by two types of growth: apical and isotropic. Apical growth is due to the polarization of the cortical actin cytoskeleton to a certain site of the plasma membrane, while isotropic growth causes bud expansion by delivering new wall components to the plasma membrane. These types of growth are regulated by Cdc28 kinase activity (Lew & Reed 1993) (Figure 1.18a). Apical growth takes place during G1/S transition, and it is mediated by G1 cyclins (Cln1, Cln2 and Cln3). Isotropic growth is promoted by Clb1 and Clb2 cyclins during mitosis. The budding yeast cell growth mainly takes place from budding to cytokinesis, and it fits with an exponential law (Di Talia *et al.* 2007) (Figure 1.18b).

This means that the growth rate is proportional to the cellular volume (Di Talia *et al.* 2007), and it is adjusted in the different phases of the cell cycle (Goranov *et al.* 2009; Leitao & Kellogg 2017) for coupling cell growth with cell division. Cellular growth needs nutrients, energy, protein synthesis and fatty acid biosynthesis, since inhibition of these processes leads to a reduction of cellular volume (Goranov *et al.* 2009; Vadia *et al.* 2017; Hannah & Barkai 2014).

1.4.1.1 Cell Size Control in G1 is implemented by an inhibitor-dilution mechanism

The best understood mechanism of cell size regulation in budding yeast takes place at the beginning of the cell cycle. Prior to bud emergence and DNA replication, cells need to pass through a START point in G1, which represents an irreversible step into the cell cycle (Figure 1.19a). During G1, cells adjust their growth rate according to the initial cell size, so that they all reach START with a critical size (Di Talia *et al.* 2007; Turner *et al.* 2012) (Figure 1.19a). For this reason, this mechanism of size control is called *sizer*. The relative growth in G1 will then be inversely proportional to the initial size of the cell: smaller cells have to prolong G1 for growing and reaching the critical size, while bigger cells have a shorter G1 (Di Talia *et al.* 2007) (Figure 1.19b).

From a molecular point of view, a switch is required for promoting bud emergence and cellular progression during START transition (Figure 1.19c). This switch involves Clns:Cdc28 activity, which is in charge of supporting apical growth as already discussed. In particular, the transcription factor Whi5 inhibits the transition through START point, by preventing synthesis of Cln1/2 in G1 cells. At the same time, Cln3:Cdc28 phosphorylates Whi5, reducing its inhibitory effect and allowing G1/S transcriptional activity (Turner *et al.* 2012) (Figure 1.19c). Relief of Whi5 repression is mediated by the G1 size control, which provides an inhibitor-dilution mechanism (Schmoller *et al.* 2015). The cellular concentration of Cln3 is constant through the size growth in G1, while Whi5 concentration decreases (Figure 1.19d, left plot); due to an increasing synthesis of Cln3 which is not matched by that of Whi5 (Schmoller *et al.* 2015) (Figure 1.19d, right plot). Therefore, the requirement of a START critical size is obtained by the critical dilution of the molecular inhibitor that prevents cell cycle progression.

1.4.1.2 Size growth during mitosis

Cell growth also takes place during M phase (Figure 1.18), via the activity of Clbs:Cdc28. We know that several molecular players take part to the progression through mitosis - as discussed in Section 1.1 - but there is no evidence about a critical mitotic size. Mitotic cell growth, however, has been partially characterized and evaluated in budding yeast, where mitosis represents the phase with the maximum growth rate (Goranov *et al.* 2009; Leitao & Kellogg 2017). Importantly, daughter cells take the major

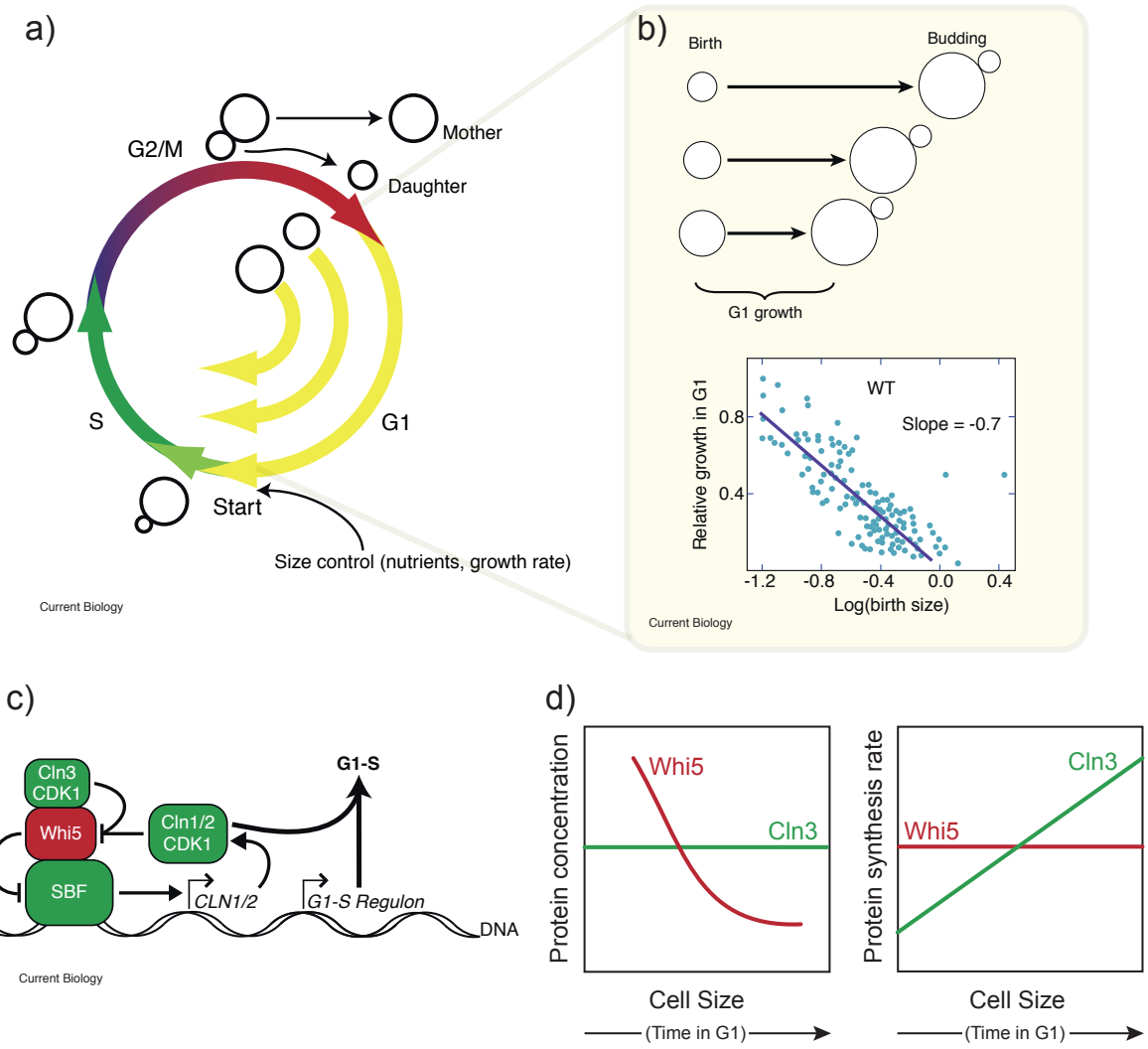

Figure 1.19: **The G1 sizer model promotes cellular proliferation by an inhibitor-dilution mechanism** - (a) Coupling of growth and proliferation in the cell cycle. When a daughter cell originates from a previous cell cycle, its size at birth will determine the amount of relative growth in G1. This size control ensures that cells go through START with a critical size. Source: (Turner *et al.* 2012). (b) Negative correlation between size at birth and relative growth on G1. While small cells have a big G1 growth, big cells have not. Source: (Turner *et al.* 2012). (c) Molecular mechanism for G1/S transition. Cln1/2:Cdc28 promotes G1/S transition, but their synthesis is inhibited during G1 by transcription factor Whi5. Phosphorylation of Whi5 by Cln3:Cdc28 allows Whi5 inhibition and progression in G1/S. Source: (Turner *et al.* 2012). (d) Inhibitor Whi5 is diluted in cells. Schematic behavior of Whi5 and Cln3 concentration (left plot) and synthesis rate (right plot) respect to an increasing cell size in time. Figure inspired from (Schmoller *et al.* 2015).

part as opposed to the mother cell (Leitao & Kellogg 2017). The combined growth of mother and daughter will follow an exponential dynamics.

1.4.2 Cell size during SAC activity: any evidence of MCC dilution?

Cell size dynamics can well play a role in adaptation to the SAC. As discussed in Section 1.2, during an active mitotic checkpoint O-Mad2 localizes to the unattached kinetochores and switches to C-Mad2, diffusing in the cytoplasm and allowing MCC assembly. Diffusion of MCC allows propagation of the "wait-anaphase" signal in the cellular volume (Heasley & of the … 2017).

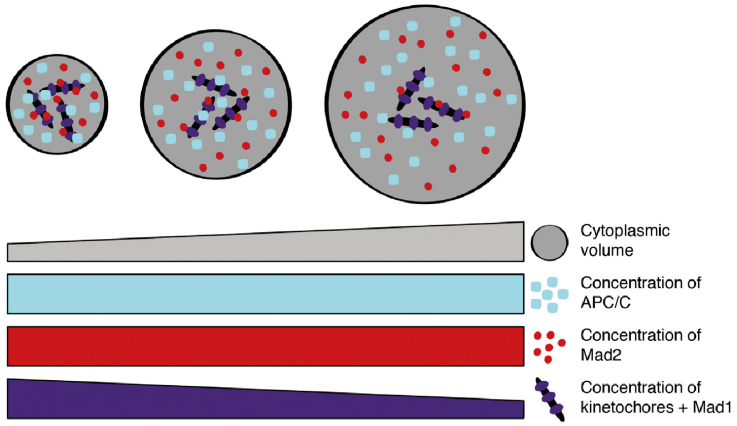

Figure 1.20: **Cell Size could impair SAC strength with an inhibitor-dilution mechanism** - Increase of cytoplasmic volume will affect concentration of unattached kinetochores, because they are present as absolute number in the cells. This dilution could potentially impair the SAC signal, creating a pool of free APC/C that is not inhibited by MCC. Figure rearranged from (Gerhold *et al.* 2016).

Assuming a constant concentration of APC/C and Mad2, Bub3 and Mad3/BubR1, any increase of cell size could causes during a mitotic arrest a decrease in the concentration of the signaling unattached kinetochores, because of their constant absolute number (Gerhold *et al.* 2016) (Figure 1.20). Moreover, a bigger cytoplasmic volume may reduce the probability of O-Mad2 to localize to the unattached kinetochores, and the distance over which MCC has to be diffused increases (Gerhold *et al.* 2016). Hence, APC/C inhibition could decrease as a consequence of cell growth in mitosis. In agreement with this possibility, it has been observed a negative correlation between cellular volumes and SAC strength in early embryogenesis of *C. elegans* (Galli & Morgan 2016). Moreover, eightfold reduction of mouse oocytes size causes an increased metaphase meiotic duration and a stalled APC/C activity upon nocodazole treatment (Lane & Jones 2017). We will explore the role of cell growth in adaptation in the Results - Section 4.1.

1.5 Cellular Memory

THe results presented in the thesis deal with molecular memory. In this section, I review some of the most recent results on the topic.

1.5.1 Cellular cognition

Cognitive biology claims that each cell is able to acquire informations from the surrounding environment. These informations are then processed and an active response towards the environment is elaborated (Lyon 2015). These abilities are based on molecular mechanisms, which determine the cognitive capacity of the cell (Lyon 2015). For this reason, it has been proposed the presence of a cellular *response regulator* (Morimoto & Koshland 1991), which summarizes incoming informations and regulates the output response, like a motherboard in computers. Upon sensing the input signal, cells assign a value to the summary of informations (*Valence* (Lyon 2015)). Then, elaboration of the input occurs. In this process, a tight interconnection between learning, adaptation and memory takes place. *Learning* represents the capacity to adapt behavior according to the past experience, which in turn is retained by the *Memory* property (Lyon 2015). The outcome of this process is an activator, which directs a specific output to the environment.

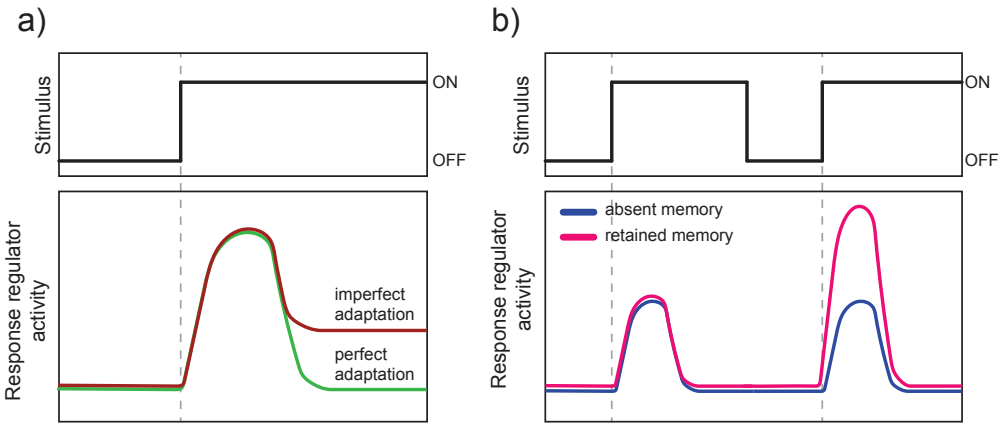

Figure 1.21: **Adaptation and Memory in Cellular Cognition** - (a) Upon introduction of a certain stimulus, response regulator activity increases and elaborates the input. In these conditions, cells can perfectly adapt to the stimulus, recovering a basal activity of the response regulator. An imperfect recovery is associated to an imperfect adaptation. (b) During subsequent introduction of a stimulus, cells can retain memory or not. In the presence of memory, the response regulator activity is higher during the second induction.

When a cell is exposed to a certain stimulus, the activity of its response regulator increases, in order to elaborate a proper output (Figure 1.21a). Once cell learns how to deal with the stimulus, it can adapt to it. In particular, a perfect adaptation is defined when the activity of the response regulator regains the basal level that was present prior to stimulus exposure (Figure 1.21a). Any retention of the activity above the basal level leads to an imperfect adaptation. Adaptation involves both cells experi-

encing the stimulus from the first time (i.e., "adapting") and cells with a continuous experience after the first exposure (i.e., "adapted"). This classical notion differs from the definition of adaptation to the SAC (or mitotic slippage - Section 1.3), in which the term "adaptation" only refers to the behavior of adapting cells upon the SAC stimulus.

Upon repetition of identical stimuli, the concept of memory can be formulated (Morimoto & Koshland 1991). The exposure to a second identical stimulus could trigger a response similar to that of the first stimulus, or even an increased response (Figure 1.21b). In the first case, memory is absent and is not retained after the elaboration of the first stimulus. In the second case, memory retains the past experience of the first stimulus and allows a better response. In the case of imperfect adaptation, the high residual activity upon the first stimulus could facilitate the achievement of a higher response when cell is exposed to the second stimulus (Morimoto & Koshland 1991).

1.5.2 Bacterial chemotaxis is a cognitive process

One of the first examples of cellular cognitive processes is represented by bacterial chemotaxis in *E. coli*. This process allows bacteria to arrange their movements, according to the gradient of chemical ligands in the surrounding environment (Figure 1.22a). Bacterial cells coordinate two types of movements: a straigthforward movement (also called *run*) and a *tumbling* one. While the run allows straight movements following the chemical gradients, tumbling is needed for changing direction (Figure 1.22a) (Webre *et al.* 2003).

Chemotaxis is well characterized from a molecular point of view in *E. coli* (Figure 1.22b) (Webre *et al.* 2003). Tumbling is promoted by the Chemotactic protein CheA, a kinase which mediates phosphorylation of CheY protein. Phosphorylated CheY then binds to flagellar motors and promotes tumbles. When random tumbling orients cell to an environmental chemical gradient, ligands bind to Methyl-accepting chemotaxis proteins (MCPs) that are located on the cellular membrane (Figure 1.22b). This event reduces activity of CheA, resulting in an inhibition of tumbling and a promotion of straightforward movement.

While ligands inhibit CheA, they progressively promote CheR activity in methylation of MCPs (Figure 1.22b), which in turn restores CheA kinase activity. MCPs methylation is a slow process - compared to the ligand-dependent response (Webre *et al.* 2003; Barkai & Leibler 1997) - but it allows bacterial cells to adapt to the chemical gradient. Indeed, progressive methylation of MCPs restores a random tumbling frequency, independently from the ligand concentration. (Barkai & Leibler 1997).

In this case, the response regulator of bacterial chemotaxis is composed by a fast ligand-dependent signal and a slow methylation-dependent signal (Morimoto & Koshland 1991). While the fast process allows to learn from the present conditions in the environment, the slow one allows the retention of

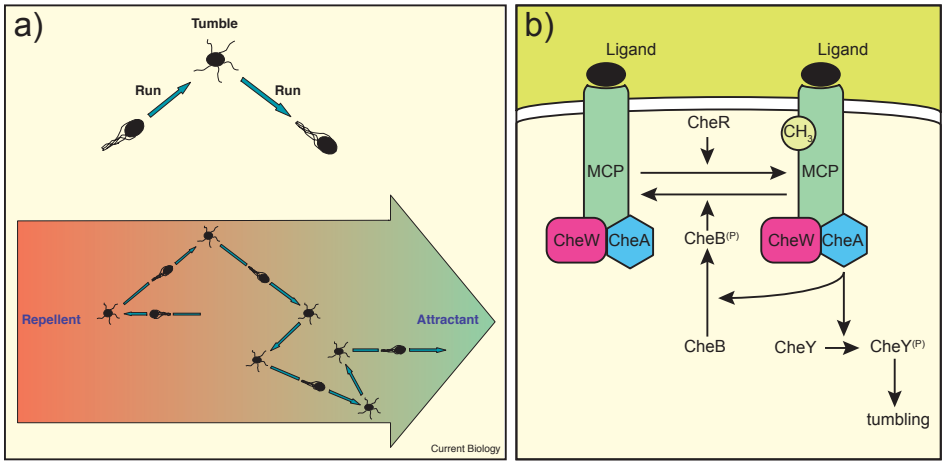

Figure 1.22: **General principles of bacterial chemotaxis** - (a) Bacteria such as E. coli exhibit two movements: runs and tumbles. In this way, they manage attraction or repulsion respect to chemical gradients in the environment. Source: (Webre *et al.* 2003) (b) Molecular pathway responsible for regulation of tumbling frequency.

past conditions. The final outcome is a robust perfect adaptation (Barkai & Leibler 1997). Upon a withdrawal and reintroduction of the gradient, bacteria do not retain any memory (Morimoto & Koshland 1991).

1.5.3 Budding yeast retains memory on deceptive mating attempt

Cellular cognition was firstly observed in bacteria. Recently, some examples of cognitive processes were also reported in higher eukaryotes. One of them includes budding yeast cells during a pheromone-induced cell cycle arrest (Caudron & Barral 2013). Administration of α-factor pheromone to cells with mating type *a* induces a signaling cascade that inhibits activation of the G1/S cyclin Cln3, therefore arresting cells in G1 (Figure 1.23d). When these cells are grown in microfluidic chambers under a constant flow of α-factor, they resume proliferation after experiencing a G1 arrest (Figure 1.23a, b), suggesting that they adapt to the pheromone and became refractory to it. Interestingly, while mother cells resume proliferation, daughter cells are competent to the G1 arrest. Interestingly, mother cells are able to retain memory of adaptation, since withdrawal of α-factor does not eliminate the refractory state (Caudron & Barral 2013).

This form of memory cannot be explained by a decreased sensing and/or valence of α-factor stimulus, since the mating signaling-cascade is still functional in refractory cells (Caudron & Barral 2013). Proliferation of refractory cells requires an active Cln3, which in turn is inhibited by the translational inhibitor Whi3 (Figure 1.23d). This means that cells somehow learn how to bypass Whi3 inhibition and resume Cln3 activity. Upon prolonged administration of the pheromone, the learning process is achieved by the assembly of Whi3 prions, which preferentially localize to the mother cells (Figure 1.23c). In this way, binding between Whi3 and mRNA of Cln3 is alleviated, and cells progress through G1/S. It also has been shown that the Hsp70 chaperone Ssa1 inhibits Whi3 assembly and

prevents adaptation to G1 arrest (Caudron & Barral 2013).

In this case, the response regulator involves two signals: the mating pathway and Whi3. During early stages of pheromone administration, both signals inhibit Cln3. As cells are arrested in G1 and fail in mating attempts, Whi3 tends to form super-assemblies, inhibiting itself and allowing Cln3 activation. Retention of memory correlates with retention of Whi3 prions in the mother cell.

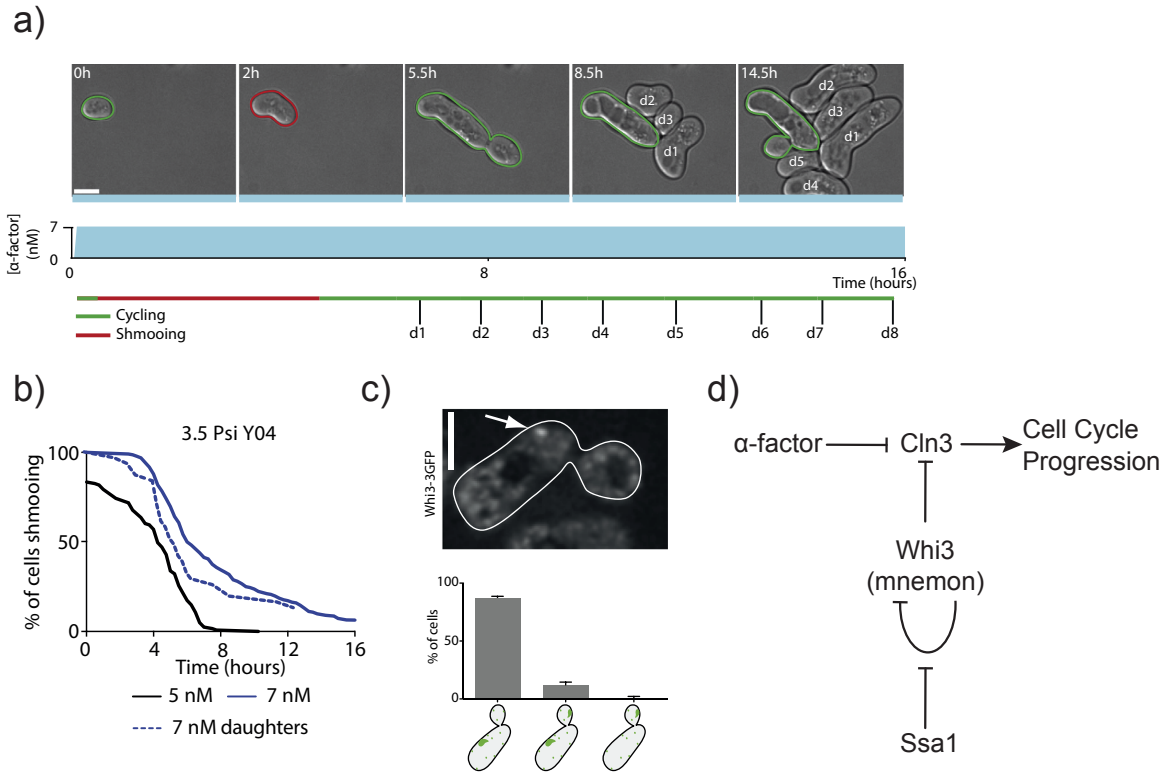

Figure 1.23: **Budding yeast cells perform a cognitive process during a prolonged exposure to α-factor** - (a) Upon a prolonged administration of α-factor 7nM, wild-type cells escape from the G1 arrest. Source: (Caudron & Barral 2013). (b) Proportion of arrested cells was plotted versus time of pheromone administration. Source: (Caudron & Barral 2013). (c) Upon α-factor administration, Whi3 forms super-assembly in mother cells, and not in daughter ones. Source: (Caudron & Barral 2013). (d) Schematic representation of the response regulator described in (Caudron & Barral 2013). At the first stages of G1 arrest, both α-factor and Whi3 inhibits Cln3 activity. The increased proportion of Whi3 prions allows activation of Cln3 and cell cycle progression, despite the continuous presence of the pheromone. Ssa1 inhibits formation of Whi3 prions.

1.5.4 Propagation of memory through the cellular progeny

The previous example provides a case in which memory is propagated through the cellular progeny. Another example of inherited cognitive process was recently proposed in human mammary epithelial cells (Yang *et al.* 2017). Upon mitotic exit of these cells, the proliferative status of the newly-born daughter cells can be evaluated, in terms of Cdk2 levels. Indeed, high Cdk2 levels positively correlate with proliferative capacity. Cdk2 is activated by chemical mitogens in growth medium, MEK/ERK pathway and CyclinD:Cdk4 (Figure 1.24a), and inhibition of these components in the mother cells abolishes Cdk2 levels and proliferative status in daughter cells (Yang *et al.* 2017). Indeed, high levels

of Cdk2 in daughter cells are stimulated by CyclinD1 mRNA and protein, which are inherited from mother cells (Figure 1.24b, c). Moreover, if mother cells experience DNA damage, p53 is activated and inherited by daughter cells, due to the high half-life of the tumor suppressor (Yang *et al.* 2017) (Figure 1.24b, c). As a result, p21 is activated and it negatively regulates Cdk2 levels (Yang *et al.* 2017) (Figure 1.24c).

The response regulator of these daughter cells relies on the ratio between Cyclin D1 and p21, which dictates the cellular fate: proliferation or quiescence (Figure 1.24d). Here, the memory is based on the past experience of mother cells, upon DNA damage and/or mitogens exposure, that is molecularly inherited by daughter cells.

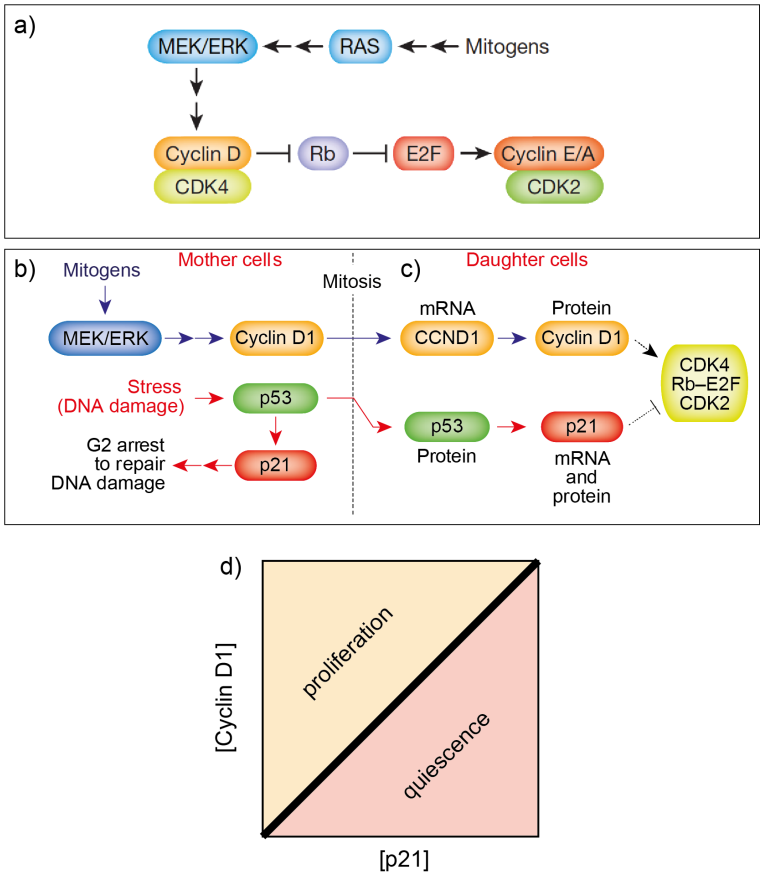

Figure 1.24: **Inheritance of mitogens and DDR activity by daughter cells influences their proliferative status** - (a) Molecular basis of CyclinE/A:Cdk2. Source: (Yang *et al.* 2017). (b) Upon exposure to mitogens and/or DNA damage, mother cells promote respectively Cyclin D1 and p53. Source: (Yang *et al.* 2017). (c) From the cellular activity of mother cell, daughter inherited mRNA of Cyclin D1 and p53 protein. Then, Cyclin D1 will compete with p21 for regulating entry into G1/S. Inheritance of Cyclin D1 and p53 is the source of cellular memory of these cells. Source: (Yang *et al.* 2017). (d) The response regulator of daughter cells is based on the ratio between p21 concentration and Cyclin D1. High levels of p21 correlates with low levels of Cyclin D1 and quiescence. On the other hand, low levels of p21 allows to high levels of Cyclin D1 to promote proliferation. Source: (Yang *et al.* 2017).

2 Aim of the Thesis

When cells are treated with antimitotic drugs, adaptation to the SAC is one of the possible outcomes of a prolonged mitotic arrest. Although several studies are focused on the overcome of this arrest, the cellular fate after adaptation has not been so well examined. To this purpose, we characterized the first cell cycles of cells that resumed proliferation after adaptation to the mitotic checkpoint: we refer to these cells as *adapted* cells.

In the first part of the Results, we described the phenotype of adapted cells in the presence of Mad2 overexpression as the source of SAC signal. Here, the absence of missegregation after adaptation allows to analyze for many hours the behavior of adapted cells. In the second part, we induce the SAC via spindle disruption to confirm the features observed in the first part in more "physiological" conditions. Finally, we report the results of Mass-Spectrometry analysis on adapted cells. Our data show at the molecular level how the cell cycle is rewired in adapted cells.

3 Material and Methods

3.1 Strains, Media and Reagents

3.1.1 Strains

All strains are listed in table 6.1 (see Appendix) and were derivative of or were backcrossed at least three times with W303 (*ade2-1, trp1-1, leu2-3, 112, his3-11, ura3*). Original construct for *GAL1-MAD2* was developed in the lab of S. Piatti (Centre de Recherche en Biologie Cellulaire de Montpellier - Montpellier, France); *cdc16-6A* mutant, *cdc27-5A* mutant and *GAL-CDC28-HA* were received from A. Murray (Department of Molecular and Cellular Biology, Harvard University, Cambridge, MA, United States); *CDC16-MYC* and *CDC27-MYC* were received from J. M. Peters (Research Institute of Molecular Pathology - Vienna, Austria); *SIC1(10x)* was received by D. P. Toczyski (Department of Biochemistry, University of California - San Francisco USA); *CFIII (CEN3.L.YPH278) URA3SUP11* was received by P. D. Wulf (Center for Integrative Biology, University of Trento - Italy).

3.1.1.1 Production of *$tetO_2$-CDC20-127* strain

$tetO_2$-CDC20-127(1x) cells were obtained by yeast transformation of wild-type strain yAC1001 with plasmid pBS94 from A. Murray (Department of Molecular and Cellular Biology, Harvard University, Cambridge, MA, United States), carrying a copy of *cdc20-127* (Hwang *et al.* 1998) with *TRP1* marker under the doxycycline-repressible promoter *$tetO_2$*. The plasmid was digested with three different restriction enzymes (EcoRV, Bsu36I, BstNI). Transformant were tested for single insertion by Southern Blot, while checkpoint-deficiency by FACS analysis. The strain was created by Luca Mariani, a former member of the laboratory.

3.1.1.2 Production of *tub2-401* mutants

tub2-401 cells were obtained by yeast transformation of wild-type strain yAC1001 with plasmid pTH18 from T. Huffaker (Department of Molecular Biology and Genetics, Cornell University - Ithaca, United States), which contains a copy of *TUB2* ORF carrying the 4 point mutations (Huffaker *et al.* 1988) with *URA3* marker. The plasmid was digested with restriction enzyme KpnI before transformation (Huffaker *et al.* 1988). Transformant were than plated on 5-fluoro-orotic acid plates to select against *URA3*, and resulting colonies were amplified and tested for cold-sensitivity at 15°C.

3.1.1.3 Strains with proteins tagged with Fluorescent Protein

CLB2-GFP was received by P.A. Silver (Department of Biological Chemistry and Molecular Pharmacology, Harvard Medical School and The Dana-Farber Cancer Institute - Boston, USA); *TUB2-mCherry* was received by Rosella Visintin (Department of Experimental Oncology, European Institute of Oncology - Milan, Italy); *MAD2-GFP* was received by T. Tanaka (Centre for Gene Regulation and Expression, College of Life Sciences, University of Dundee, Scotland, UK). Tagging of endogenous Clb2 with mCherry was performed in the lab by Paolo Bonaiuti (Bonaiuti *et al.* 2017).

3.1.2 Media and reagents

All population experiments were performed using YEP medium (1% yeast extract, 2% Bacto Peptone, 50 mg/l adenine) supplemented with 2% glucose (YEPD), 2% raffinose (YEPR), or 2% raffinose and 2% galactose (YEPRG). Live-cell imaging experiments were performed using synthetic complete medium supplemented with ammonium sulfate. For chromosome loss assay, cells were grown in synthetic medium lacking uracile before plating them.

α-factor (GenScript®) was used at 5 μg/ml for 1h 30 min, followed by 2.5 μg/ml for 30 min; readdition was performed at 20 μg/ml. Nocodazole (Sigma-Aldrich®) was used at 3, 5 or 15 μg/ml, while readdition at 1.5, 2.5 or 7.5 μg/ml. Readdition of α-factor was performed when more than 90% of the cells were budded, and starting from this event every 2h. Readdition of nocodazole was performed after 3h from the inoculum, and then every 2h. Doxycycline hyclate (Sigma-Aldrich) was used at 10 μg/ml according to (Barnhart *et al.* 2011), in order to repress *cdc20-127* expression in *tetO$_2$-CDC20-127(1x)* cells. When cells were synchronized in G1 before releasing them without *cdc20-127* expression, doxycycline was added together with 2.5 μg/ml of α-factor, in order to allow an optimal G1 synchronization while starting to repress cdc20-127.

In population and single-cell experiment with *GAL1-MAD2(3x)* and *GAL1-CDC28-HA* cells, galactose 2% was added 1 hour before the release from α-factor. Except for *tub2-401* cells, all the experiment

were performed at 30°C.

3.2 Western Blot Analysis

3.2.1 Protein Lysate Preparation

Cells were sampled and centrifuged at 4000 rpm, 2 min. Once supernatant was discarded, pellet was resuspended in 1 ml of Trichloroacetic acid (TCA) 20%. Pellet was centrifuged again (13200 rpm, 3 min), separated from supernatant via aspiration and resuspended in 100 μl of TCA 20% to precipitate proteins. Samples were stored at -20°C.

Glass beads were added to the stored pellets, allowing a complete lysis in a vortex, for 10 min, at room temperature. Then, 400 μl of TCA 5% were added in each sample, in order to slightly increase pH. Liquid volume was separated from glass beads, transferring it in a new tube and centrifugating it at 4000 rpm, 10 min. Supernatant was aspirated carefully, and pellet was centrifuged again at 4000 rpm for 5 min, for achieving a better collection of pellet.

For each sample, 1 part of Laemmly Buffer (SDS 2%, Tris-HCl 60 mM pH 6.8, glycerol 10%, bromophenol blue 0.01%, 2-mercaptoethanol 10%) and half-part of basic tris 1M were added, in order to further increase pH. Then, samples were incubated at 95°C for 2 min, in order to allow protein denaturation and breakage of disulfide bonds (Fraschini *et al.* 1999). Finally, samples were centrifugated at 13200 rpm, 5 min. Supernatant was collected and stored at -20°C.

3.2.2 Western and Transfer Blot

Lysates were then loaded and separated by SDS-page gels. In Western Blots reported in Section 4.1, home-made gels were used, with 10% or 12.5% polyacrylamide containing an acrylamide-to-bisacrylamide ratio of 29/1. In Sections 4.3, 4.4 and Appendix, Criterion™ TGX Stain-Free™ Precast Gels from Bio-Rad © 10% were used. In both cases, proteins were separated applying a voltage of 100-140 V, in a running buffer (Glycine 2M, Tris 0.25 M, SDS 0.02 M, pH 8.3).

Wet transfer blot on Amersham Protran Nitrocellulose Membranes (GE © Healthcare) was performed for home-made western blot, using a transfer buffer (1% glycine, 0.02M basic Tris, 20% methanol) and applying a voltage of 100 V for 1h 15min, at 4°C. For precast gels, semi-dry transfer blot was performed, using Trans-Blot® Turbo™ Transfer Pack (Midi Format, 0.2 μm Nitrocellulose) on a Trans-Blot® Turbo™ Transfer System, setting 25 V, 2.5 A for 7 min.

3.2.3 Protein detection

Membranes coming from transfer blot were incubated with TBS-Tween and milk 5% for 1h at room temperature. Then, they were incubated overnight with primary antibodies. The next day, membranes were washed with TBS-Tween for 30 min, and then incubated with HRP secondary antibodies for 1h, at room temperature. After an additional washing phase of 1h, proteins were detected by an enhanced chemiluminescence system (Pierce ECL; Thermo Fischer Scientific) and digitalized images were acquired with a Chemidoc XRS+System (Bio-Rad©).

The following primary antibodies were used: anti-ScMad2 (from Monoclonal Antibodies Facility at the IFOM-IEO Campus), anti-MYC (from Monoclonal Antibodies Facility at the IFOM-IEO Campus), anti-Clb2 (sc-9071; Santa Cruz Biotechnology, Inc.), anti-Pgk1 (D660; Invitrogen), anti-Tub1 (MCA78G, Bio-Rad), anti-Cdc28 (sc-6709; Santa Cruz Biotechnology, Inc.), anti-Mad1 (IQ242; ImmuQuest Ltd). Secondary antibodies came from Bio-Rad laboratories.

3.2.4 Quantification of Western Blot

Quantification of signal coming from chemiluminescence reaction was performed with Image Lab ™ Software (Bio-Rad©). In Western Blot reported in Section 4.1, each band was quantified with Volume Tool, taking a fixed rectangular area for each lane and considering as background the same fixed area in a portion of membrane without signal. Western Blot in Sections 4.3 and 4.4 were quantified with Lane and Bands Tool, manually adjusting lane profiles.

In both cases, signal coming from any protein of interest was normalized to the signal coming from the housekeeping protein (Pgk1, Tub1 or Mad1).

3.2.5 Phos-Tag Western Blot

Detection of phosphorylated Cdc16 and Cdc27 was performed by Phosphate-affinity Mn^{2+}-Phos-tag Western Blot (Kinoshita *et al.* 2006; Kinoshita *et al.* 2009). For Cdc27, home-made gels 7.5% were prepared adding to the regular recipe Phos-Tag™ AAL-107 5mM reagent (Wako Chemicals GmbH ©) and $MnCl_2$ 10 mM. In the presence of manganese ions, Phos-Tag reagent binds specifically to phosphate groups, allowing separation of phosphorylated isoforms from the non-phosphorylated one. For Cdc16, half doses of Phos-Tag™ AAL-107 5mM reagent and $MnCl_2$ 10 mM were used. Protein separation was achieved applying a constant amperage (15 mA/gel) for about 3/4 hours.

Before proceeding with wet transfer blot, gels were incubated in transfer buffer supplemented with 100 mM EDTA pH 8 for 30 min, in order to chelate the manganese ions. Then, gels were washed for 15 min with transfer buffer, and regular wet transfer blot protocol was performed on nitrocellulose

membranes. Membranes were incubated with TBS-Tween with milk 2% and BSA 2% for 1 h. Then, they were incubated overnight with anti-MYC primary antibodies, 4°C. From this point, the regular procedure for protein detection was performed, using HRP anti-mouse secondary antibodies.

3.3 Proteomic Analysis

Here we report the workflow for LC/MS-MS proteome analysis of adapted cells, performed by Vittoria Matafora (Lab. of Functional Proteomics - A. Bachi - IFOM, Milan - IT), except for the last subsection that was performed by myself. For further details, see (Matafora *et al.* 2017).

3.3.1 Protein Lysate Preparation

From a culture in log phase growth, 10 mL were sampled and centrifuged (4000 rpm, 2 min, room temperature). Supernatant was discarded, while pellet was resuspended in 1 ml of 100 mM Tris/HCl pH 7.6. Once supernatant was discarded again (13200 rpm, 3 min, 4°C), pellet was subjected to rapid cooling in dry ice plus denatured alcohol, and stored at -80°C.

From -80°C, pellet was resuspended in 70-80 μL of 100 mM Tris pH 7.6, 100 mM dithiothreitol, 5% SDS and heated at 95°C for 5 min. Then, glass beads were added and sample was vortexed for 10 min, at room temperature, for a complete lysis. Subsequently, 35-40 μl of 100 mM Tris pH 7.6, 100 mM dithiothreitol (DTT), 5% SDS were added. Sample was centrifuged (13200 rpm, 5 min, room temperature), and supernatant was collected and stored at -20°C.

3.3.2 Protein Digestion for MS analysis

For digestion, 50 μg of lysate were added to 200 μL of 8 M urea in 0.1 M Tris/HCl, pH 8.5 (UA buffer) and transferred to YM-30 microcon filters (Cat No. MRCF0R030, Millipore©). After centrifugation (14000 $\times g$, 15 min), three washing with 400 μl of UA buffer were done (14000 $\times g$, 15 min). Lysate was reduced with 0.01 M DTT in UA buffer for 30 min at room temperature. Then, 2 washing with 400 μl of UA buffer were repeated; 100 μl of 0.05 M iodoacetamide in 8 M urea were added, in order to alkylating proteins, and samples were incubated in the dark for 5 min. Filters were washed twice with 100 μl of UA buffer, followed by two washing with 100 μl of 40mM NH_4HCO_3. Subsequently, sample was resuspended in 95 μl of 40 mM NH_4HCO_3, supplemented with 120 mM $CaCl_2$ and 1 μg of trypsin, and incubated overnight at 37°C. Then, an additional incubation with 1 μg of trypsin for 3 h was performed. Peptides resulting from the digestion were collected by centrifugation and purified on a C18 StageTip (Proxeon Byosystems©, Denmark). Once concentrated, peptides were splitted in independent samples for technical replicates.

3.3.3 Mass Spectrometry Analysis

From digested samples, 1 μg was injected in a quadrupole Orbitrap Q-exactive HF mass spectrometer (Thermo Scientific ©). Peptides separation was achieved on a linear gradient from 95% solvent A (2% ACN, 0.1% formic acid) to 55% solvent B (80% acetonitrile, 0.1% formic acid) over 240 min, and to a final 100% of solvent B in 3 min at a constant flow rate of 0.25 $\mu l/min$ on UHPLC Easy-nLC 1000 (Thermo Scientific ©). The LC system was connected to a 23 cm fused-silica emitter of 75 μm inner diameter (New Objective, Inc. Woburn, MA, USA), packed in-house with ReproSil-Pur C18-AQ 1.9 μm beads (Dr Maisch Gmbh, Ammerbuch, Germany) using a high-pressure bomb loader (Proxeon, Odense, Denmark). A Data-Dependent Acquisition (DDA) was performed on the mass spectrometer, with the following settings: dynamic exclusion of 15 s enabled, MS1 resolution of 70000 at m/z 200, MS1 automatic gain control target of 3e+6, MS1 maximum fill time of 60 ms, MS2 resolution of 17500, MS2 automatic gain control target of 1e+5, MS2 maximum fill time of 60ms, MS2 normalized collision energy of 25. For each DDA cycle, one full MS1 scan range of 300-1650 m/z was followed by 12 MS2 scans, using an isolation window size of 2 m/z.

3.3.4 Database Search and Spectral Library Construction

Files with raw data coming from MS analysis were processed with MaxQuant software (1.5.6.0) (Cox & Mann 2008), using Andromeda search engine (Cox *et al.* 2011). MS/MS peak lists were searched against the UniProtKB/Swiss-Prot protein sequence Yeast complete proteome database (release 2014). A reverse decoy database was generated within Andromeda, setting a 0.01 False Discovery Rate (FDR) for Peptide Spectrum Matches (PSMs) and proteins. A filtering was applied to the resulting list, asking at least two peptides identifications per protein, of which at least one peptide had to be unique to the protein group. Spectral libraries were generated using Skyline (2.5.0.6157) (MacLean *et al.* 2010) and Andromeda search results.

3.3.5 Protein Quantitation using Data-Dependent Acquisition Analysis

DDA files were analyzed in a label-free manner, using MaxQuant software (Cox & Mann 2008) for protein quantitation. Quantitation was provided by Label-Free Quantification intensities (LFQ intensities), which represent the intensities values coming from MS/MS normalized across the entire data set.

3.3.6 Data Normalization and Statistics

Once LFQ intensities were obtained for identified protein of adapted and not adapted cells, Z-scores were evaluated for each protein. In order to identify any significant increase or decrease in protein abundance, a t-test was performed on Z-scores, using Perseus software (1.5.6.0) (Tyanova *et al.* 2016). For *GAL1-MAD2(3x)* cells, a FDR of 0.01 was set, while for *tub2-401* 0.05. Then, a hierarchical cluster analysis was performed on Z-scores. Each analysis included two biological replicates, both of them with two technical replicates.

3.3.7 Exploring significant and not-significant proteome enrichment

Protein lists resulting from hierarchical cluster analysis were submitted to PANTHER database (Mi *et al.* 2013; Mi *et al.* 2017), performing a statistical overrepresentation test across Gene Ontology (GO) Slim Biological Process terms of *Saccharomyces cerevisiae* (p-value < 0.05). Fold-enrichment was evaluated for any significant GO term, as reported in (Mi *et al.* 2013). Each list was also subjected to a statistical overrepresentation test of *Saccharomyces cerevisiae* pathways, using ConsensusPathDB-yeast database (Herwig *et al.* 2016; Kamburov *et al.* 2013; Kamburov *et al.* 2011; Pentchev *et al.* 2010) (FDR < 0.05). Beyond significant enrichment, each list was submitted to SGD Gene Ontology Slim Mapper (Cherry *et al.* 2012) and pathways of interest were identified. Selected proteins were inserted in Protein-to-Protein Interaction (PPI) network, using Cytoscape software (Cline *et al.* 2007; Saito *et al.* 2012; Shannon *et al.* 2003; Smoot *et al.* 2011). GeneMANIA plugin (Montojo *et al.* 2010) was used for querying proteins of interest, looking only for physical interactions.

3.4 Single Cell Experiments

3.4.1 Image acquisition settings

Each single-cell experiment was performed via monitoring cells growing in microfluidic chambers (CellASIC®), in which flowing medium was maintained with a ONIX microfluidic perfusion system (CellASIC®). Time-lapse movies of *GAL1-MAD2(3x)* were recorded using a DeltaVision Elite imaging system (Applied Precision) based on an inverted microscope (IX71; Olympus) with a camera (CoolSNAP HQ2; Photometrics) and a UPlanFL N 60x (1.25 NA) oil immersion objective lens (Olympus). During experiments at 30°C, an oil immersion with refractive index n=1.516 was used. In the case of experiment performed at temperatures lower than 21°C, we used oil immersion with n = 1.512. GFP, and mCherry were acquired using single bandpass filters (EX475/28 EM523/36 for GFP, EX575/25 EM632/60 for mCherry). Time-lapses of *tub2-401* and *GAL1-CDC28-HA* cells were

acquired with another DeltaVision system, with the same settings as described above but with a different camera (Scientific CMOS Camera). Excited and non-excited fields were acquired, in order to evaluate any phototoxicity of the acquisition setting by comparing the cell cycle duration in excited and non-excited cells.

3.4.2 *GAL1-MAD2(3x)* adapting and adapted cells

3.4.2.1 Experimental setup

Log-phase cells growing at 30°C in synthetic medium with raffinose were diluted to $OD_{600} \sim 0.1$ and α-factor 5 $\mu g/ml$ was added in each volume. After 1h 30 min, α-factor 2.5 $\mu g/ml$ was added. Cells were diluted to $OD_{600} \sim 0.15$, sonicated and loaded in the microfluidic plate. Then, cells were kept in G1 while exposing them to galactose, in order to pre-induce *GAL1pr*. After 1h, cells were released in synthetic medium with galactose, leaving them to grow at 30°C.

3.4.2.2 Excitation settings

The following excitation settings were used:

- **POL**: 1 z-stack, exposure time 0.08s, power lamp 32%, every 10 min
- **GFP (Clb2)**: 1 z-stack, exposure time 0.15s, power lamp 32%, every 10 min
- **mCherry (Tub2)**: 3 z-stacks (0.85 μm), exposure time 0.10s, power lamp 10%, every 10 min

3.4.3 *GAL1-CDC28-HA* adapting cells in nocodazole

3.4.3.1 Experimental setup

Log-phase cells growing at 30°C in YEPR were diluted to $OD_{600} \sim 0.15$ and α-factor 5 $\mu g/ml$ was added in each volume. After 1h 30 min, α-factor 2.5 $\mu g/ml$ was added. Cells were diluted to $OD_{600} \sim 0.2$, sonicated and loaded in the microfluidic plate. Then, cells were kept in G1 while exposing them to galactose, in order to pre-induce *GAL1pr*. After 1h, cells were released in YEPRG supplemented with nocodazole 15 $\mu g/ml$, leaving them to grow at 30°C. When most of the cells were budded and entered in mitosis, α-factor 20 $\mu g/ml$ was added in the flowing medium, in order to re-synchronize cells in the subsequent G1 after adaptation.

3.4.3.2 Excitation settings

The following excitation settings were used:

- **POL**: 1 z-stack, exposure time 0.08s, power lamp 32%, every 10 min
- **GFP (Mad2)**: 11 z-stacks (0.3 μm), exposure time 0.07s, power lamp 10%, every 10 min
- **mCherry (Clb2)**: 1 z-stack, exposure time 0.5s, power lamp 10%, every 10 min

Images for Mad2-GFP were deconvoluted with SoftWoRx software, and a maximum intensity projection was performed with all the z-stacks.

3.4.4 *tub2-401* adapting and adapted cells

3.4.4.1 Technical specifications

Experiments with *tub2-401* cells were performed at lower temperature (15-21°C), enveloping the microfluidic plate in a incubating metallic chamber (Figure 3.1a) in which a refrigerated antifreeze mixture was flowing. Temperature control was performed by a BOLD LINE Water-Jacket Top Stage Incubation System (OKOlab ©). In this system, refrigeration and flow of antifreeze was performed by an immersion thermostat (LAUDA© DR. R. WOBSER GMBH & CO. KG, Germany) which was connected to the incubating chamber with several insulated tubes. Moreover, an objective cooler was connected to the same system, in order to refrigerate the objective during the timelapse. Temperature control was performed by BOLD LINE T-unit, together with SmartBox (OKOlab ©). The system took into account room temperature (measured by a thermistor) and temperature inside the incubating chamber (monitored by a fine gauge thermocouple). T-unit allowed two ways of temperature control: Sample Mode (keeping constant the temperature of specimen monitored by thermocouple) or Chamber Mode (maintaining a constant temperature of chamber). A BOLD LINE Logger Software (OKOlab ©) allowed communications with OKOlab system in order to log data from it.

3.4.4.2 Calibration of Incubator System before the timelapse

In order to properly set temperature control before doing the timelapse, the following pipeline was performed :

1. **Measuring temperature in the imaging region**

   A fake microfluidic plate was put in the incubating chamber and filled with mineral oil in the corresponding cavity of imaging region. Then, objective was put in contact with plate, under the imaging region. Thermocouple was inserted in the mineral oil, and incubating chamber was closed (Figure 3.1c). Incubation system was set to Chamber Mode at $\sim$ 16°C, allowing to keep constant temperature of chamber while monitoring the one in the imaging region. Moreover, we put a cylinder full of mineral oil inside the chamber, on the bottom part of it (Figure 3.1b).

Once temperature reached a steady state, we turned on the DeltaVision imaging system, and we left the entire system to reach an equilibrium temperature for 24 hours.

2. **Calibration**

   Once the system reached the equilibrium, we moved the thermocouple from the imaging region to the cylinder (Figure 3.1d). This allowed to evaluate the difference between temperature of imaging region and that of the inside part of chamber. Usually, imaging region was 2/3°C higher than the bottom part of the chamber. Assuming a linear relationship between these two temperatures, we set incubation system in Sample mode, in order to maintain constant the temperature of the cylinder region. During this mode, thermocouple was shifted in the cylinder and cylinder temperature was adjusted, according to the desired temperature in the imaging region.

3. **Incubation of the experimental microfluidic plate** Before closing the chamber, a new microfluidic plate was inserted. PBS was removed from wells, which were filled with synthetic medium. Once closed, we allowed the system to reach an equilibrium for 24 hours. In this way, medium was refrigerated before the experiment.

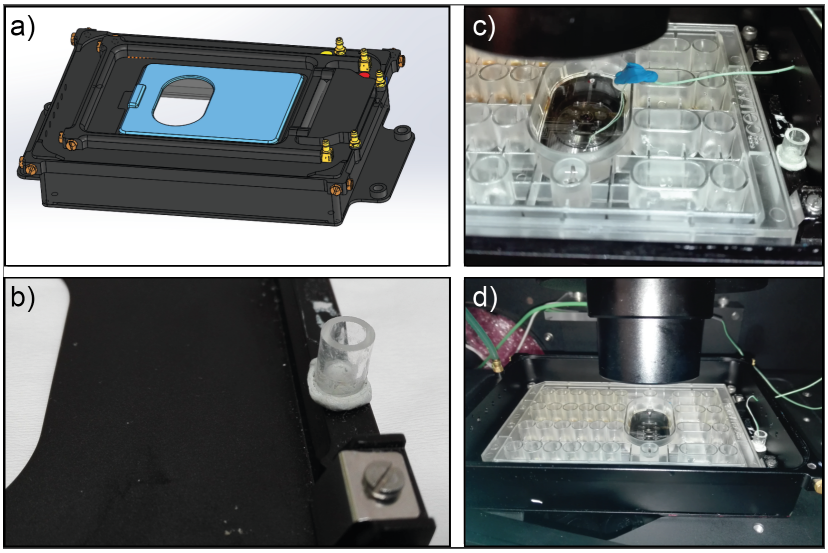

Figure 3.1: **Details of incubator system** - (a) Design of incubating chamber (OKOlab©). (b) Details of cylinder located on the bottom part of chamber. (c) Details of temperature measurement in the imaging region. (d) Calibration of temperature between imaging region and cylinder. Settings of incubator system were performed by Okolab© and with the support of Imaging Technological Development Unit at IFOM - Milan, IT.

3.4.4.3 Experimental setup

Log-phase cells growing at 30°C in synthetic medium were diluted to $OD_{600} \sim 0.2$ and α-factor 5 $\mu g/ml$ was added in each volume. After 1h 30 min, α-factor 2.5 $\mu g/ml$ was added. After 2 hours from the first α-factor addition, cells were release in synthetic medium supplemented with α-factor 5 $\mu g/ml$ and leaving them to grow at low temperature for 1 hour. This additional phase allowed cells

to keep the G1 arrest, while starting to sense the low temperature. After 1h from release, cells were diluted again to $OD_{600} \sim 0.2$, sonicated and loaded in the microfluidic plate. Once all the positions to be monitored were chosen, cells were released from α-factor, leaving them to grow in cold synthetic medium. During the entire timelapse, temperature was continuously monitored.

3.4.4.4 Excitation Settings

For these experiment, we identified the following excitation settings:

- **POL**: 1 z-stack, exposure time 0.08s, power lamp 32%, every 15 min
- **GFP (Clb2)**: 1 z-stack, exposure time 0.15s, power lamp 32%, every 15 min

3.5 Single Cell Analysis

3.5.1 Segmentation and tracking of cell bodies

Timelapse were imported in Phylocell (Charvin *et al.* 2008), an open-source software written in MATLAB® by G. Charvin (Institut de Génétique et Biologie Moléculaire et Cellulaire - Illkirch-Graffenstaden, France), and available at `https://github.com/gcharvin/phyloCell`. Using Phylocell, segmentation of cell bodies was achieved with homothetic inflation and/or watershed algorithms, manually adjusting the obtained areas where necessary. Tracking of segmented area in time was performed by Iterative Closest Point algorithm. Software was further improved by Emanuele Martini (Technical Development Imaging Unit, IFOM - Milan, Italy), in order to achieve a better segmentation of adapted cells.

From segmented area, we extracted informations about cellular dimension and fluorescence in time, by ad-hoc software written in MATLAB® by Paolo Bonaiuti in the lab. During data extraction, background fluorescence was subtracted from the cellular one. Moreover, each couple "mother-and-daughter" was considered as an unique Region of Interest (ROI).

3.5.2 Image Analysis of *GAL1-MAD2(3x)* and *tub2-401* cells

To the purpose of simplifying the analysis, we followed only the progeny coming from each mother cells at the beginning of the timelapse, ignoring the one originated from daughter cells of adapting mother cells. Evaluation of mitotic duration in *GAL1-MAD2(3x)* and *tub2-401* cells was performed via evaluating nuclear signal of Clb2-GFP, using the same procedure described in (Vernieri *et al.* 2013) and developed in the lab by Fridolin Gross. Briefly, by k-means algorithm on Clb2 fluorescence we

were able to identify the nucleus for each cell. Since Clb2 is expresses only in mitosis, estimation of nuclear area was accurate only during mitotic phase (Figure 3.2a). In this way, mean nuclear fluorescence of Clb2 was estimated in mitosis. Each trajectory was smoothed and plotted, in order to check one by one the behavior of each cell (Figure 3.2b) and manually defining mitotic entry and exit from the plotted trajectory, with a basic user interface. Selection of mitotic entry was defined by the user at the time in which Clb2 started to increase, while mitotic exit when Clb2 started to decrease. Mitotic duration was defined as the difference between these two timepoints. Moreover, we also recorded information about cellular area of mother and daughter cells within these timepoints (Figure 3.2c).

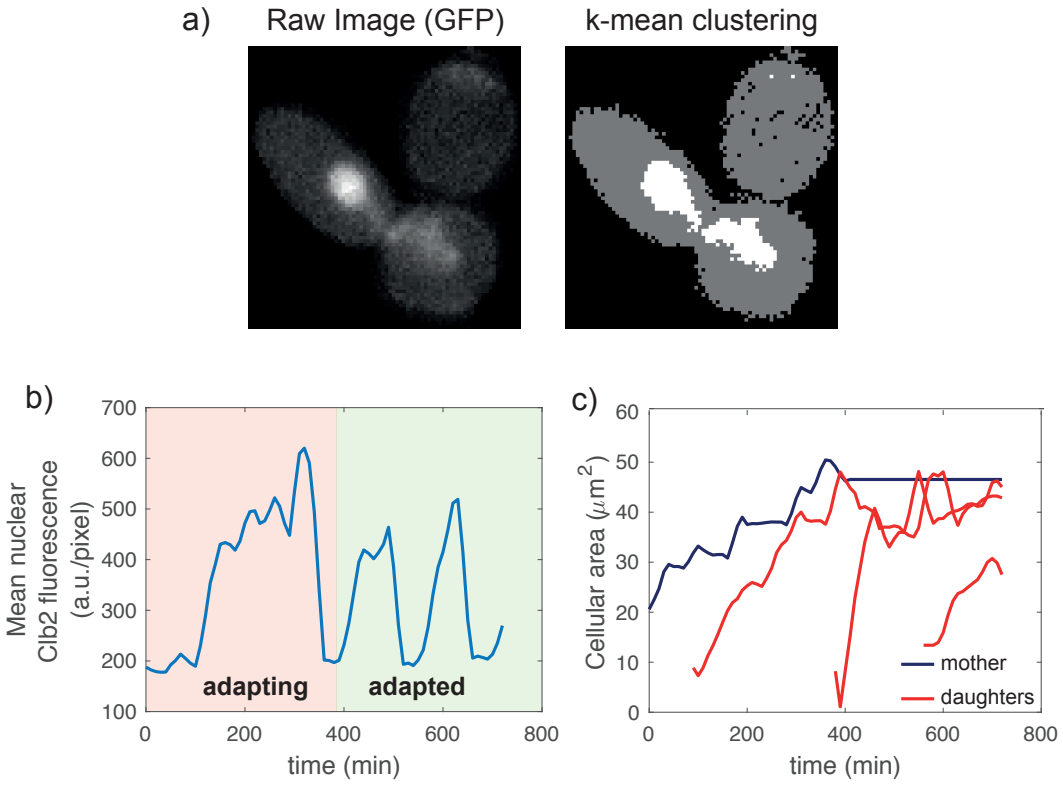

Figure 3.2: **Measuring Clb2 nuclear levels and cellular area in *GAL1-MAD2(3x)* and *tub2-401* cells** - (a) Raw image of GFP signal in a *GAL1-MAD2(3x)* cell. (b) Processed image with k-means algorithm. Basing on Clb2-GFP fluorescence, the algorithm allowed to identify: extracellular region (black), cytosolic region (grey), nuclear region (white). Mean levels of Clb2 were evaluated in the white region. (c) Evaluation of Clb2 mean nuclear fluorescence in adapting and adapted cells during a shift to galactose. (d) Monitoring cellular size of adapting and adapted cells. For each mitotic round of adapting and adapted cells, we monitored cellular growth of mother and daughter cells. Area in pixel was converted to μm^2 according to the pixel size of the objective.

3.5.3 Image Analysis of *GAL1-CDC28-HA* cells in nocodazole

Image analysis of nocodazole-arrested cells was performed with the same procedure described in (Bonaiuti *et al.* 2017) and developed in the lab by Paolo Bonaiuti. For each cell, mean cellular value of Clb2-mCherry signal was evaluated in time, and each resulting trajectory was smoothed (Figure 3.3a). Meanwhile, Mad2-GFP Localization Index (LI) signal (Primorac *et al.* 2013) was evaluated in time: for a segmented area A, LI is defined as

$$LI(A) = \frac{\langle A_{1\%} \rangle - \langle A \rangle}{std\,(A)}, \tag{3.1}$$

where $\langle A_{1\%} \rangle$ is the mean of the 1% brightest pixels inside A, $\langle A \rangle$ is the mean fluorescence in A, $std\,(A)$ standard deviation of fluorescence in A. The procedure allowed to automatically identify the time by which Clb2 started to increase and decrease (Figure 3.3a). Since adapted cells degrade Clb2 in the presence of localized Mad2 to the unattached kinetochores (Bonaiuti *et al.* 2017), we set a threshold for LI equal to 5 in order to better discriminate good localizations for bad ones (Figure 3.3b-c). As a negative control for localization, Mad2 LI was under the fixed threshold in cells at the beginning of the timelapse (i.e. during G1 arrest), where Mad2 does not localize by definition.

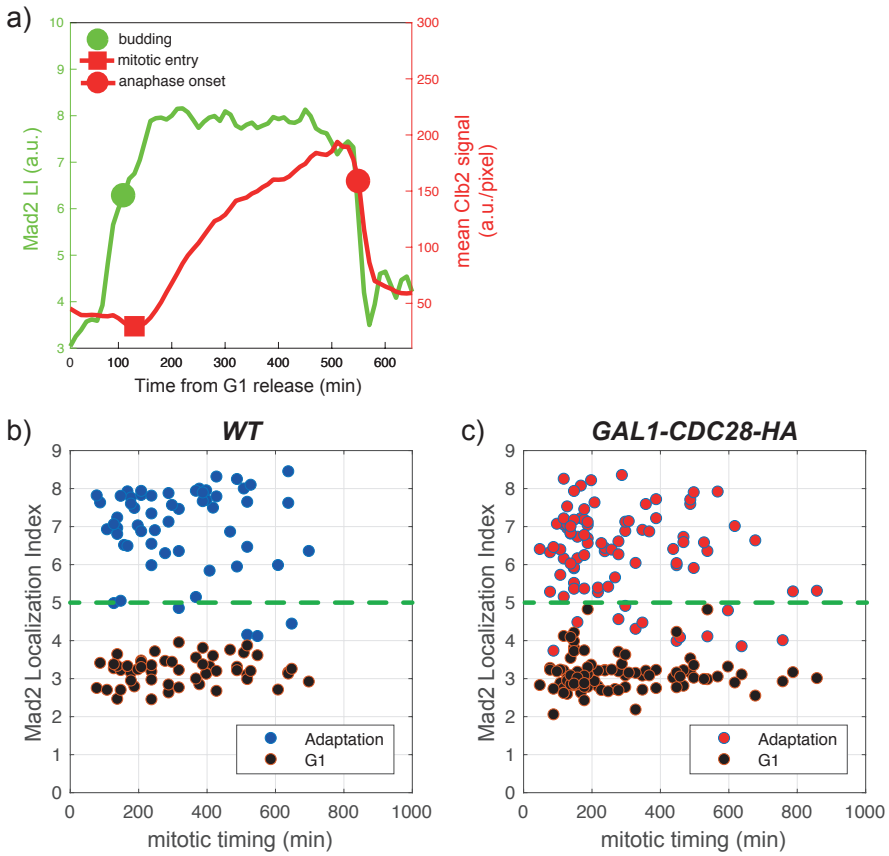

Figure 3.3: **Evaluating Clb2 levels and Mad2 Localization Index during a mitotic arrest** - (a) An example of raw trajectory coming from analysis of nocodazole-arrested cells. For each cells we monitored in time the behavior of mean levels of Clb2 (red) and of Mad2 Localization Index (LI) (green). The automatic procedure allowed to automatically detect mitotic entry and anaphase onset, according to the rising levels of Clb2 and their decay. (b-c) For each cell, we plot mitotic duration versus localization index of Mad2 during G1 arrest (black dot) and during adaptation (blue or red dot). A threshold equal to 5 for LI (green dashed line) allowed to better isolate cases in which cells adapted with an active Mad2 localization. All the MATLAB scripts for evaluation of Clb2 and Mad2 signals were designed by Paolo Bonaiuti in the lab (Bonaiuti *et al.* 2017).

3.5.4 Cell Size Control Analysis

This analysis was adapted from (Di Talia *et al.* 2007), in which a theoretical framework was applied for explaining cell size control during G1/S transition. We arranged this analysis in the metaphase-to-anaphase transition of adapting cells, as described in Section 4.1. Considering mother and daughter as an unique cell body during the measured mitosis, we wanted to fit raw data with an exponential law:

$$A(t) = A_0 \exp(\alpha t), \tag{3.2}$$

where $A(t)$ represents the cellular area at time t, A_0 cellular area at mitotic entry, α growth rate. By normalizing Equation 3.2 by A_0 and applying logarithm to both members of the equation, we obtain the following relation:

$$ln\left[\frac{A(t)}{A_0}\right] = \alpha t, \tag{3.3}$$

which represent a line with slope α. Therefore, trajectories of cellular area during mitosis of adapting cells were normalized to the value at the mitotic entry, and their logarithmic values were fitted with the linear law 3.3 (Figure 3.4). For each fitting, we estimated a goodness of fit (adjusted R^2) and the growth rate α. Together with raw data, these parameters were evaluated for testing cell size control hypothesis, as described in Section 4.1.

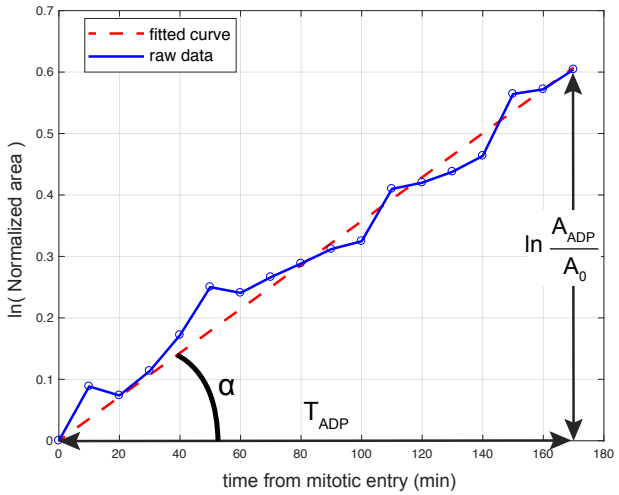

Figure 3.4: **Fitting cellular size raw data with an exponential growth** - An example of fit with raw data coming from one adapting cell. The result is a line with slope α (i.e. growth rate).

3.5.5 Statistical Methods

Sample size was not evaluated a-priori for each experiment. Statistical analysis were performed with GraphPad Prism ®, with significance level $\alpha = 0.05$. Normality of each sampled distribution was

tested, using D'Agostino-Pearson omnibus and Shapiro-Wilk tests, and not rejecting the normality hypothesis when both tests returned a p-value p greater than the significance level.

For comparison of two normal distributions, a two-tailed unpaired t-test with Welch's correction was performed; in the case of not-normal distributions, a two-tailed Mann-Whitney test was used. Evaluation of linear correlation coefficient was performed with Pearson coefficient - for normal distributions - or Spearmann coefficient - for not-normal distributions.

Comparison of three or more normal distributions was performed with an ordinary one-way ANOVA, testing multiple comparisons with Tukey test. In the case of not-normal distributions, a Kruskal-Wallis test with Dunn's multiple comparisons test were used. For multiple comparisons, the following symbols were reported: ns ($p > 0.05$), * ($p < 0.05$), ** ($p < 0.01$), *** ($p < 0.001$), **** ($p < 0.0001$).

3.6 Other Techniques

3.6.1 FACS Analysis

In this study, FACS analysis was used for an evaluation of DNA content in a population of cells. For each timepoint, 1 ml of cells was collected and centrifugated (13200 rpm, 1-3 min). Then, supernatant was discarded and pellet was resuspended with 1 ml of ethanol 70%, in order to fix cells. Fixed cells were then incubated at 4°C.

Then, ethanol was discarded from each sample (13200 rpm, 3 min) and resulting pellet was resuspended with 1 ml of Tris HCl 50 mM pH 7.6. After another centrifugation (13200 rpm, 3 min), cells were incubated at 37°C with 500 μl of Tris HCl 50 mM pH 7.6 supplemented with RNAse 1 mg/ml, for 4-5 hours or during an entire overnight. Subsequently, supernatant was discarded (13200 rpm, 3 min) and each sample was washed with PBS(1x) or FACS Buffer (Tris HCl 1 M pH 7.6, NaCl 5 M, $MgCl_2$ 1 M). After another centrifugation (13200 rpm, 3 min), pellet was resuspended in 300 μl of Propidium Iodide (PI) in order to stain DNA. Cells were incubated at 4°C for at least 20 min, then 100 μl were diluted in 1 ml of Tris HCl 50 mM pH 7.6.

After a proper sonication, diluted cells were processed at flow cytometry (FACScalibur, DB), scoring 10000 event for each sample. Raw data were then analyzed with FlowJo® software.

3.6.2 Immunofluorescence (IF) Analysis

This technique was used for visualization of spindle in population experiments. Via looking at spindle morphology, we were able to distinguish cell cycle phase of each cells: interphase (only one dot visible), metaphase (short spindle) and anaphase (elongated spindle). Moreover, IF of nocodazole-

arrested cells allowed to evaluate the efficiency of the drug in depolymerizing mitotic spindle.

For each timepoint, 1 ml of cells was collected and centrifugated (13200 rpm, 1-3 min). Then, supernatant was discarded and pellet was resuspended with 1 ml of KPi buffer (0.1 M Kphos pH 6.4 - obtained by mixing K_2HPO_4 with KH_2PO_4 - 0.5 mM $MgCl_2$) supplemented with formaldehyde 3.7%, in order to fix cells. Samples were then incubated at 4°C.

Then, 3 washes were performed with 1 ml of KPi buffer for each sample (4000 rpm, 2 min), discarding supernatant each time. Then, one final wash with 1 ml of sorbitol solution (Sorbitol 1.2 M, 0.1 M Kphos pH 7.4, 0.5 mM $MgCl_2$) was performed. Supernatant was discarded (4000 rpm, 2 min) and each pellet was resuspended in 200 μl of mix solution (sorbitol solution supplemented with zymolase 10 mg/ml and 2-mercaptoethanol), leaving in a thermomixer at 37°C, 400 rpm, 15/20 min, in order to allow cell wall digestion.

When spheroplasts were visible, each sample was centrifuged (3800 rpm, 1.5 min), supernatant was discarded and each pellet was resuspended with 1 ml of sorbitol solution. After an additional wash (3800 rpm, 1.5 min), pellet was stored at -20°C. 5 μl of treated spheroplasts were loaded to glass slides (Thermo-Scientific) coated with polylysine (Sigma-Aldrich). After 15/20 min, slides were immersed in cold methanol (-20°C) for 3 min - in order to dehydrate samples - and then in cold acetone (-20°C) for 10 s, in order to fix samples. Then, each sample was incubated with anti-Tub1 primary antibody (MCA78G, Bio-Rad), allowing incubation for 2h at room temperature. Subsequently, 3 washes were performed with BSA-PBS solution (containing PBS plus bovine serum albumin BSA), and each sample was incubated with secondary antibody (FITC-conjugated anti-rat antibody from Jackson ImmunoResearch Laboratories) for 1h, at room temperature, in a dark place. Finally, after 4 washes with BSA-PBS solution, DAPI was added in each sample - in order to also detect DNA - and slides were closed.

3.6.3 Serial dilution and droptest assay

Cells were grown overnight in 5 ml of liquid medium, allowing them to rich a high concentration during the overnight. Then, the strain with the lowest concentration was identified and all the other strains were diluted to that concentration in 1 ml. For each strain, 100 μl of diluted cells were added to 1 ml of sterile water, and from this final volume 200 μl were loaded on the first column of a 96 well. 180 μl of sterile water were added from second to sixth column. Then, 20 μl of cells from the first column were collected, and serial dilution were performed from the second to the sixth column. Finally, cells were spotted on agar plates with a mold or multichannel pipette.

3.6.4 Measuring concentration and cell size

Monitoring of cellular concentration and/or size in *GAL1-MAD2(3x)* (see Section 4.1) and *tub2-401* cells (see Section 4.2) was performed using Scepter ™ Handheld Automated Cell Counter (© Millipore Corporation) with Scepter ™ Sensors 40 μm. Each log-phase cell culture was diluted 1:100 in 1 ml of PBS(1x), sonicated and then processed at the counter. Data log were handled with Scepter ™ Software Pro.

3.7 Biological replicates

For each experiment showed in Results, the number of technical replicates - where present - is reported in the caption of the associated figure. Here, we summarize the number of biological replicates:

- **1 replica**: Figures 4.3, 4.6, 4.9, 4.16, 4.19, 4.20, 4.21, 4.35, 4.36b-c, 4.38, 4.39, 4.40, 6.1, 6.2
- **2 replicates**: Figures 4.2, 4.4, 4.5, 4.7, 4.8, 4.10, 4.11, 4.12, 4.14, 4.15, 4.18 (more than 2), 4.22, 4.28, 4.36a, 4.41

4 Results

4.1 Proliferating Cells after Adaptation to the Mitotic Checkpoint induced by Mad2 overexpression

An ectopic activation of the Mitotic Checkpoint can be achieved by overexpressing Mad2, placing 3 copies of the gene under the galactose-inducible promoter *GAL1pr* (*GAL1-MAD2(3x)*, (Rossio *et al.* 2010b)). When grown in galactose, cells exhibit an arrest in mitosis (Rossio *et al.* 2010b; Mariani *et al.* 2012) that lasts several hours, after which they adapt to the mitotic block (Rossio *et al.* 2010b; Vernieri *et al.* 2013), resuming APC/C activation, and thus enter anaphase and eventually exit from mitosis. In this section, we describe features of cells that resume proliferation after adaptation.

4.1.1 Adaptation to the SAC induced by Mad2 overexpression establishes a Refractory State

A live-cell imaging approach allows to appreciate the large cell-to-cell variability and stochasticity of adaptation (Vernieri *et al.* 2013; Bonaiuti *et al.* 2017). To minimize such variability, we synchronized *WT* and *GAL1-MAD2(3x)* cells in G1, and then we released them in microfluidic chambers, under a constant flow of galactose-containing medium (Figure 4.1). Under these conditions, both strains experienced the same metabolic alterations due to the shift of carbon source, but only *GAL1-MAD2(3x)* cells arrested in mitosis (Rossio *et al.* 2010b; Mariani *et al.* 2012; Vernieri *et al.* 2013). We thus refer to *WT* cells as "cycling" (Figure 4.1a), while *GAL1-MAD2(3x)* cells in the first arrest caused by Mad2 overexpression as "adapting" cells (Figure 4.1b). After adaptation, we noticed that *GAL1-MAD2(3x)* cells resume proliferation: we called these cells "adapted" (Figure 4.1b).

We monitored the dynamics of mitotic spindles, using β-tubulin *TUB2* tagged with mCherry, and mitotic progression with the endogenous mitotic cyclin B (*CLB2*) tagged with GFP. Tagged Clb2 allowed us to estimate the duration of mitotic arrest for each cell: mitotic entry was identified by the

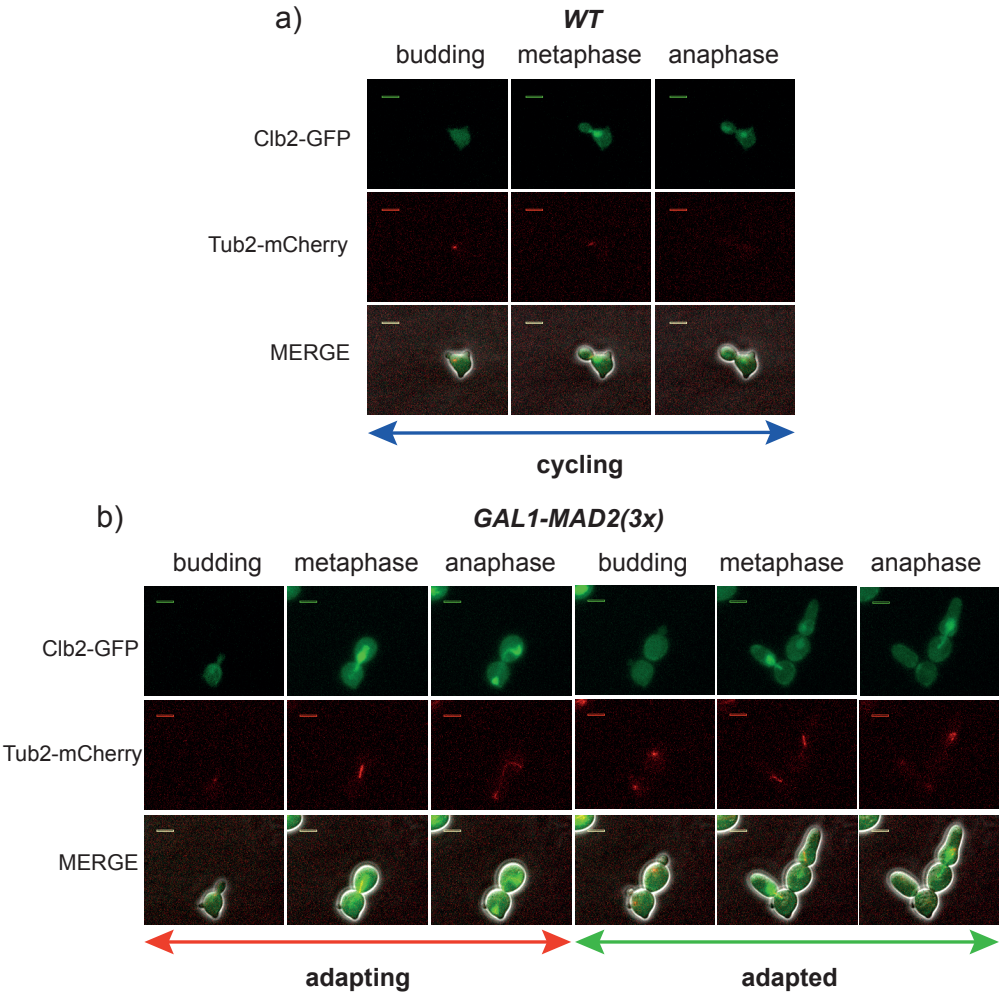

Figure 4.1: **Monitoring Proliferating Cells after Adaptation to the SAC induced by Mad2 overexpression** - *WT* cells (yAC2006 - *MATa, TUB2-mCherry CLB2-GFP*) and *GAL1-MAD2(3x)* cells (yAC2671 - *MATa, TUB2-mCherry CLB2-GFP GAL1-MAD2(3x)* were grown in synthetic medium containing raffinose, synchronized in G1 and then released in synthetic medium containing galactose). Clb2 and Tub2 fluorescence was monitored for each cell. (a) An example of *WT* cell - "cycling" condition. (b) An example of *GAL1-MAD2(3x)* cell. The first cell cycle upon Mad2 overexpression is reported as "adapting", while the subsequents are named "adapted"

time Clb2 levels start to increase, and anaphase onset by the time of Clb2 degradation (Figure 4.2a). Confirming our previous work (Vernieri *et al.* 2013), we observed a significant difference in mitotic duration between cycling and adapting cells (Figure 4.2b). As mentioned above, we observed that cells are able to proliferate again after adaptation, with a mitotic length significantly shorter compared to adapting cells (Figure 4.2b). This result suggests that cells become partially refractory to the Mitotic Checkpoint, with mitotic timing still significantly longer than that of cells in unperturbed conditions (Figure 4.2b). In conclusion, after adaptation to Mad2 overexpression, we were able to observe a population of proliferating cells which seemed to become refractory to the SAC. We define these cells adapted refractory cells.

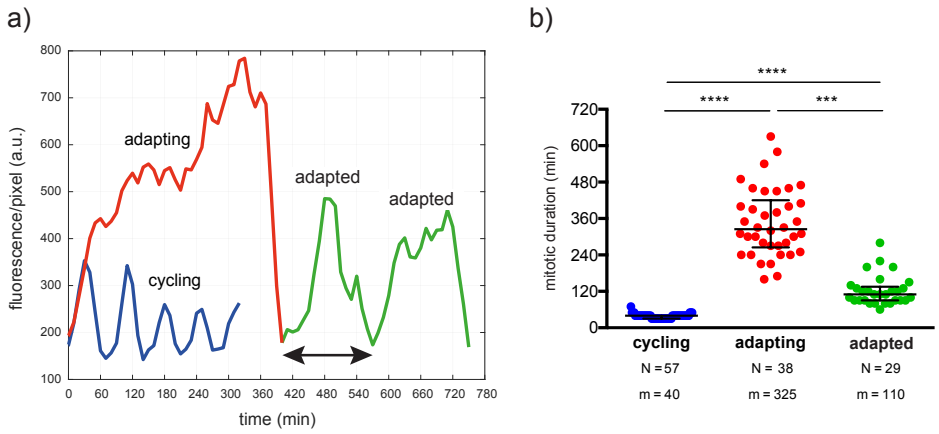

Figure 4.2: **Proliferating Cells after Adaptation exhibit a decreased mitotic duration** - Single cells analysis of *WT* cells (yAC2006 - *MATa TUB2-mCherry CLB2-GFP*) and *GAL1-MAD2(3x)* cells (yAC2671 - *MATa TUB2-mCherry CLB2-GFP GAL1-MAD2(3x)* described in Figure 4.1. (a) Mean nuclear Clb2 signal was estimated for each cell, as reported in (Vernieri *et al.* 2013) - see an example in the figure for adapted cells (black arrow). Clb2 trajectories were plotted in time, synchronizing them when Clb2 signal started to increase. (b) Comparison of mitotic duration. For each condition reported in a), timespan between Clb2 increase and decrease was estimated and defined as mitotic duration. Statistical analysis were performed with GraphPad Prism ®, using Kruskal-Wallis test with Dunn's Multiple Comparison Test (significance level 0.05). N: number of observation. m: median of population. For each population, median and interquartile range were reported. The same significant differences were also observed in a previous biological replica, in which cells were not pre-synchronized in G1 before inducing Mad2 overexpression.

4.1.2 Refractoriness is not due to a decrease in *GAL1* promoter activity in time

In the experiment shown in Figures 4.1 and 4.2, we induced the SAC by overexpressing Mad2. We thus asked whether the refractory state was simply due to a physiological decrease in Mad2 overexpression during the long time-course of the experiment. We thus followed in *GAL1-MAD2(3x)* cells the levels of Mad2 upon 24h of galactose exposure (Figure 4.3). The analysis suggests that Mad2 overexpression seems to slightly decrease in time.

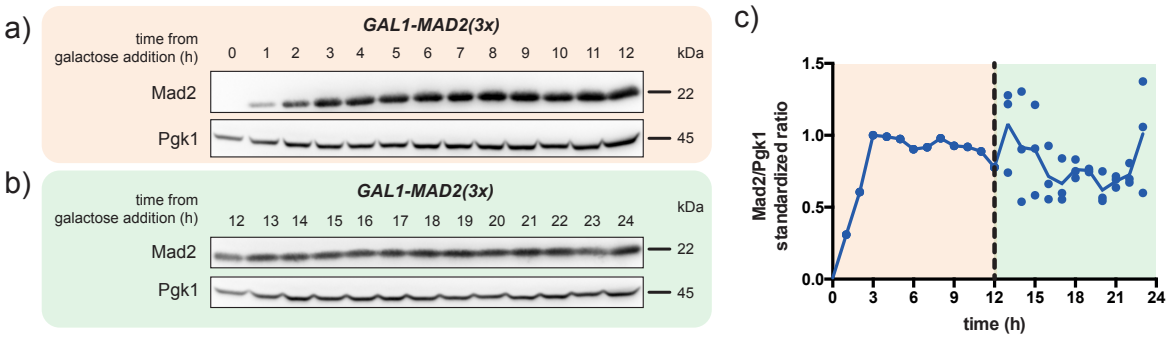

Figure 4.3: **Mad2 levels slightly decrease during 24h of induction** - A population of asynchronous *MATa, GAL1-MAD2(3x)* cells (yAC2465) was shifted from YEPR to YEPRG, in order to induce Mad2 overexpression. Cells were monitored for 12h. (a) Western Blot analysis of Mad2 levels at early stages of overexpression. (b) Western Blot analysis of Mad2 levels at late stages of overexpression. (c) Quantification of Mad2 levels. For each timepoint, Mad2 levels were normalized to the housekeeping protein levels, i.e. Pgk1. Ratios from a) were normalized to their maximum levels, while ratios from b) were normalized to the value of the ratio at 12h in a). Each dot correspond to a single data (1 technical replica for a), 3 technical replicates for b))

Mad2 levels may decrease in time owing to the prolonged activation of the *GAL1* promoter. To test this possibility, we aimed at comparing the SAC arrest in two *GAL1-MAD2(3X)* strains, both overexpressing Mad2 from the *GAL1* promoter for the same amount of time. Both strains were grown for 12h in galactose, arrested in α-factor and released again in galactose: the *GAL1* promoter is supposed to be under identical conditions in the two strains. However, during the 12 hours of growth in galactose one strain expressed an allele of *CDC20* (*cdc20-127*) which produces a mutant Cdc20 able to bypass the SAC (Hwang *et al.* 1998) (Figure 4.4a, adapting). The other strain, instead, expressed wild type Cdc20 (Figure 4.4a, adapted refractory). Thus, the first strain neither experienced a SAC arrest nor adaptation during the 12 hours of growth in galactose, regardless of the high levels of Mad2. The second strain instead adapted and entered the refractory state. In this setting, a difference in cell cycle timing between adapted refractory cells and cells adapting to the SAC for the first time could not be explained with difference in *GAL1* activation time. It would rather be due to the fact that one class of cells had previously adapted to the SAC and the other did not.

We expressed the *cdc20-127* gene under the doxycycline-repressible $tetO_2$ promoter. The ability of this mutant form of Cdc20 to bypass the spindle checkpoint was tested and confirmed in our *GAL1-MAD2(3x)* system (See Appendix). *GAL1-MAD2(3x)* $tetO_2$*-CDC20-127(1x)* cells were grown overnight with galactose and without doxycycline (i.e. with cdc20-127). After 12 h, doxycycline was added to silence the $tetO_2$ promoter, cells were arrested in G1 and monitored in the continuous presence of galactose (Figure 4.4b). After repression of cdc20-127 synthesis, cells that never experienced adaptation (Figure 4.4b, adapting) exhibited an arrest in mitosis longer than cells that had experienced adaptation (Figure 4.4b, adapted refractory). This result suggests that the refractory state is not due to alterations in *GAL1pr* activity in time, but cells acquire "experience" from a prolonged mitotic arrest which allows them to have a faster mitotic phase. We argue that they become specialized "adapted" cells. At this stage, we cannot exclude the possibility that for reasons other than time of activation, *GAL1pr* activity is reduced in continuous presence of SAC. We will address this criticism in the Discussion.

4.1.3 Refractoriness is lost upon microtubules depolymerization

We next asked if refractoriness induced by Mad2 overexpression would be maintained changing SAC-inducing stimuli. To answer this question, we used nocodazole to activate the SAC in cells adapted to Mad2 overexpression. We synchronized adapted refractory cells in G1 and released them in different concentrations of nocodazole. Regardless of the concentration of nocodazole, adapted refractory cells exhibited a 5h-long arrest in mitosis (Figure 4.5) without detectable microtubules polymerization and rebudding cells. *WT* cells showed the same behavior. These results suggest that refractoriness is

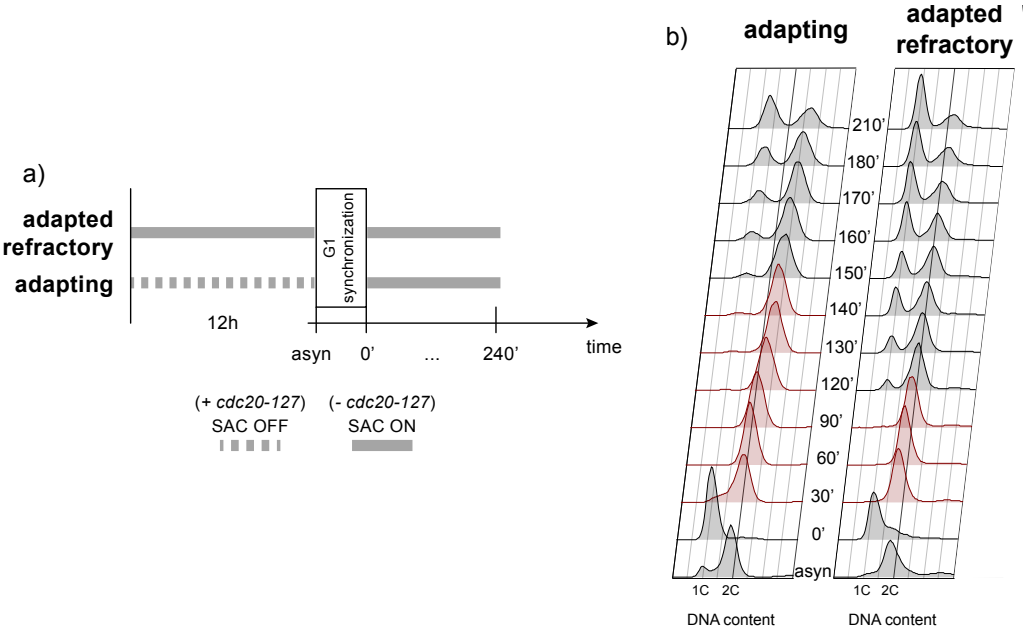

Figure 4.4: **Overexpression of Mad2 is still able to induce the SAC after 12 hours from its induction** - (a) Scheme of the experiment. *MATa, tetO$_2$-CDC20-127(1x), GAL1-MAD2(3x)* cells (yAC2807) were grown for 12h in YEPRG medium in order to induce overexpression of Mad2. During this first phase, SAC was only active in adapted refractory cells, since they were not expressing cdc20-127. Then, cells were synchronized in G1 by α-factor and released in YEPRG medium supplemented with doxycycline hyclate 10 $\mu g/ml$ (Barnhart *et al.* 2011) in both conditions, in order to repress cdc20-127 synthesis. After 1,5h from release, α-factor was readded in order to resynchronize cells in G1. (b) FACS analysis of the experiment described in a). Red profiles correspond to timepoints in which more than 80% of scored cells exhibit a 2C DNA content.

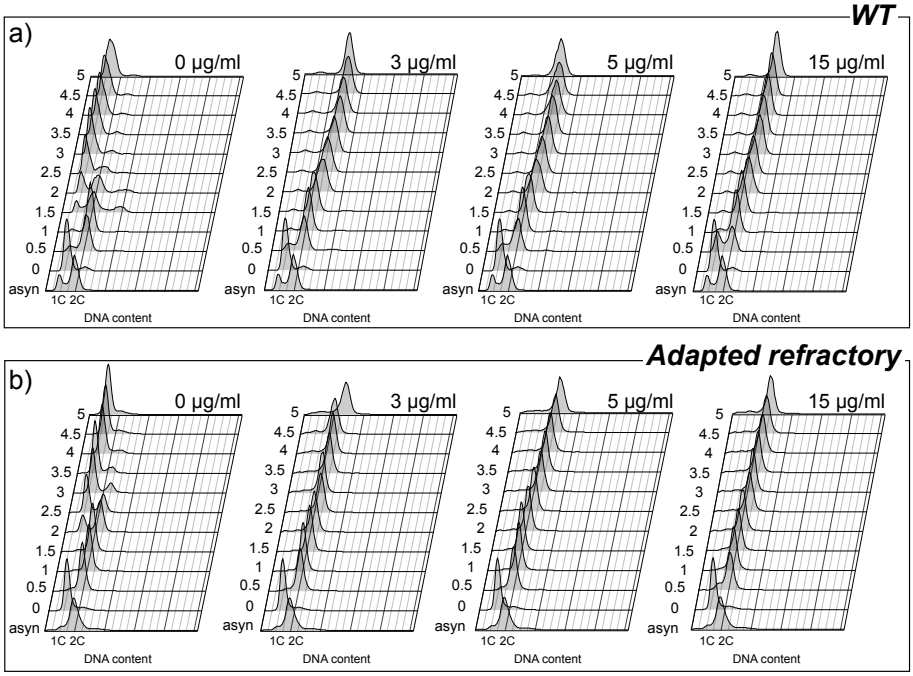

Figure 4.5: **Adapted refractory cells become competent to the SAC induced by nocodazole** - *MATa, WT* (yAC3202) and *MATa, GAL1-MAD2(3x)* (yAC2465) cells were grown overnight for 15h in YEPRG, in order to produce a population of adapted refractory cells from yAC2465. Then, cells were synchronized in G1 with α-factor and released in YEPRG supplemented with 0, 3, 5 or 15 $\mu g/ml$ of nocodazole, monitoring them for 5h. For each condition, α-factor was readded after 1.5h and 3.5h from release, while nocodazole was readded after 3h from release. (a) FACS profiles for WT cells. (b) FACS profiles for adapted refractory cells.

unable to overcome the effects of nocodazole, maybe due to the fact that the latter induces a stronger SAC response (e.g. enhanced MCC assembly).

4.1.4 Memory in Adaptation to the Checkpoint has a timespan

So far, we described a form of refractoriness which takes place in the continuous presence of SAC-inducing stimuli. We next asked whether the refractory state is maintained when the stimulus is transiently removed. If this were the case, we would conclude that cells have a memory of adaptation (Caudron & Barral 2013), as described in the Introduction (Section 1.5). In the next subsections, we describe two experimental approaches to remove transiently the stimulus inducing the SAC.

4.1.4.1 Loss of memory upon removal of Mad2 overexpression

Removal and reintroduction of Mad2 overexpression in Adapted Refractory Cells We induced the SAC by overexpressing Mad2. To relieve cells from the SAC transiently, we restored the endogenous levels of Mad2. We grew Adapted refractory cells and we released them in glucose-containing medium, in order to completely repress *GAL1pr* activity and Mad2 overexpression. Via Western Blot analysis, we observed that cells took 12h for restoring Mad2 endogenous levels (Figure 4.6a-b), assuming a cellular size that was similar to that of cells that never experience Mad2 overexpression (data not shown). This result sets the minimum length of stimulus removal with this approach.

After cells had regained endogenous levels of Mad2, we needed to re-introduce proper Mad2 overexpression. It is known that activation of *GAL1pr* is different in budding yeast cells grown in glucose or in raffinose (Stockwell *et al.* 2015) because glucose strongly represses *GAL* transcription as opposed to raffinose. It is reported that upon a shift in galactose, cells grown in raffinose activate the *GAL1pr* within 20 min (Kundu *et al.* 2007); on the other hand, cells that grow in glucose show a slower kinetics of induction (Kundu *et al.* 2007). Indeed, when we evaluated Mad2 overexpression in *GAL1-MAD2(3x)* cells grown in raffinose (Figure 4.6c, Induction) or in glucose (Figure 4.6c, Induction w/o derepression), we observed that Mad2 overexpression started after 4 hours in cells grown in glucose, exhibiting a lag-phase of 3h respect to cells grown in raffinose (Figure 4.6d, Induction vs Induction w/o derepression). In order to eliminate this lag-phase, we introduced in cells grown in glucose an intermediate phase of 2h in raffinose, before releasing them in galactose (Figure 4.6c, Induction with derepression). With this protocol, Mad2 overexpression behaved similarly in cells pre-grown in glucose and raffinose.

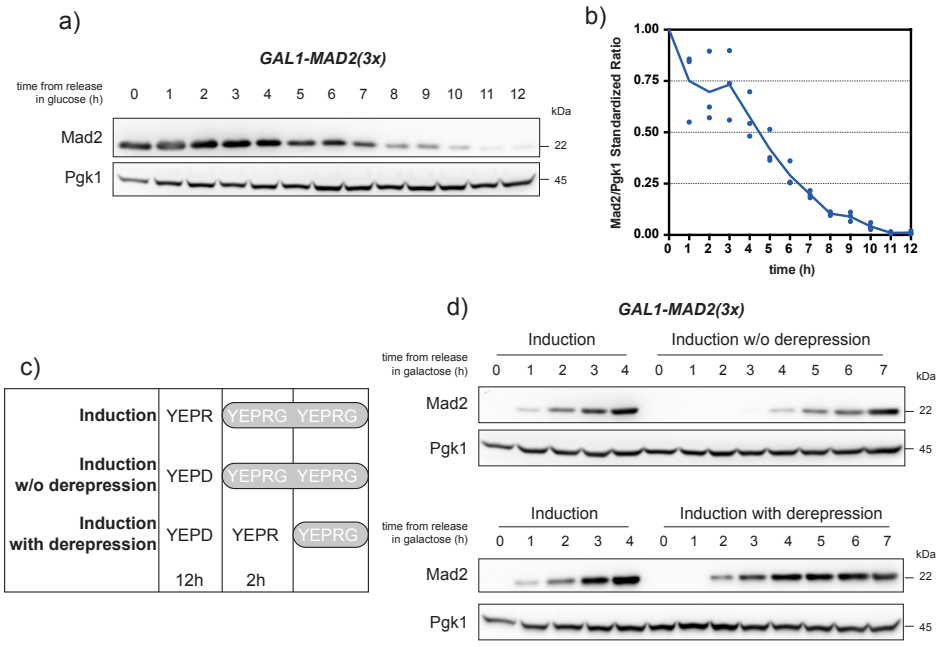

Figure 4.6: **Removal and reinduction of Mad2 overexpression in adapted refractory cells** - (a) Removal of Mad2 overexpression in *GAL1-MAD2(3x)* cells. *MATa GAL1-MAD2(3x)* (yAC2465) cells were grown overnight in galactose, in order to make them adapted refractory. Then, they were shifted in YEPD in order to repress *GAL1pr* activity. Cells were monitored for 12h, and cells were sampled each hour for Western Blot analysis. (b) Quantification of Western Blot in a), normalizing Mad2 signal by the housekeeping Pgk1 signal. Each normalized ratio was divided by the ratio at time 0, and plotted in time. Each dot represent a technical replicate, while the continuous line connects mean value for each timepoint. (c) Experimental setup for optimizing Mad2 re-induction. *MATa GAL1-MAD2(3x)* (yAC2465) cells were grown overnight in YEPR or YEPD. The next day, cells that grew in YEPR where released in YEPRG (Induction). On the other hand, cells grown in YEPD were directly release in YEPRG (Induction w/o derepression) or in YEPR for 2h and then in YEPRG (Induction with derepression). Gray boxes correspond to the timespan in which cells were monitored. Cells were sampled for Western Blot analysis. (d) Western Blot of the experiment described in c). Upper part: comparison of Mad2 levels in Induction and Induction w/o derepression. Lower part: comparison of Mad2 levels in Induction and Induction with derepression.

Memory is erased upon 12h We then produced adapted refractory cells and shifted them in glucose-containing medium for removing the SAC-inducing stimulus for 12h. Then, *GAL1pr* was de-repressed in raffinose for 3 hours and consequently re-induced with a new round of galactose exposure (Figure 4.7a, Withdraw condition). We compared these cells to cells where the *GAL1pr* was induced for the first time (Figure 4.7a, Adapting condition). In the second induction on agar plates, Withdraw cells exhibited a growth similar to cells under their first induction (Figure 4.7b, Adapting vs Withdraw). When re-induction occurred in liquid medium, the proportion of dumbbell cells was very similar to cells experiencing their first induction (Figure 4.7c), indicating a similar arrest in mitosis. These results suggest that adapted refractory cells after the removal of the SAC-inducing stimulus for 12 hours become again fully competent to the SAC.

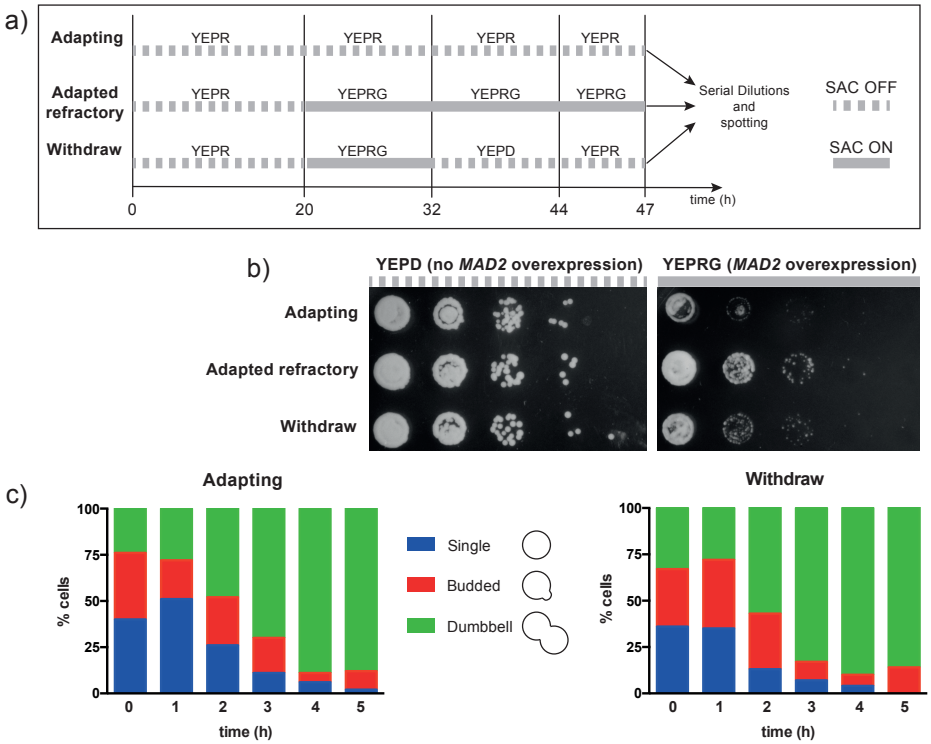

Figure 4.7: **Adapted refractory cells become competent again to the SAC upon 12h of overexpressed Mad2 removal** - (a) Experimental Setup. *MATa GAL1-MAD2(3x)* (yAC2465) cells were grown in YEPR liquid medium. Subsequently, they were grown in three different conditions until 47 hours from their inoculum. Then, they were diluted to ∼ 9e+7 cells/ml and serial dilutions and spotting were performed on YEPD and YEPRG agar plates. (b) Serial dilution and spot assay for yAC2465 cells described in a). (c) Analysis of cellular morphology in liquid medium. Adapting and Withdraw cells were released in YEPRG liquid medium, instead of plating them. They were monitored for 5h, and cellular morphology was scored for 100 cells every hour.

4.1.4.2 Memory experiment using *cdc20-127* expression

The type of experiment just described is based on several changes in carbon-source, which could introduce alteration in metabolic pathways (Paulo *et al.* 2015). Moreover, Mad2 being a very stable protein (Figure 4.6a-b), we could not test a transient removal of the SAC stimulus shorter than 12 hours. Therefore, as a second approach we withdrew the SAC stimulus using the transient cdc20-127 expression. Since Cdc20 is degraded with a half-life of ∼ 7 minutes (Bonaiuti *et al.* 2017; Pan & Chen 2004), it is much easier and faster to add and remove the SAC stimulus by modulating cdc20-127 levels than changing levels of Mad2.

Expression of *cdc20-127* in adapted refractory cells is able to uncouple proliferation and SAC

First, we tested how efficiently *cdc20-127* expression silences the SAC in adapted refractory cells. To this purpose, *tetO$_2$-CDC20-127(1x) GAL1-MAD2(3x)* cells were grown in galactose-containing medium with endogenous Cdc20 for 12h, in order to allow them to acquire refractoriness to the SAC. Then, expression of *cdc20-127* was established for 3h or 12h. (Figure 4.8a, Withdraw). Finally, we synchronized cells in G1 and released them while expressing cdc20-127 (Figure 4.8, Withdraw). Cel-

lular size was monitored for the entire timespan of withdrawal (Figure 4.9). As controls, we used cells that were grown all the time with an active SAC (Adapted refractory) or never (Adapting). Notice, for Adapting cells we use the same terminology of Figure 4.4 although these cells are not really adapting after the arrest in α-factor. These are actually cycling cells.

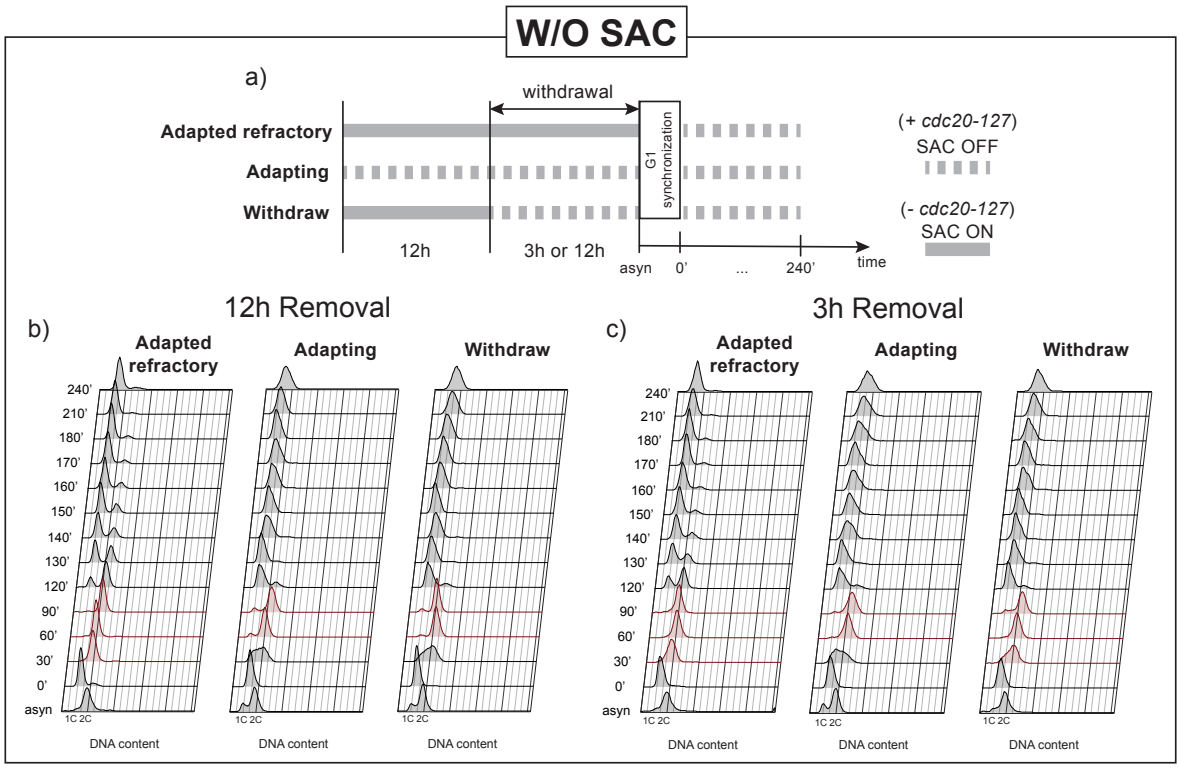

Figure 4.8: **Uncoupling Mad2 overexpression from SAC activity in adapted refractory cells** - (a) Experimental Setup. *MATa, tetO$_2$-CDC20-127(1x), GAL1-MAD2(3x)* (yAC2807) cells were inoculated in YEPR liquid medium. Then, they were shifted in YEPRG for 12h - in order to induce Mad2 overexpression - and immediately splitted in 3 different conditions, modulating the SAC activity via activation or inactivation of cdc20-127 synthesis. Then, cells were synchronized in G1 with α-factor and released in YEPRG, monitoring them for 4h in the presence of cdc20-127. α-factor was re-added after 1h and 3h from release, in order to re-synchronize cells in the subsequent G1 phase. Samples were collected for FACS analysis, both for (b) 12h of stimulus removal and (c) 3h removal. Red profiles correspond to timepoints in which more than 80% of scored cells exhibit a 2C DNA content.

Both with 3h and 12h removal, Withdraw and Adapting cells assumed a very similar cell cycle progression, (Figure 4.8b-c, Adapting vs Withdraw), while assuming different size (Figure 4.9b). Upon a removal of 3h, Withdraw cells assumed an Adapted refractory-like cell size, while after 12h their size decreased to Adapting-like size. Removing the stimulus for 3 or 12h suffices to show the same cell cycle kinetics after the release from α-factor as cells that were never arrested. Without withdrawal, the expression of *cdc20-127* is not sufficient to reset perfectly the cell cycle. We estimate in $\sim$ 20 min the residual delay. We conclude that the SAC stimulus can be effectively removed with either a 3h or 12h expression of *cdc20-127*.

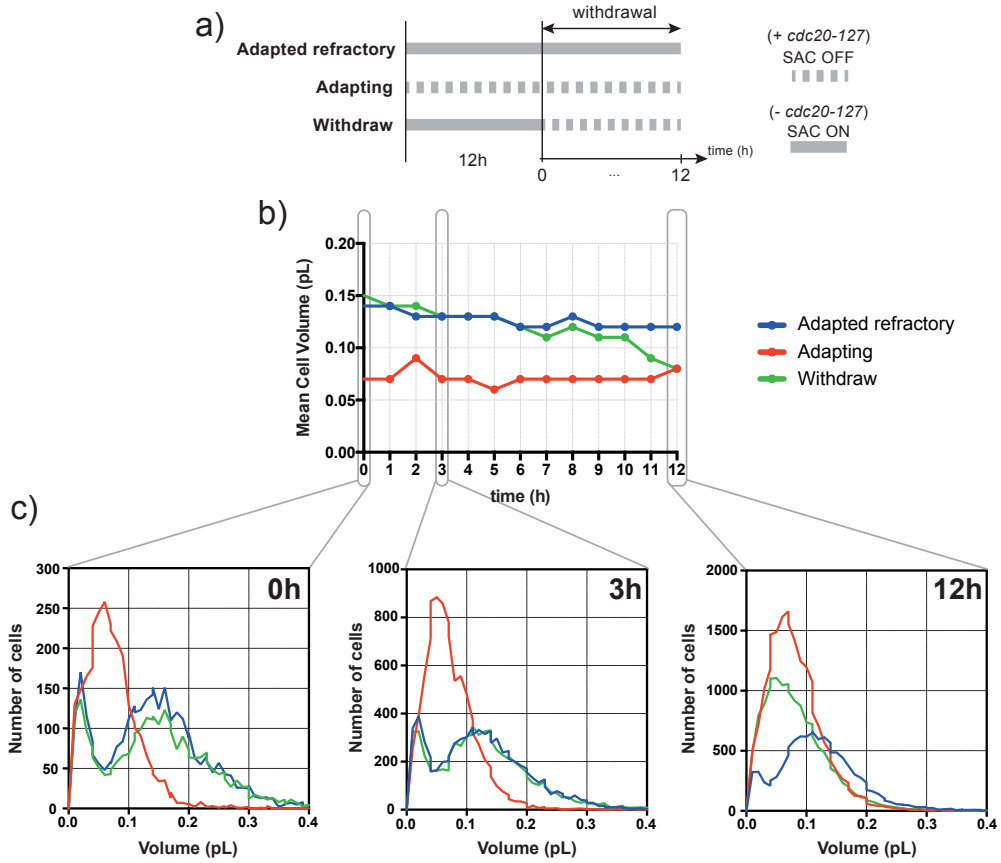

Figure 4.9: **Cell size behavior during SAC-withdrawal by *cdc20-127* expression** - (a) *MATa, tetO$_2$-CDC20-127(1x), GAL1-MAD2(3x)* (yAC2807) cells were grown as Adapting, Adapted refractory and Withdraw as indicated in the experimental setup of Figure 4.8a. Cells were monitored from the beginning of the withdrawal for 12h, recording informations about cellular size using Scepter ™ Handheld Automated Cell Counter (© Millipore Corporation). (b) Plot of mean cell volume for each condition. (c) Histograms of cell volume recorded by Scepter™: at the beginning of the withdrawal (0 h), after 3h and 12h from withdrawal.

Memory is retained for 3h, but not for 12h Once we validated the expression of cdc20-127 for SAC-stimulus removal, we tested the presence of memory in Withdraw cells, by releasing them from G1 in the presence of an active checkpoint - i.e., without cdc20-127 (Figure 4.10, WITH SAC, a). Withdraw cells experienced the SAC for the second time, while Adapting cells for the first time. Adapted refractory cells experienced a continuous activity of SAC for the entire experiment, as described in Section 4.1.2.

In agreement with previous data, Withdraw cells that experienced a 12h removal were again competent to the SAC, exhibiting a mitotic arrest that was similar to that of cells that experienced SAC activity for the first time (Figure 4.10b, Withdraw vs Adapting). Withdraw cells that experienced a 3h removal, instead, exhibited a mitotic duration similar to Adapted refractory cells (Figure 4.10c, Withdraw vs Adapted refractory), although the latter were slightly faster. In summary, our data suggest that refractoriness to the SAC is erased upon 12h of SAC-inducing stimulus removal, while it is still preserved upon a withdrawal of 3h.

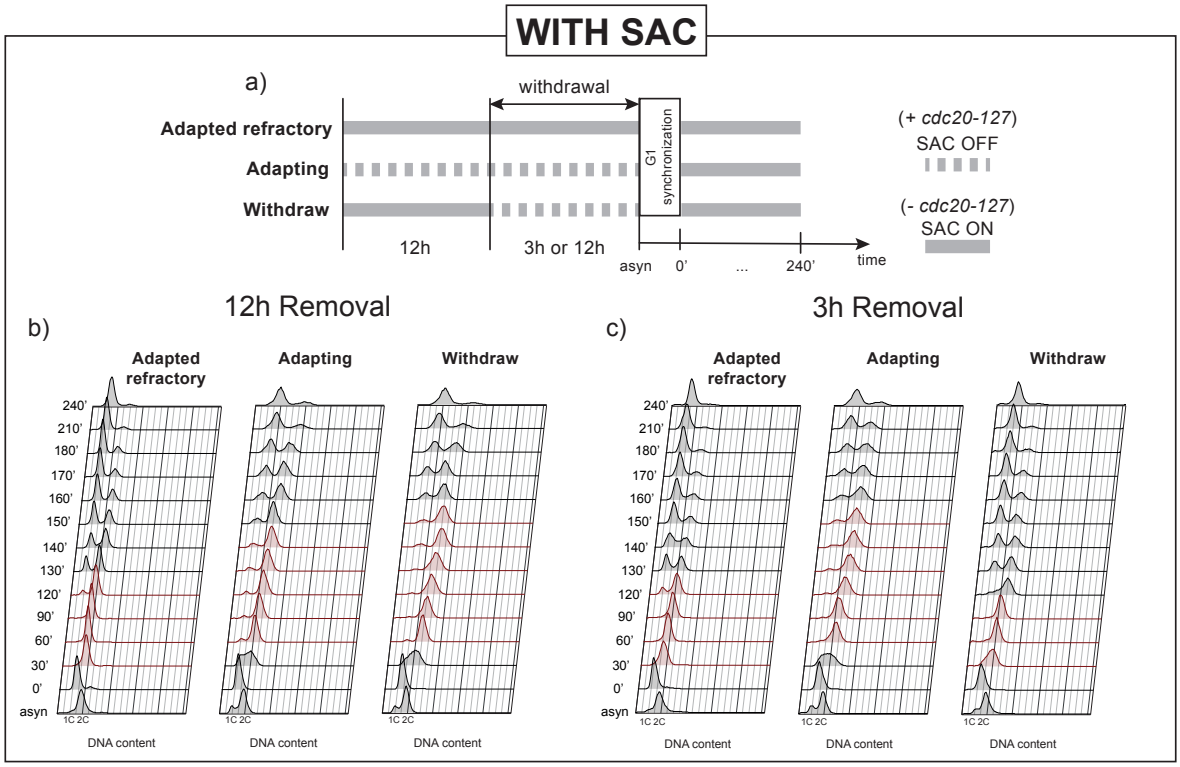

Figure 4.10: **Removal of SAC signal for 3h, but not for 12h, does not alter Refractoriness to the Checkpoint** - (a) Experimental Setup. *MATa, tetO$_2$-CDC20-127(1x), GAL1-MAD2(3x)* (yAC2807) cells were inoculated in YEPR liquid medium. Then, they were shifted in YEPRG for 12h - in order to induce Mad2 overexpression - and immediately splitted in 3 different conditions, modulating the SAC activity via activation or inactivation of cdc20-127 synthesis. Then, cells were synchronized in G1 with α-factor and released in YEPRG supplemented with doxycycline hyclate 10 $\mu g/ml$ (Barnhart *et al.* 2011). We monitored them for 4h. α-factor was re-added after 1h and 3h from release, in order to re-synchronize cells in the subsequent G1 phase. Samples were collected for FACS analysis, both for (b) 12h of stimulus removal and (c) 3h removal. Red profiles correspond to timepoints in which more than 80% of scored cells exhibit a 2C DNA content.

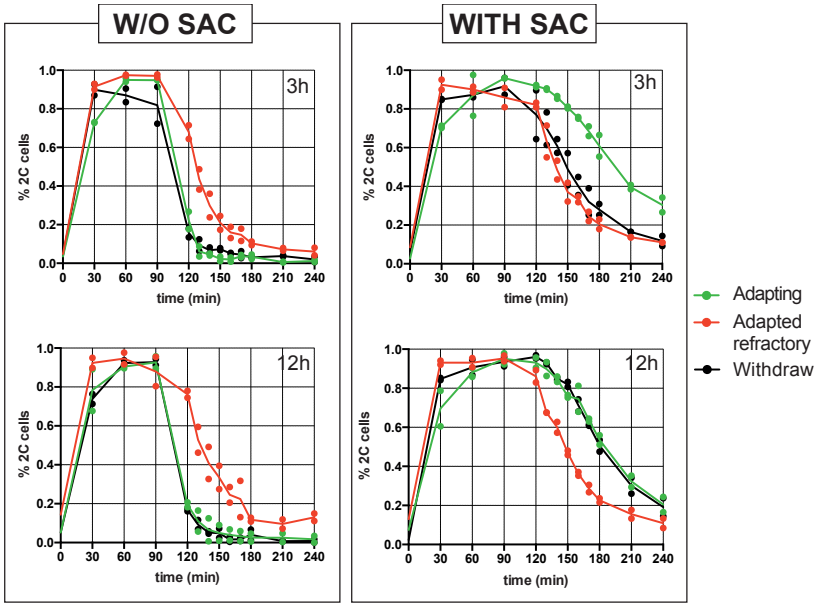

Figure 4.11: **Recap of the results from memory experiment with cdc20-127** - For each of the FACS profiles reported in Figure 4.8 and Figure 4.10, we evaluate the proportion of cells with a double DNA content (2C cells). On the left: W/O SAC, i.e. cells released without checkpoint activity. On the right: WITH SAC, i.e. cells released with checkpoint activity. Proportion of 2C cells was evaluated with FlowJo® software.

4.1.5 Understanding Cell Size Control during Refractoriness

Figure 4.9 shows that upon silencing the SAC for 3h, size of Withdraw cells was similar to size of Adapted refractory cells. Both assumed wild type-like dimensions after 12h of *cdc20-127* expression (Figure 4.9c). This result may suggest that faster mitotic timing of adapted refractory cells correlates with increased cellular dimensions. In molecular terms, larger size may weaken the SAC by diluting MCC component (Galli & Morgan 2016), as discussed in the Introduction (see Section 1.4). In cells adapted to Mad2 overexpression, the checkpoint strength is not due to the kinetochore-to-cytoplasm ratio, since the SAC signal does not originate from any unattached kinetochores (Mariani *et al.* 2012). However, MCC still constitutes a limiting factor and it could be diluted in the cell if synthesis of MCC components does not correlate with cell size. An implication of this hypothesis is that cells adapt when they reach a critical size. We thus asked whether this was the case.

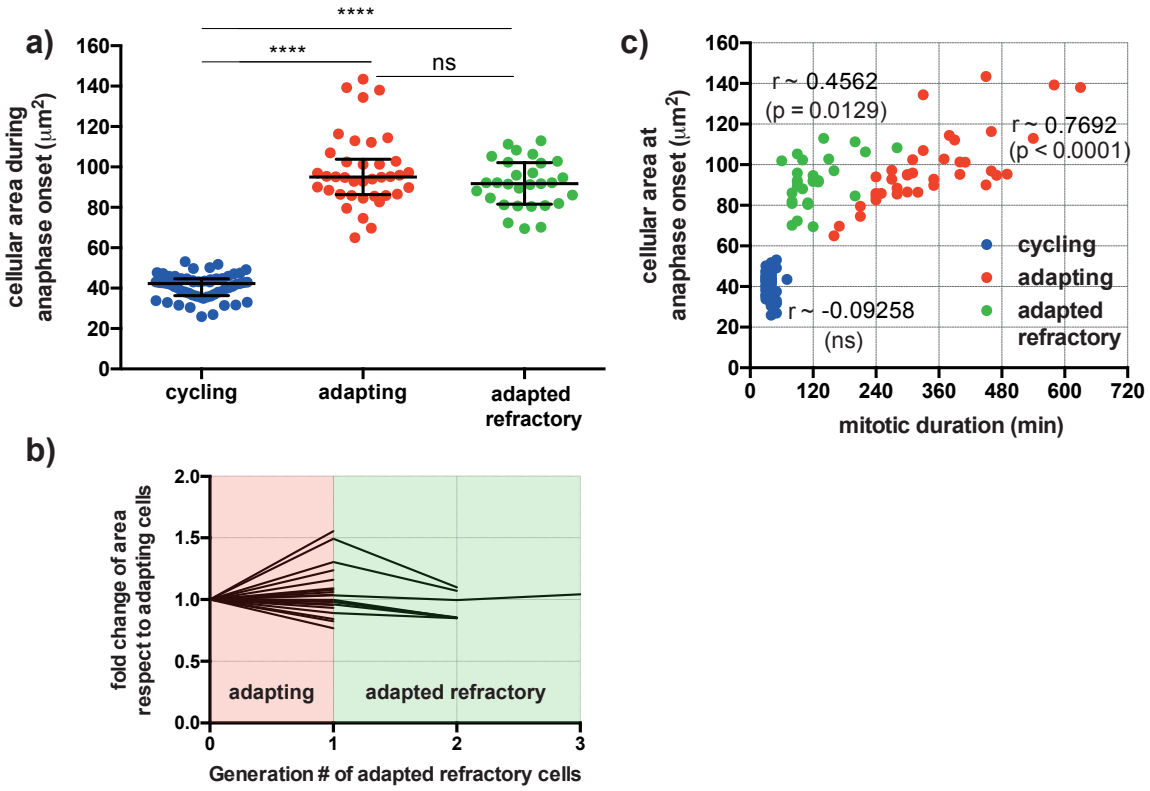

Figure 4.12: **Evaluation of time and size in cycling, adapting and adapted refractory cells** - (a) Distributions of size in cycling, adapting and adapted refractory cells at anaphase onset. Statistical analysis were performed with GraphPad Prism ®, using Kruskal-Wallis test with Dunn's Multiple Comparison Test (significance level 0.05) For each population, median and interquartile range were reported. (b) Monitoring cell size at anaphase onset in the progeny of each adapting cells. For each adapting cell that exhibit at least one adapted refractory cell cycle, cell size of adapted refractory cell was normalized to the size of the ancestral adapting cell and plotted as a function of generation number after adaptation to the SAC. Number of trajectories: 20. (c) Scatter plot between time and size in cycling, adapting and adapted refractory cells at anaphase onset (i.e. when Clb2 started to be degraded). According to the normality of distributions, Pearson or Spearman correlation coefficient were evaluated, testing whether they were significantly different from 0 (significance level 0.05).

To study cell size in adapted refractory cells, we further analyzed the single-cell experiment described in Subsection 4.1.1, measuring the area of segmented cells at mitotic entry (i.e. when Clb2 started to increase) and at anaphase onset (i.e. when Clb2 started to decrease). We considered cellular area as the sum of mother with daughter cell. We noticed that adapted refractory cells tended to acquire an area that was similar to adapting cells during anaphase onset (Figure 4.12a, b), although with reduced mitotic timing (Figure 4.2). These data are consistent with the idea that cells are able to adapt and become refractory to the Mitotic Checkpoint by reaching a critical size.

We thus directly evaluated correlation between time and size during adaptation (Figure 4.12c). We observed a positive and significant correlation in adapting cells (i.e., cells that adapt later reach a larger size), which puts in doubt the existence of a critical size of adaptation. In the following subsection, we are going to use a theoretical approach (Di Talia *et al.* 2007) for clarifying the existence or not of this critical size.

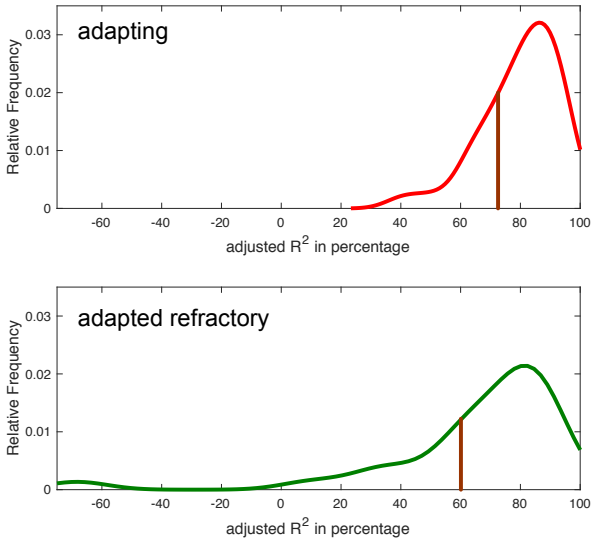

Figure 4.13: **Goodness of fit with an exponential function for adapting and adapted refractory cells** - Distribution of adjusted R^2 coming from experimental fitting of mitotic behavior of cell size adapting cells (in red) and adapted refractory cells (in green) with an exponential function. Distributions were plotted with MATLAB®, using kernel density estimator method. For each probability function, observations above the brown line correspond to the 75% of the right-tail distribution.

4.1.5.1 Refractoriness to the SAC does not require a critical size

We focused our analysis on adapting cells, measuring the behavior of their area during the timecourse. As already mentioned, for each mitosis we considered mother and its daughter cell as a unique cell body. Via fitting the raw data with an exponential law, we obtained an adjusted R^2 greater than 0.7 for 75 % of cells in our sample (Figure 4.13 - adapting). Under this degree of confidence, we assumed an exponential growth of cellular area in adapting cells:

$$A_{ADP} = A_0 \exp\left(\alpha T_{ADP}\right), \tag{4.1}$$

where A_{ADP} and T_{ADP} represent area and time during adaptation (i.e., between entry in mitosis and anaphase onset, measured by Clb2-GFP); A_0 cellular area at mitotic entry; α growth rate. Note that α is the only parameter which is estimated from the fitting procedure, while the others are coming from single-cell measurements. By applying logarithmic transformation to equation 4.1, we obtain the following equivalent formula:

$$\log\left(A_{ADP}\right) = \log\left(A_0\right) + \alpha T_{ADP}. \tag{4.2}$$

If there is a critical adaptation size, we expect that size at adaptation $\left[\log\left(A_{ADP}\right)\right]$ does not correlate neither with size at mitotic entry $\left[\log\left(A_0\right)\right]$, nor with cellular expansion $\left[\alpha T_{ADP}\right]$ (Figure 4.14, I and II). Instead, we expect a negative correlation between size at mitotic entry and cellular growth (Figure 4.14, III). A negative slope equals to -1 corresponds to a perfect sizer model (Di Talia *et al.* 2007). Our experimental data from adapting cells show a significant negative correlation between cellular expansion and size at mitotic entry (Figure 4.14, III), therefore suggesting the presence of a moderate size control mechanism. However, the critical size hypothesis also postulates that all cells adapt with the same size, regardless of the time spent in metaphase T_{ADP} and of the size at mitotic entry A_0. This was not the case, since adaptation size positively correlates with both (Figure 4.14, I and II). We conclude that adaptation is not triggered by the achievement of a critical size volume, although some aspect of size control is probably present.

4.1.5.2 Control of size growth in Adapting Cells

Despite the absence of a critical size of adaptation, Figure 4.14-III suggests the presence of some element of size control. A better comprehension about this control would be achieved by uncoupling the cellular expansion αT_{ADP} and evaluating the individual contribution of growth rate α and adaptation time T_{ADP} in the observed negative correlation (Osella *et al.* 2014). We discovered that growth rate negatively correlates with size at mitotic entry, while adaptation time does not (Figure 4.15). Therefore, cells that enter with a small size in mitosis tend to assume a high growth rate (Figure 4.15, $\log\left(A_0\right)$ vs α) and adapt with a small size (Figure 4.14-I). Our results suggest that a control of size growth in adapting cells takes place during mitosis. This mechanism would act on modulating growth rate rather than adaptation timing (Figure 4.14).

4.1.5.3 Cellular Growth of Adapted refractory cells resume properties of cycling cells

Once adapting cells become refractory, they maintain a size at anaphase onset which is similar to what was achieved in adaptation (Figure 4.12a and b). At the same time, these cells have a faster cell

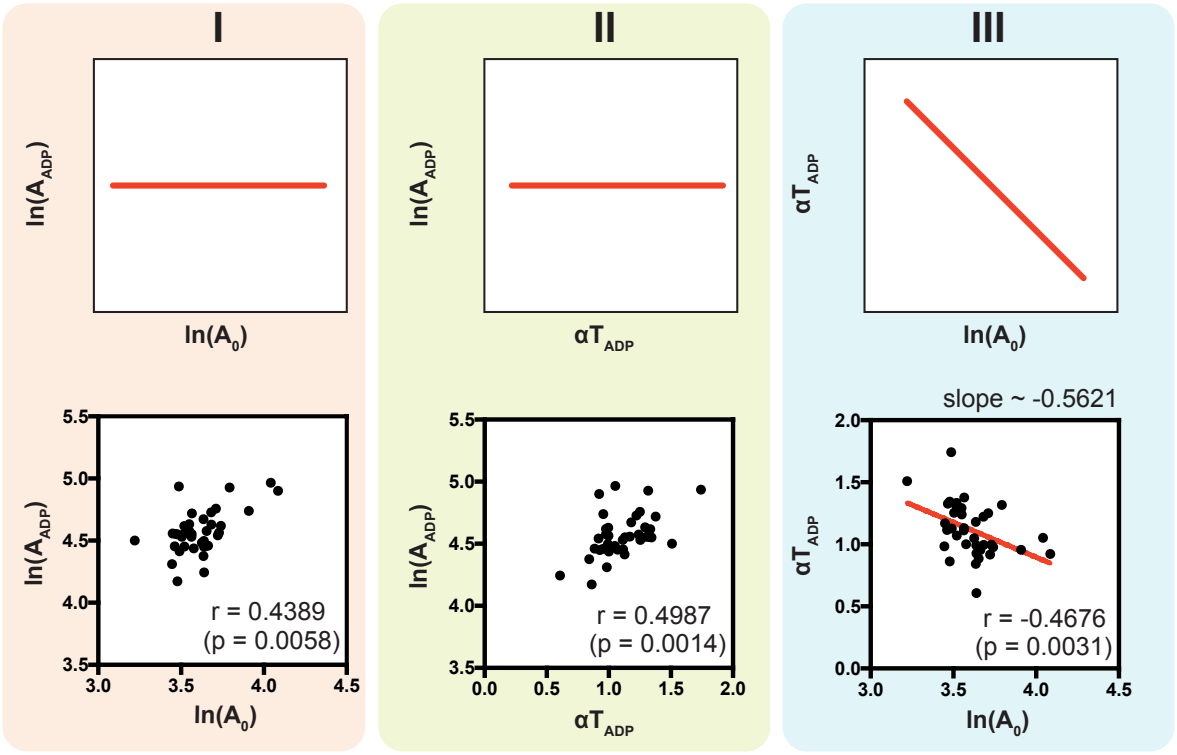

Figure 4.14: **Absence of a critical size in Adapting Cells** - (I-III) Theoretical behavior of a cell size control in which size at adaptation is constant. Each behavior was tested on experimental data coming from adapting cells, by scatter plot. Number of observations: 38. For each comparison, Pearson or Spearman correlation coefficient were evaluated - according to the normality of distributions or not - testing whether they were significantly different from 0 (significance level 0.05). In III), a linear fitting was performed (red line, adjusted $R^2 \sim 0.1606$)

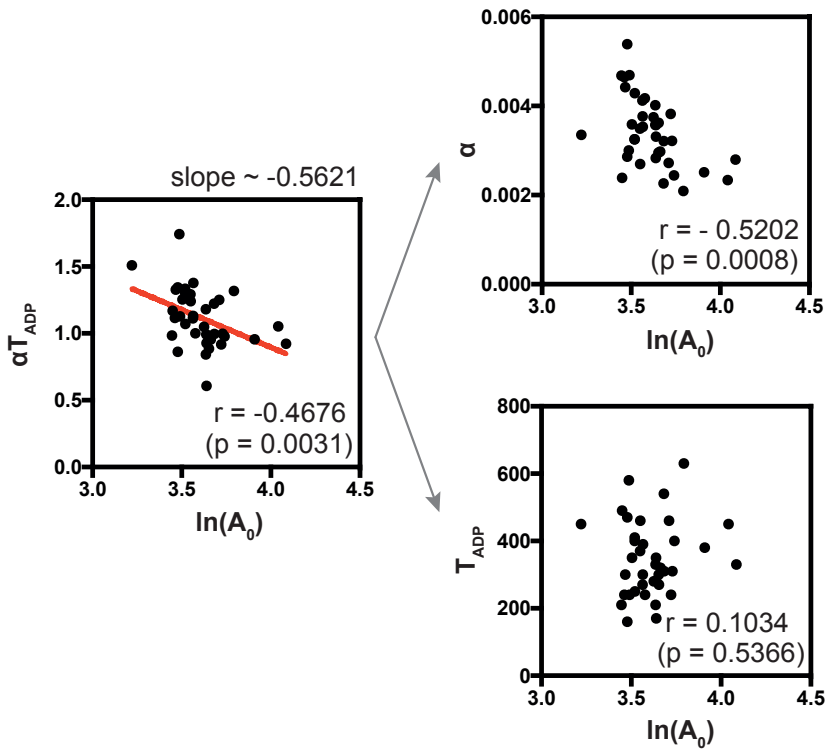

Figure 4.15: **Size Control in Adapting Cells** - Testing single contribution of growth rate α and adaptation timing T_{ADP} in cell size control, by scatter plot. Number of observations: 38. For each comparison, Pearson or Spearman correlation coefficient were evaluated - according to the normality of distributions or not - testing whether they were significantly different from 0 (significance level 0.05). On the left plot, a linear fitting was performed (red line, adjusted $R^2 \sim 0.1606$)

cycle compared to adapting cells. To shed light on the interplay between size and cell cycle time, we proceeded with the same theoretical workflow (Di Talia *et al.* 2007; Osella *et al.* 2014) that was applied in Section 4.1.5.1 for adapting cells.

75 % of sampled adapted refractory cells exhibit adjusted R^2 greater than 0.59 when their size behavior was fitted with an exponential law (Figure 4.13 - adapted), and some values were lower than 0.5 and negative. Hence, we had to reject the hypothesis of exponential growth, and we could not assume Equations 4.1 and thus 4.2 for adapted cells. Likewise, all the analysis shown in Figure 4.14 could not be repeated.

Nevertheless, a general description of cell size in these cells can be performed. Assuming that a mother cell M and its daughter D define a couple "mother-and-daughter" C from mitotic entry to anaphase onset, we can evaluate growth rate as

$$a_C = \frac{\Delta C}{\Delta T} = \frac{C_{exit} - C_{entry}}{T_{exit} - T_{entry}}, \tag{4.3}$$

where $\Delta C = C_{exit} - C_{entry}$ defines the difference between the area of C at entry and exit from mitosis, while $\Delta T = T_{exit} - T_{entry}$ refers to the mitotic duration (Figure 4.16a). Since $C = M + D$ by definition,

$$a_C = \frac{\Delta C}{\Delta T} = \frac{\Delta (M + D)}{\Delta T} = \frac{\Delta M}{\Delta T} + \frac{\Delta D}{\Delta T} = a_M + a_D, \tag{4.4}$$

allowing us to evaluate the single contribution of mother and daughter cells during mitotic cellular growth for C. We evaluated experimental growth rates for adapted refractory cells, comparing them to the growth rate of cycling and adapting cells. The analysis reveals that growth rate in adapted refractory cells is higher than in adapting cells (Figure 4.16b, left plot), while ΔC is lower (Figure 4.16b, right plot). A higher growth rate depends on a shorter mitotic timing of adapted refractory cells respect to adapting cells. A lower ΔC is explained by the fact that adapted refractory cells enter into mitosis with a larger size than adapting ones, while reaching a similar size at the anaphase onset (Figure 4.12c-d).

In this framework, we also evaluated the contribution of mother and daughter cell growth separately. We discovered that mother cells did not contribute to cellular growth of adapted refractory cells (Figure 4.16c), since the median values of a_M and ΔM were null, as in cycling cells. On the other side, behavior of daughter cell growth recapitulated what we observed from couple "mother-and-daughter" C (Figure 4.16d). These data suggest that growth rate of adapted refractory cells increases after adaptation, resuming a daughter-driven growth and cycle times similar to cycling cells, while preserving the size variability obtained during the first adaptation event. We have not explored further

the basis of this unique growth, which would surely require further analysis.

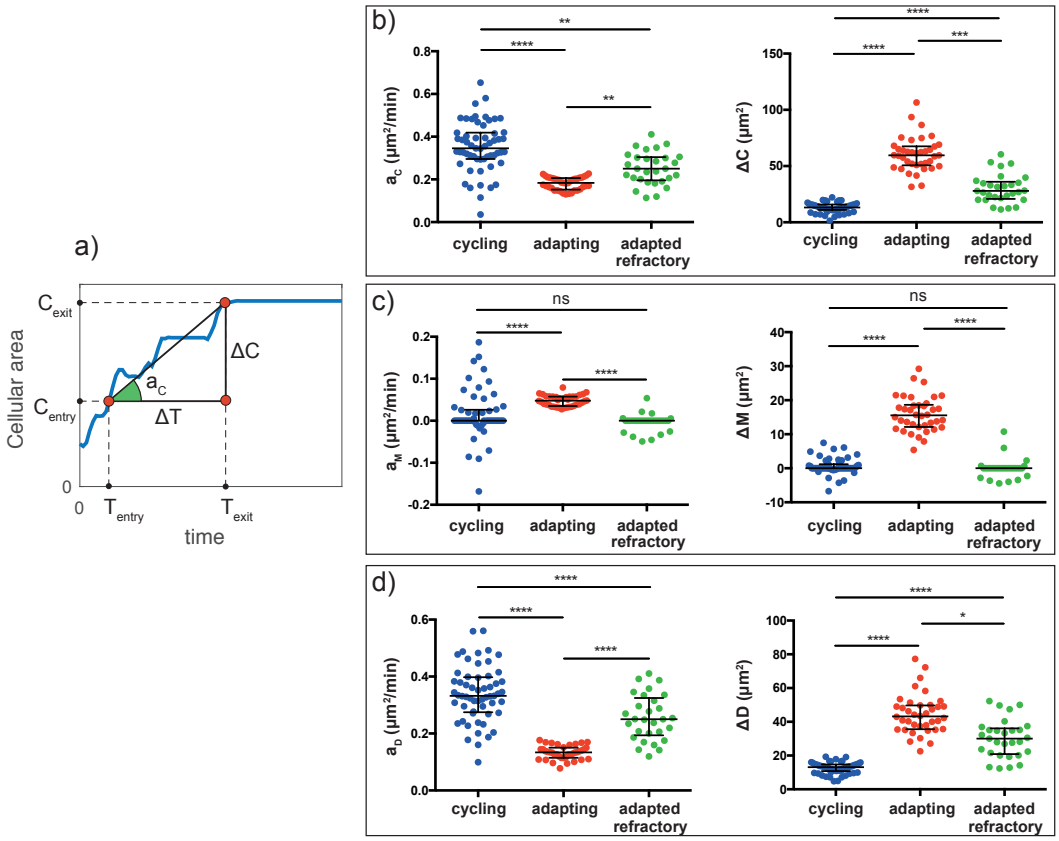

Figure 4.16: **Evaluation of experimental growth rate in cycling, adapting and adapted refractory cells** - (a) An example of how experimental growth rate is evaluated for a cell. (b) Evaluation of experimental growth rate and added cellular area for: (b) each couple, (c) each mother cell, (d) each daughter cell. Statistical analysis were performed with GraphPad Prism ®, using Kruskal-Wallis test with Dunn's Multiple Comparison Test (significance level 0.05). For each population, median and interquartile range were reported.

4.1.6 Some conclusions on proliferating cells after adaptation

Upon ectopic overexpression of Mad2, we characterized a population of proliferating cells after adaptation to the SAC. These cells are refractory to the checkpoint (Figure 4.17a), and maintain memory of adaptation between 3-12h of stimulus removal (Figure 4.17c, d). Moreover, refractory state is lost when adapted refractory cells are treated with nocodazole (Figure 4.17b). One very important property of adapted refractory cells concerns their ploidy: as revealed by FACS analysis, there is no any (sub-)population of aneuploid cells arising from adaptation to the Mad2 overexpression, suggesting the absence of missegregation events.

In this section we also explored cell size as a possible explanation for refractory state. Despite a positive correlation between refractoriness and size, we discovered that adaptation is not triggered by a critical size (Figure 4.17f). Instead, Adapted refractory cells adopt a new growth rate, resuming properties that are similar to that of cycling cells, while preserving the size that was reached in adaptation (Figure 4.17e, f).

One may ask whether these results are specific of Mad2 overexpression, or if they represent general properties of proliferating cells after adaptation to the SAC. To answer this question, we induced adaptation with other experimental means.

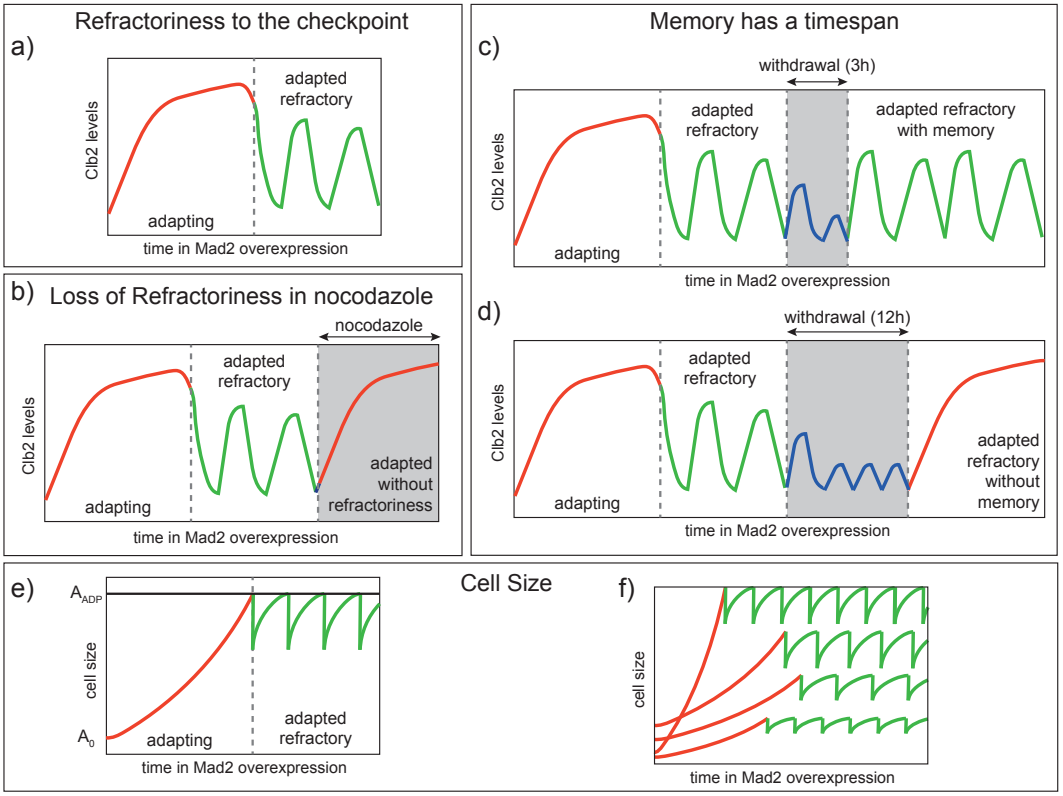

Figure 4.17: **Properties of cells adapted to Mad2 overexpression** - Schematic representation of properties reported in this section. (a) Proliferating cells after adaptation become refractory to the SAC. (b) Refractoriness to the checkpoint is lost upon nocodazole administration. (c-d) Memory has a timespan, according to the duration of SAC withdrawal. (e) Cell size increase exponentially in adapting cells. Once adapted, cells perform faster cell cycle with an increased growth rate and similar size at the anaphase onset. (f) Absence of a critical size by which cells become refractory to the SAC.

4.2 Proliferating Cells after Adaptation to the Mitotic Checkpoint induced by spindle depolymerization

So far, we studied a population of proliferating cells after adaptation to the SAC, inducing ectopically the Mitotic Checkpoint via overexpression of one of its molecular player. Overexpression of SAC molecular players represents an easy way to arrest cells in mitosis and evaluate the short- and long-term effect of this block. However, this method may have off-target effects, and it is artificial since it does not require unattached kinetochore in checkpoint signaling (Mariani *et al.* 2012). Thus, even if Mad2 overexpression comes with the advantage of uncoupling adaptation from chromosome missegregation, it would be important to use other methods for inducing SAC and characterizing adaptation and refractoriness to the checkpoint in more "physiological" conditions.

One option would be to treat cells with nocodazole. However, nocodazole starts to decrease its effectiveness without any proper re-addition after 5-6h (data not shown). In order to induce the SAC via a constant disruption of mitotic spindle, we used cold-sensitive mutants of β-tubulin *tub2-401* which are not able to properly polymerize microtubules at low temperatures (Huffaker *et al.* 1988; Sullivan & Huffaker 1992). In this section, we report preliminary results about cells adapted to microtubules depolymerization in Tub2 mutants grown at low temperatures.

4.2.1 A viable population of adapted cells arise from *tub2-401* mutants at semi-permissive temperatures

4.2.1.1 Screening of semi-permissive temperatures on agar plates

As a preliminary experiment, we screened cellular growth of *tub2-401* at different temperatures. As a readout for SAC activity, we used *tub2-401 mad*2Δ cells: these cells should be checkpoint-deficient, therefore becoming not viable upon restrictive conditions (K. G. Hardwick *et al.* 1999). Moreover, we also monitored *WT* and *mad*2Δ cells, in order to test whether the low temperature per-se activates the Mitotic Checkpoint.

Cells were grown in liquid medium at 30°C, and subsequently spotted on agar plates at different temperatures, and monitored day by day (Figure 4.18). At permissive temperature (30°C), all strains exhibited a similar growth. When temperature was decreased to semi-restrictive conditions ($\sim$ 22-25°C), the mitotic checkpoint started to be activated, since viability of *tub2-401 mad*2Δ cells decreased compared to the other strains (Figure 4.18, 22 and 25°C). Probably thanks to checkpoint activity, we appreciated a population of viable *tub2-401* cells after 2 days from their spotting. This population was not present for restrictive temperatures (lower than 18°C), where *tub2-401* and *tub2-401 mad*2Δ exhibited similar impaired growth (Figure 4.18, 18 and 15°C). In conclusion, we identified

as 21-25°C a range of semi-permissive conditions for *tub2-401*, in which the SAC is engaged and cells are capable to proliferate after adaptation.

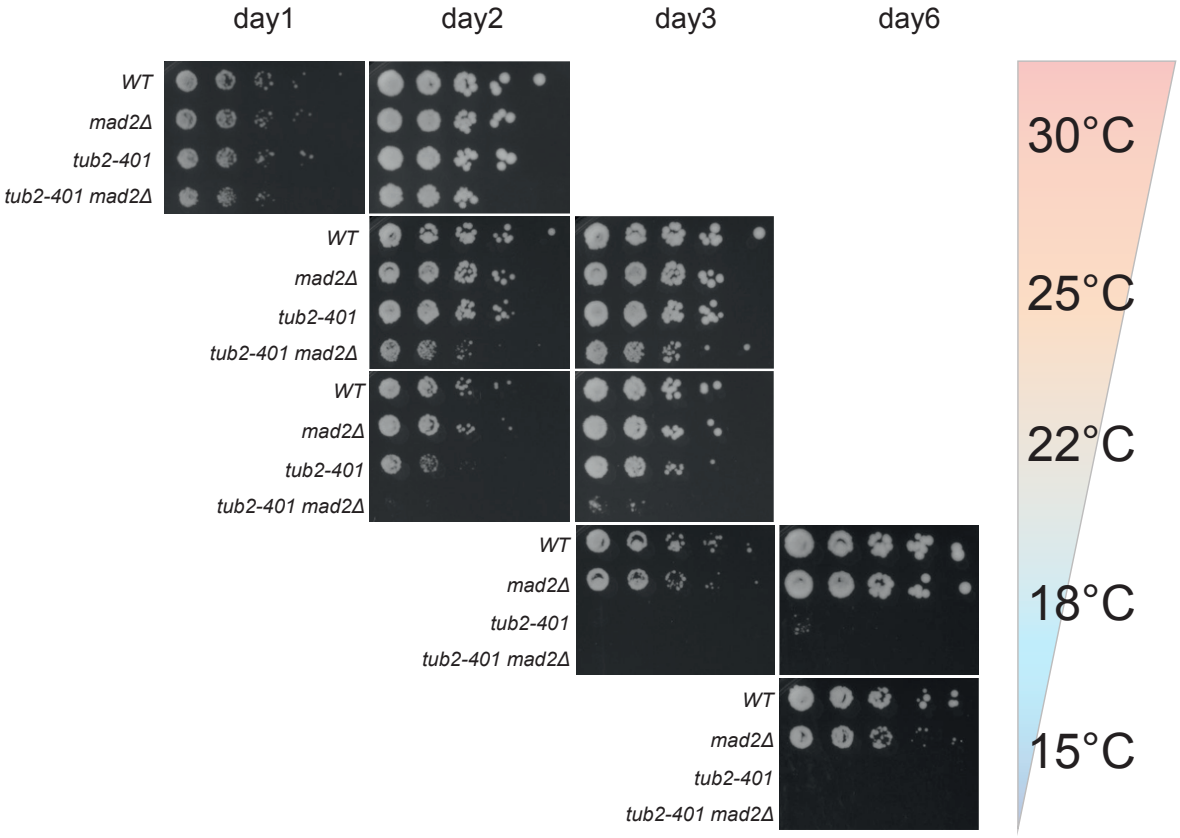

Figure 4.18: **Evaluating viability of *tub2-401* adapted cells upon different temperatures** - *WT* (yAC3568), *mad*2Δ (yAC3372), *tub2-401* (yAC3220) and *tub2-401 mad*2Δ cells (yAC2946) were grown in YEPD liquid medium at 30°C. Then, they were diluted to ∼ 5e+7 cells/ml and serial dilutions were performed. Strains were spotted on YEPD agar plates, which were incubated at 30, 25, 22, 18 and 15°C and monitored.

4.2.1.2 Cellular growth in liquid medium at 21°C

We next analyzed cellular growth in liquid medium, choosing 21°C as semi-restrictive temperature. Cells were grown at 30°C and then shifted to 21 (Figure 4.19a). During the first 4h after the shift, no differences were detectable, maybe because strains needed to get used to low temperature (delay in Figure 4.19b). However, after 4h *tub2-401* and *tub2-401 mad*2Δ cells grew slower than the other strains (Figure 4.19b), while increasing their volume (Figure 4.19d). During the second day, differences were clearer: *tub2-401 mad*2Δ cells stopped to grow, likely due to massive missegregation (Figure 4.19c). On the other hand, *tub2-401* cells continued to grow, with a doubling time of ∼ 4h (Figure 4.19c, Table 4.1), while maintaining a size that was 2.5 bigger than *WT* (Figure 4.19e, f). Moreover, we noticed that doubling time of *tub2-401* cells decreased by one hour from day 1 to day 2 (Table 4.1), suggesting the presence of a faster cell cycle 22h after the decrease of temperature. Taken together, our data suggest the presence of a viable population of adapted cells, which proliferate faster

after a slow transient at low temperature, and with a constant volume. These properties remind those observed in the previous section, in cells adapting to Mad2 overexpression.

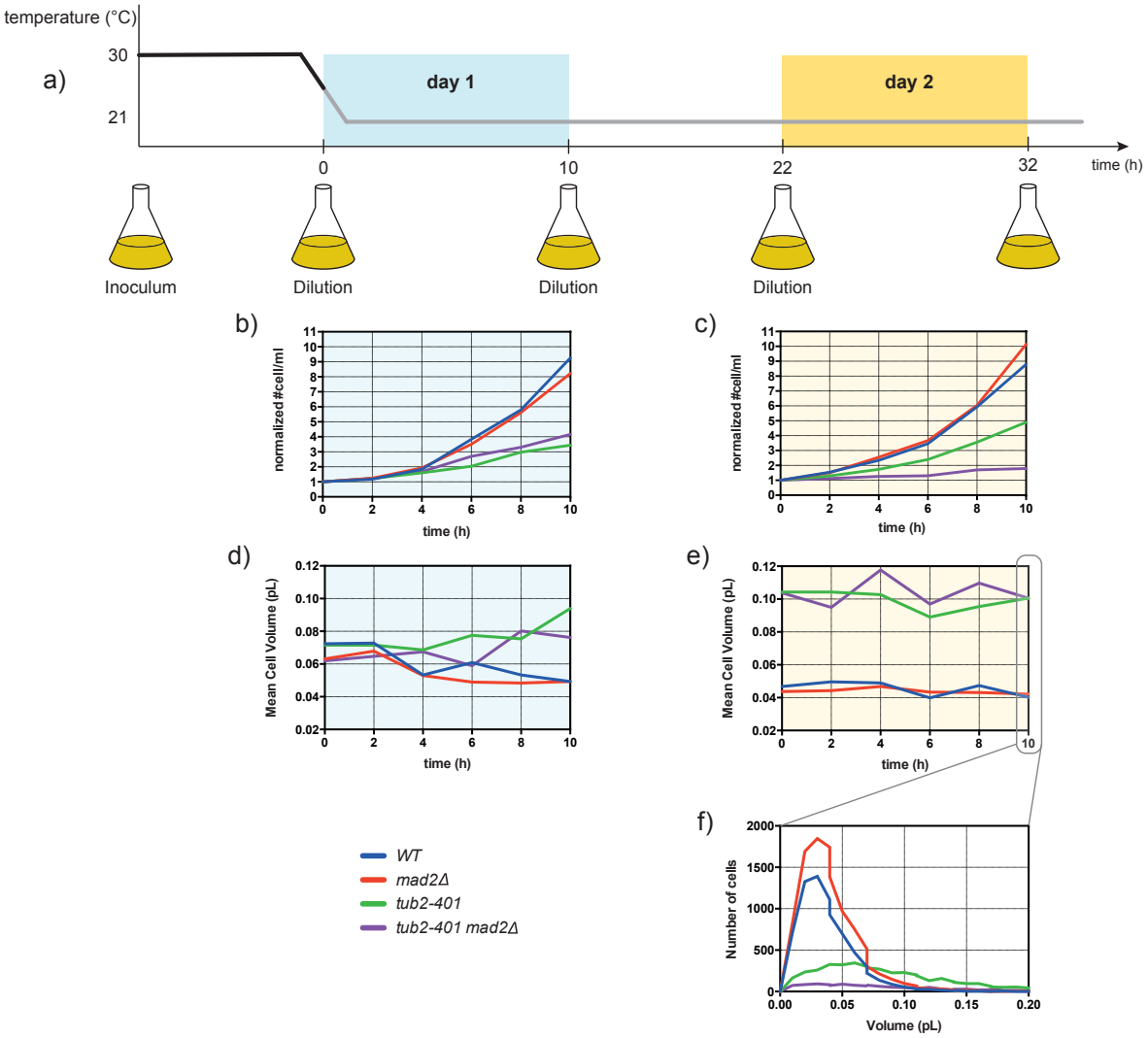

Figure 4.19: **Growth of *tub2-401* cells at 21°C** - (a) Experimental Setup. *WT* (yAC3717), *mad*2Δ (yAC3372), *tub2-401* (yAC3220) and *tub2-401 mad*2Δ (yAC2946) cells were inoculated in liquid YEPD, allowing them to grow overnight at 30°C. The day after (day 1), they were diluted to ∼ 1e6 cell/ml and monitored every 2h, for 10h. At the end of day 1, cells were diluted to ∼ 1.5e6 cell/ml, allowing them to grow overnight at 21°C. In the following day (day 2), cells were diluted to ∼ 1.8e6 cell/ml and monitored every 2h, again for 10h. (b-c) Growth curves of the reported strains. Number of cells per ml was normalized to the initial concentration at the beginning of monitoring (time 0). (d-e) Behavior of mean cell volume of the reported strains. (f) Histogram of cell volumes of the reported strains at the end of the experiment. Informations about cellular concentration and volume were recorded with Scepter ™ Handheld Automated Cell Counter (© Millipore Corporation).

4.2.2 Single-cell analysis of *tub2-401* adapted cells

To confirm the presence of a refractory state in *tub2-401* cells, we then performed a single-cell analysis of *tub2-401* cells growing at low temperature. We synchronized *WT*, *mad2*Δ, *tub2-401* and *tub2-401 mad2*Δ cells in G1 and released them in a microfluidic chamber, which was incubated at ∼ 19.5-20°C for the entire experiment (Figure 4.20a - see Material and Methods for details). *tub2-401* cells

	WT		*mad2*Δ		*tub2-401*		*tub2-401 mad2*Δ	
	Day1	Day2	Day1	Day2	Day1	Day2	Day1	Day2
growth rate ($1/min$)	0.2215	0.2179	0.2212	0.2298	0.1262	0.1576	0.1458	0.0590
doubling time (min)	3.130	3.181	3.282	3.017	5.493	4.399	4.755	11.74
adjusted R^2	0.9903	0.9976	0.9930	0.9976	0.9837	0.9944	0.9837	0.9509

Table 4.1: **Fitting of growth curves at 21°C with an exponential law** - Raw data coming from Figure 4.19b-c were fitted with the following mathematical law: $N = exp(kt)$, where N represents normalized number of cell per ml, t time and k growth rate. From the fitting, an estimation of doubling time $\ln(2)/k$ was performed, together with adjusted R^2 for goodness of fit. Fitting was performed with GraphPad Prism ®.

exhibited a first mitotic arrest, followed by at least another cell cycle for ∼ 56% of the monitored cells. Similarly to what was observed in Section 4.1, we refer to the first mitosis as "adapting" cells, and to the subsequent ones as "adapted" cells.

The mitotic duration was evaluated in each condition, according to the increase and decrease of Clb2-GFP levels (Bonaiuti *et al.* 2017). Mitotic length of *WT* cells was comparable to that of *mad2*Δ cells, showing that low temperature per se did not activate the SAC in wild-type cells. Adapting cells, instead, exhibited a mitotic duration that was longer compared to *WT* cells (Figure 4.20b); the delay was due to the SAC activity, since checkpoint deficient *tub2-401 mad2*Δ cells showed a wild-type mitotic duration (Figure 4.20b). Once adapted to the SAC, cells resumed proliferation with a mitotic duration that was not significantly different from that of adapting cells (Figure 4.20b, adapted). There was not a clear prevalence of adapted cells with a shorter mitotic duration (Figure 4.20c). This result is different to that of adapted cells upon Mad2 overexpression (see Section 4.1, Figure 4.2) and does not support the presence of a refractory state in *tub2-401* adapted cells.

The absence of a refractory state is in contrast with the decreased doubling time that was observed in liquid medium (see the experiment of Subsection 4.2.1.2). This discordance could be explained by a difference in proliferation between cells growing in liquid medium and those monitored in microfluidic chambers. Indeed, in the microfluidic chamber (Figure 4.20d) the doubling time of *tub2-401* cells was ∼ 3-4 times slower than that measured in liquid medium experiment. Once adapted, most of *tub2-401* cells resumed proliferation without cytokinesis, forming a cluster of 3 cell bodies (Figure 4.20d). Eventually, cellular proliferation decreased, since most of cells underwent to death. This result is in accordance with a previous study (Sullivan & Huffaker 1992), in which *tub2-401* cells produced microcolonies with at least 3-4 cells at semi-restrictive temperature (18°C). In those microcolonies, daughter cells were anucleated, because the absence of cytoplasmic microtubules allowed mother cells to detain DNA.

The disagreement between these data and those obtained with the *GAL1-MAD2(3x)* system is likely to be due to the missegregation that comes with adaptation in the *tub2-401* system. To produce comparable results, we may have to reduce the extent of missegregation, possibly by increasing the

temperature.

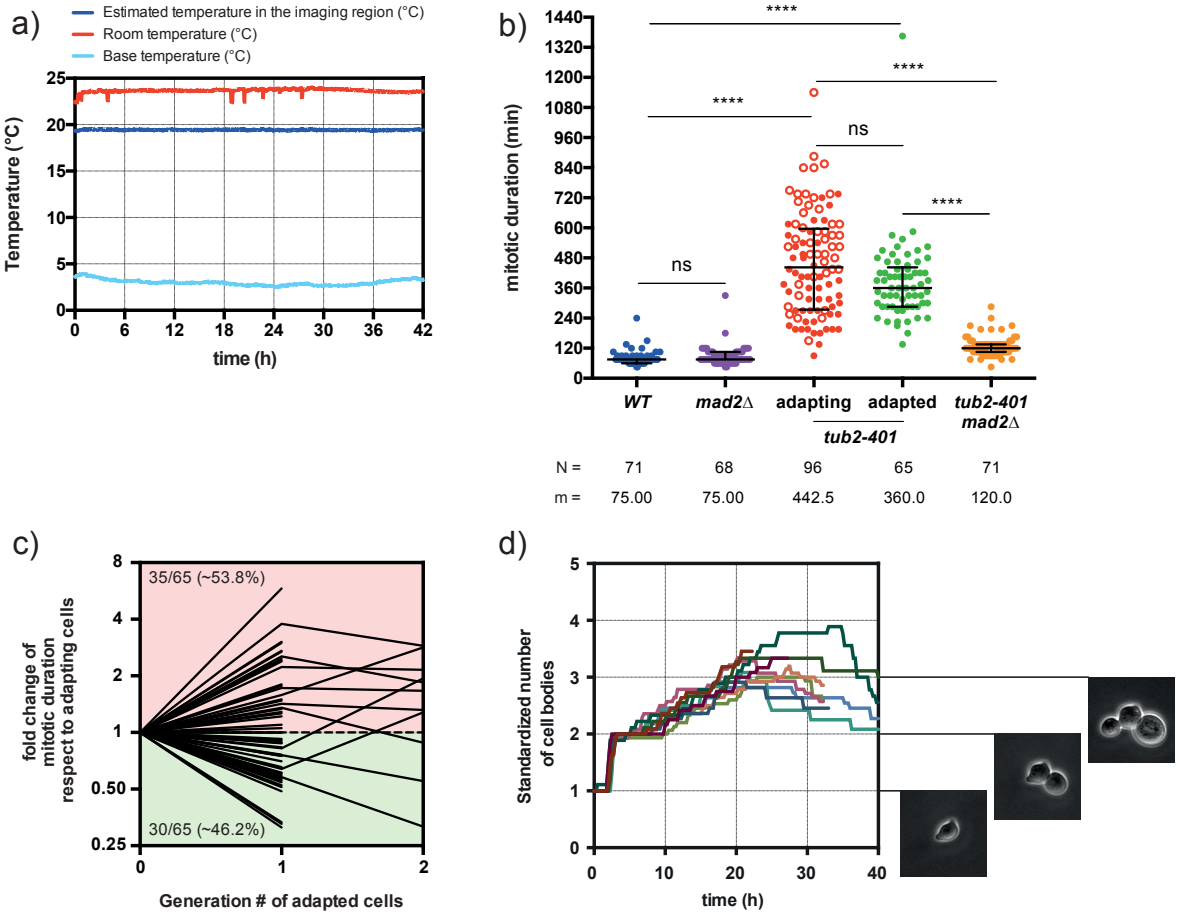

Figure 4.20: **Single cell analysis for *tub2-401* cells at ~ 20°C** - *MATa CLB2-GFP* (yAC3491), *MATa CLB2-GFP mad2*Δ (yAC3041), *MATa CLB2-GFP tub2-401* (yAC2970), *MATa CLB2-GFP tub2-401 mad2*Δ (yAC3034) cells were grown in synthetic medium, synchronized in G1 and then released in microfluidic chamber at low temperature. Cells were monitored for 40h. (a) Temperature was constantly maintained and monitored during the entire timelapse, as described in Material and Methods (see Chapter 3 for details). (b) Evaluation of mitotic duration for each condition, following the same procedure that was reported in Section 4.1 - Figure 4.2. Statistical analysis were performed with GraphPad Prism ®, using Kruskal-Wallis test with Dunn's Multiple Comparison Test (significance level 0.05). N: number of observation. m: median of population. For each population, median and interquartile range were reported. In adapting population (in red), white circle correspond to that cells that did not proliferate after adaptation during the 40 hours. (c) Monitoring mitotic duration in the progeny of each adapting cell. For each adapting cell that exhibit at least one adapted cell cycle, mitotic duration of adapted cell was normalized to mitotic duration of the ancestral adapting cell and plotted as a function of generation number after adaptation to the SAC. Quantification of fold changes higher or lower than 1 is reported. (d) For each of the ten monitored *tub2-401* colonies during the live cell imaging experiment, the number of cell bodies was measured. The resulting trajectories were normalized to the initial number of cells and plotted versus time. Examples of 1, 2, 3 cell bodies are reported.

4.2.3 A preliminary estimate of missegregation rates in *tub2-401* cells

Differently from cells adapted upon Mad2 overexpression (Section 4.1), cells adapting to spindle depolymerization could missegregate chromosome, with deleterious effects on cellular proliferation (Santaguida & Amon 2015). To estimate the extent of missegregation, we evaluated the loss rate of a Chromosome III Fragment (CFIII) (Spencer *et al.* 1990; Warren *et al.* 2002). This fragmented chromosome carries *SUP11*, an ochre-suppressing tRNA that suppresses the red pigment phenotype of W303 strains carrying *ade2-101* mutation. After crossing our *WT*, *mad*2Δ, *tub2-401* and *tub2-401 mad*2Δ strains with *CFIII URA3 SUP11*, we grew double mutants at 30°C in synthetic medium without uracile, in order to prevent spontaneous loss of CFIII. Then, cells were diluted and plated on agar plates with low concentration of adenine. Plates were then incubated at different temperatures, monitoring colonies growth. While colonies carrying CFIII chromosome were white, cells that lost the fragmented chromosome became red. Following (Warren *et al.* 2002), we counted the number of colonies that were at least one-half red as a readout for chromosome loss events during the first cell division upon plating. By normalizing this number by the total number of colonies in each plate, we obtained an estimation of loss-rate. As expected, *tub2-401 mad*2Δ cells exhibited a higher loss-rate than the other strains (Figure 4.21). On the other hand, loss rate of CFIII in *tub2-401* cells was lower than 5% for 23-25°C (Figure 4.21). An increase of loss rate was appreciable at 20°C (Figure 4.21), even if the total number of colonies was less than in the other conditions (Table 4.2), probably due to a higher sensitivity to temperature. These preliminary data suggest the presence of a negative correlation between CFIII loss rate and viability of adapted cells. These data could explain the reduced viability that was monitored in *tub2-401* adapted cells grown in the microfluidic chamber (Figure 4.20d).

		WT	*mad2Δ*	*tub2-401*	*tub2-401 mad2Δ*
30°C	# ≥ half-sectored colonies	0	11	4	16
	# total colonies	27	121	97	115
	loss-rate %	0	9,1	4,1	13,9
25°C	# ≥ half-sectored colonies	0	2	2	36
	# total colonies	66	95	121	155
	loss-rate %	0	2,1	1,7	23,2
23°C	# ≥ half-sectored colonies	4	5	3	31
	# total colonies	111	159	119	122
	loss-rate %	3,6	3,1	2,5	25,4
20°C	# ≥ half-sectored colonies	0	7	3	n.a.
	# total colonies	98	171	12	n.a.
	loss-rate %	0	4,1	25	n.a.
18°C	n.a.# ≥ half-sectored colonies	0	16	n.a.	n.a.
	# total colonies	83	123	n.a.	n.a.
	loss-rate %	0	13	n.a.	n.a.
15°C	# ≥ half-sectored colonies	0	13	n.a.	n.a.
	# total colonies	80	151	n.a.	n.a.
	loss-rate %	0	8,6	n.a.	n.a

Table 4.2: **Evaluation of CFIII chromosome loss for *tub2-401* mutants** - Evaluation of loss-rate of CFIII chromosome in the experiment described in Section 4.2.3 (see also Figure 4.21). "n.a." stands for "not-available", due to the absence of viable colonies on plates.

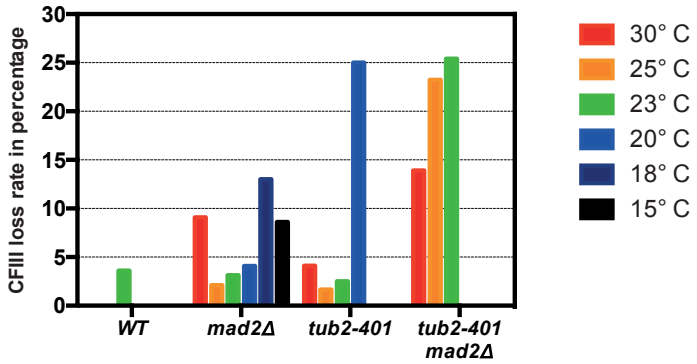

Figure 4.21: **Chromosome loss assay for *tub2-401* mutants** - *URA3 SUP11* (yAC1749), *mad2Δ URA3 SUP11* (yAC3252), *tub2-401 URA3 SUP11* (yAC3228) and *tub2-401 mad2Δ URA3 SUP11* (yAC3251) cells were grown in synthetic medium lacking uracile. Then, they were diluted to ∼ 1e3 cells/ml, and 200 μl were plated on agar plates with low amount of adenine. Plates were incubated at 30, 25, 23, 20, 18 and 15°C and monitored. Loss-rate were evaluated (see Table 4.2), as shown in (Warren *et al.* 2002) and reported in the plot.

4.3 Proteomic Screening of Adapted cells

Having defined different phenotypic properties of adapted/adapted refractory vs cycling cells, we aimed at providing a molecular rationale for these differences. To this purpose, we performed a Shotgun Label-Free LC/MS-MS (Matafora *et al.* 2014; Matafora *et al.* 2017) of the adapted proteome, inducing the checkpoint via Mad2 overexpression or *tub2-401* mutants. This analysis allowed us to evaluate which part of the proteome is up- or down-regulated compared to a control condition. In this section, we report our results.

4.3.1 Proteomic Analysis of *GAL1-MAD2(3x)* Adapted refractory cells

As discussed in Section 4.1, expression of *CDC20* allele *cdc20-127* is able to uncouple Mad2 overexpression from checkpoint activity, introducing a population of cycling cells (Adapting W/O SAC, see Section 4.1, Subsection 4.1.4.2) that overexpress Mad2 as Adapted refractory cells. We used these cells as our negative control, and compared them to cells overexpressing Mad2 and wild-type Cdc20 only. *tetO$_2$-CDC20-127(1x), GAL1-MAD2(3x)* cells were inoculated in YEPR liquid medium (no Mad2 overexpression) and subsequently shifted in galactose supplemented or not with doxycycline, in order to modulate *cdc20-127* synthesis. We will refer to cells expressing cdc20-127 as "not Adapted", and to cells that not express cdc20-127 as "Adapted refractory". After ∼19h from the shift, cells were collected and processed for LC/MS-MS analysis. Adapted refractory and not Adapted cells are identical in terms of carbon source shift, but different in their SAC response (as discussed in Section 4.1).

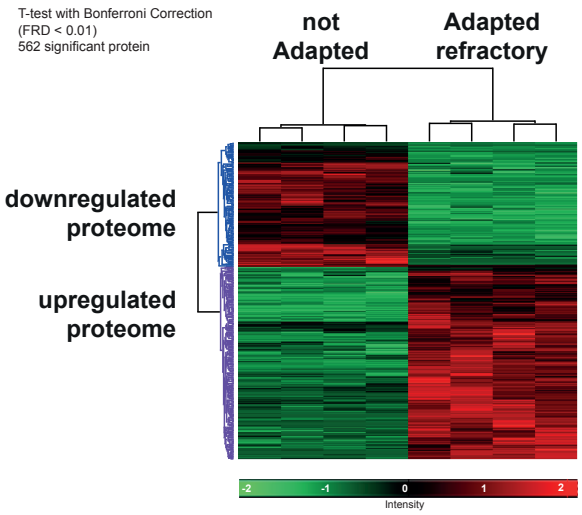

Figure 4.22: **Heatmap of the identified proteome in Adapted refractory cells** - Out of ∼ 3800 proteins, 562 exhibited a significant increase (in red) or decrease (in green) in Adapted refractory cells. The analysis was performed on two biological replicates, with two technical replicates, by Vittoria Matafora - Lab of Functional Proteomics (A. Bachi) - IFOM, Milan - IT.

We identified about 3800 proteins, of which 562 showed significant differences between Adapted refractory and not Adapted cells (Figure 4.22). By a hierarchical cluster analysis, we detected two sets of genes differentially expressed in the two conditions. In the next subsections we describe them.

4.3.1.1 Upregulated proteome of Adapted refractory cells

We identified 341 proteins upregulated in Adapted refractory cells. Via a Gene Ontology and Pathway enrichment analysis, we observed that most of them belong to metabolic pathways (Figure 4.23), suggesting that Adapted refractory cells rewire their metabolism while proliferating in the continuous presence of SAC-inducing stimuli. In particular, we observed a ~ 2 fold enrichment of "phosphate-containing compound metabolic processes" (Figure 4.23a). Since this Gene Ontology (GO) entry refers to the chemical reactions and pathways involving phosphate groups, Adapted refractory cell cycle may require a high consumption of phosphate. Moreover, the significant enrichment of the chitin biosynthesis pathway (Figure 4.23b) suggests a high requirement of cell wall components. This is in accordance with the fact that Adapted refractory cells are larger than not Adapted ones, as discussed in Section 4.1.

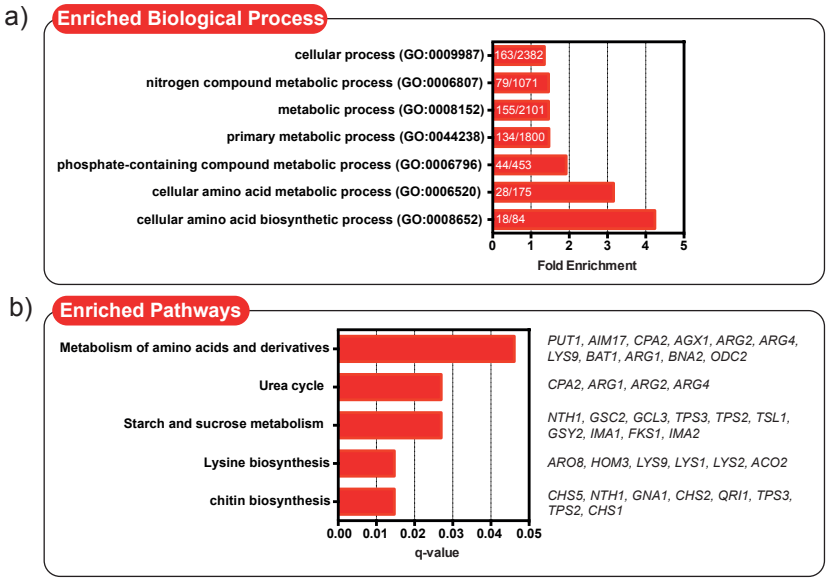

Figure 4.23: **Analysis of Enriched Biological Processes and Pathways in the upregulated proteome of Adapted refractory cells** - (a) Statistical Overrepresentation Test of upregulated proteome in Adapted refractory cells was performed on PANTHER GO-Slim Biological Process Entries (Mi *et al.* 2013; Mi *et al.* 2017) (`www.pantherdb.org`). Entries significantly enriched (adjusted p-value < 0.05) are reported, in terms of fold-enrichment compared to the reference list. For each term, the ratio between protein identified in our study and protein in the reference list is reported. (b) - Statistical Overrepresentation Test of upregulated proteome in Adapted refractory cells was performed on ConsensusPathDB-yeast (Herwig *et al.* 2016; Kamburov *et al.* 2013; Kamburov *et al.* 2011; Pentchev *et al.* 2010) Pathway Entries (`cpdb.molgen.mpg.de/YCPDB`). Pathways significantly enriched (q-value < 0.05) are reported, together with the genes obtained from our study.

Beyond metabolism, we focused our attention on the GO entry "enriched cellular process". Inside this entry, we noticed several upregulated proteins belonging to cell cycle-related processes (Figure 4.24b). Most of them are involved in the mitotic cell cycle, DNA replication and DNA Damage Re-

sponse (DDR). Moreover, some proteins are member of the GO term "Protein Phosphorylation", in accordance with what mentioned above (Figure 4.23a). Interestingly, physical interactions of these proteins gives rise to a well-defined topological network (Figure 4.24a), in which Cyclin dependent kinase 1 Cdc28 has the highest number of interactions. Polo-like Kinase Cdc5 was also present in the same network. Given the constant arrest in mitosis experienced by these cells, the result is maybe not so surprising. However, levels of Cdc5 are cell cycle regulated, while Cdc28 levels are not. Moreover, asynchronous Adapted refractory Cells are more enriched in G2/M phase than not Adapted asynchronous cells, as revealed by FACS analysis (see Section 4.1, Figure 4.4, asynchronous timepoint - asyn). Therefore, while Cdc5 upregulation may be due to a significant enrichment of mitotic cells in Adapted refractory population, Cdc28 upregulation may be independent from the cell cycle phase.

Concluding, these data suggest a high requirement of phosphate for Adapted refractory cells, and an increased abundance of key mitotic regulators like Cdc28 and Cdc5 kinases.

a)

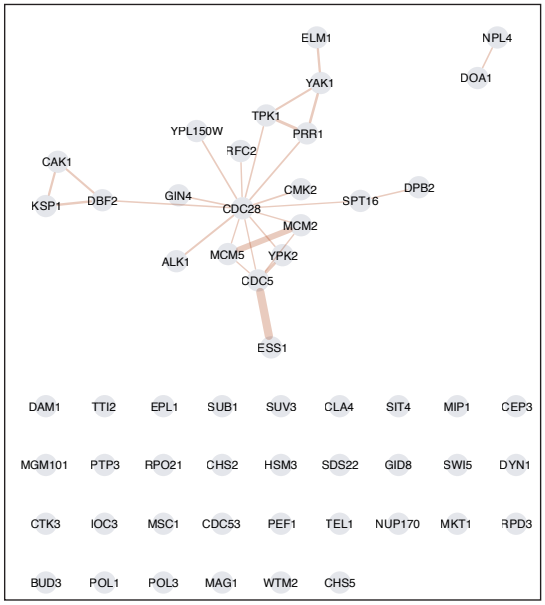

b)

Gene Ontology term	Genes
Protein phosphorylation	*TEL1,CDC28,GIN4,PTP3,CAK1,ALK1,DBF2,KSP1,YAK1,TPK1, ESS1,ELM1,PRR1,CTK3,CDC5,YPK2,CLA4,CMK2,YPL150W*
Mitotic cell cycle	*CDC28,NPL4,BUD3,SIT4,CDC53,SWI5,GIN4,CAK1,ALK1, PEF1,ESS1,ELM1,DYN1,CHS5,CDC5,GID8,CEP3,CLA4,RPD3*
Cellular Response to DNA damage stimulus	*MCM2,TEL1,CDC28,HSM3,SIT4,RPO21,MAG1,EPL1,RFC2, TTI2,MGM101,DOA1,MCM5,SUB1,MKT1,POL1,WTM2,DPB2*
DNA repair	*MCM2,TEL1,CDC28,HSM3,SIT4,RPO21,MAG1,EPL1,RFC2, MGM101,DOA1,MCM5,SUB1,POL1,DPB2*
Regulation of cell cycle	*CDC28,GIN4,DBF2,DAM1,RFC2,CDC5,SUB1,GID8,CEP3, CLA4,RPD3*
DNA replication	*MCM2,CDC28,POL3,SPT16,RFC2,MCM5,POL1,RPD3,MIP1, SUV3,DPB2*
Chromosome segregation	*NUP170,CDC28,IOC3,DAM1,RFC2,SDS22,DYN1,CDC5,CEP3*
DNA recombination	*MCM2,CDC28,MGM101,MCM5,MSC1,CDC5,RPD3*
Cytokinesis	*CHS2,BUD3,PEF1,DBF2,ELM1,CHS5*
Cell budding	*CDC28,BUD3,GIN4,PEF1,ELM1*

Figure 4.24: **Network analysis of upregulated cell cycle proteins in Adapted refractory cells** - (a) Network of the identified proteins involved in cell cycle processes. Edges are related to physical interaction between proteins, and their width correlates with consensus number in interaction databases. The network was created with Cytoscape (Cline *et al.* 2007; Saito *et al.* 2012; Shannon *et al.* 2003; Smoot *et al.* 2011), using GeneMANIA plugin (Montojo *et al.* 2010) and only referring to physical interactions among protein. (b) Selection of cell cycle protein in Adapted refractory cells. The list was obtained by performing SGD (Cherry *et al.* 2012) Gene Ontology Slim Mapper (`https://www.yeastgenome.org/cgi-bin/GO/goSlimMapper.pl`) on upregulated proteome of Adapted refractory cells.

4.3.1.2 Downregulated proteome of Adapted refractory cells

In the same proteomic screening, we identified 221 proteins with a decreased protein abundance in Adapted refractory cells compared to not Adapted ones. Here, we noticed again an involvement of metabolic pathways, but the major enrichment was observed in translational processes (Figure 4.25a):

cytoplasmic translation, rRNA processing, translational control and protein folding (Figure 4.25b and 4.26b). In particular, the protein with the maximum number of physical interaction was Ssb1, a ribosome-associated molecular chaperone (Figure 4.26a). Downregulation of these component could suggest the presence of defects in translational processes of Adapted refractory cells, possibly concerning not only protein biosynthesis, but also protein quality control mechanisms. The experienced stressful condition during a prolonged mitotic arrest may lead to this phenomenon. Otherwise, since it is known that transcription is strongly inhibited during mitosis, the observed downregulation may be explained by a significant enrichment of mitotic cells.

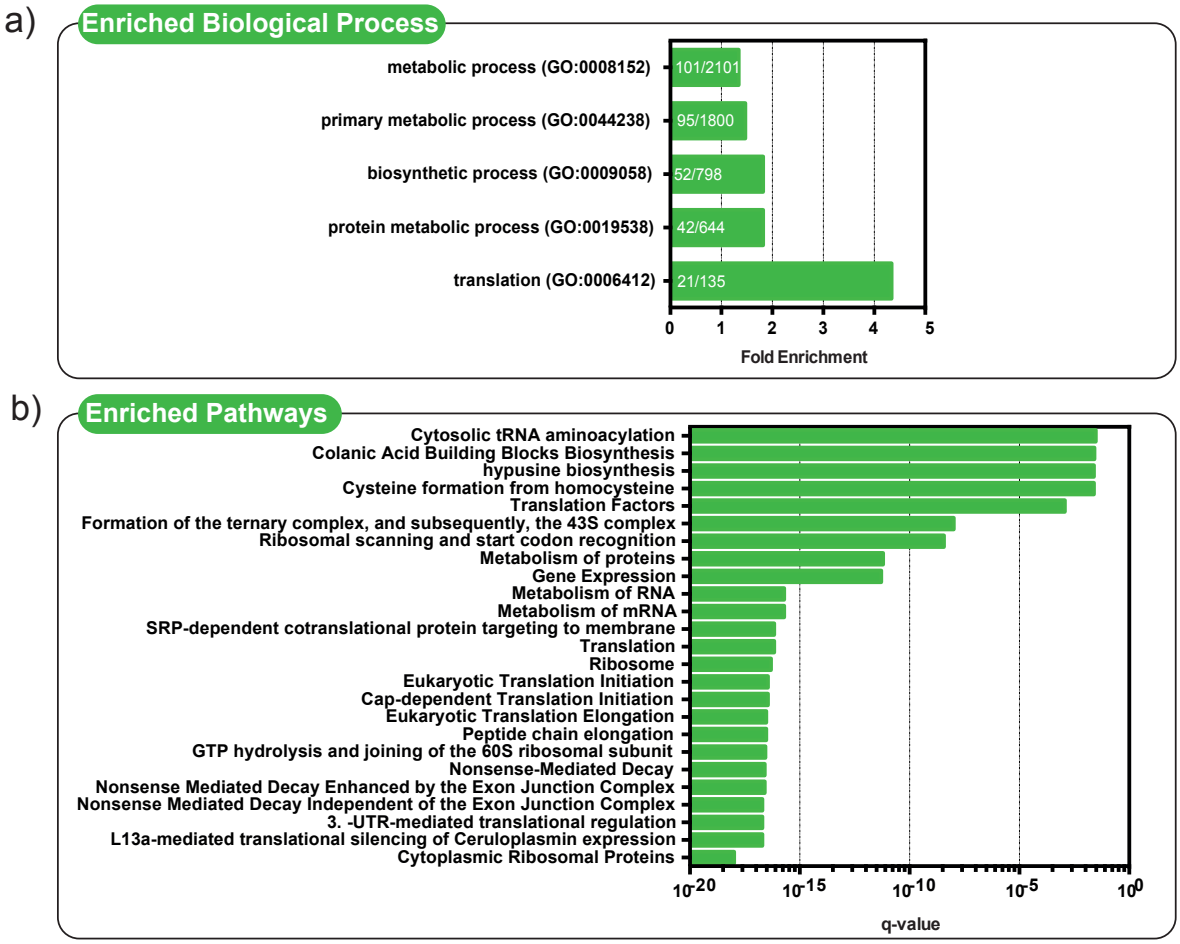

Figure 4.25: **Analysis of Enriched Biological Processes and Pathways in the downregulated proteome of Adapted refractory cells** - (a) Statistical Overrepresentation Test of downregulated proteome in Adapted refractory cells was performed on PANTHER GO-Slim Biological Process entries (Mi *et al.* 2013; Mi *et al.* 2017) (`www.pantherdb.org`). Entries significantly enriched (adjusted p-value < 0.05) are reported, in terms of fold-enrichment compared to the reference list. For each term, the ratio between protein identified in our study and protein in the reference list is reported. (b) - Statistical Overrepresentation Test of downregulated proteome in Adapted refractory cells was performed on ConsensusPathDB-yeast (Herwig *et al.* 2016; Kamburov *et al.* 2013; Kamburov *et al.* 2011; Pentchev *et al.* 2010) Pathway Entries (`cpdb.molgen.mpg.de/YCPDB`). Pathways significantly enriched (q-value < 0.05) are reported.

Beyond translational processes, we also detected downregulation of several cell cycle proteins (Figure 4.27b). Among them, Mad2 was identified. The presence of Cdc20 is due to the expression of *cdc20-127* from an exogenous promoter in not Adapted cells. Finally, we observed several proteins

involved in nuclear transport, chromatin organization, mitosis and DNA damage (Figure 4.27b). In this network, the molecular chaperone Ssb1 was again the protein with the maximum number of physical interactions (Figure 4.27a).

a)

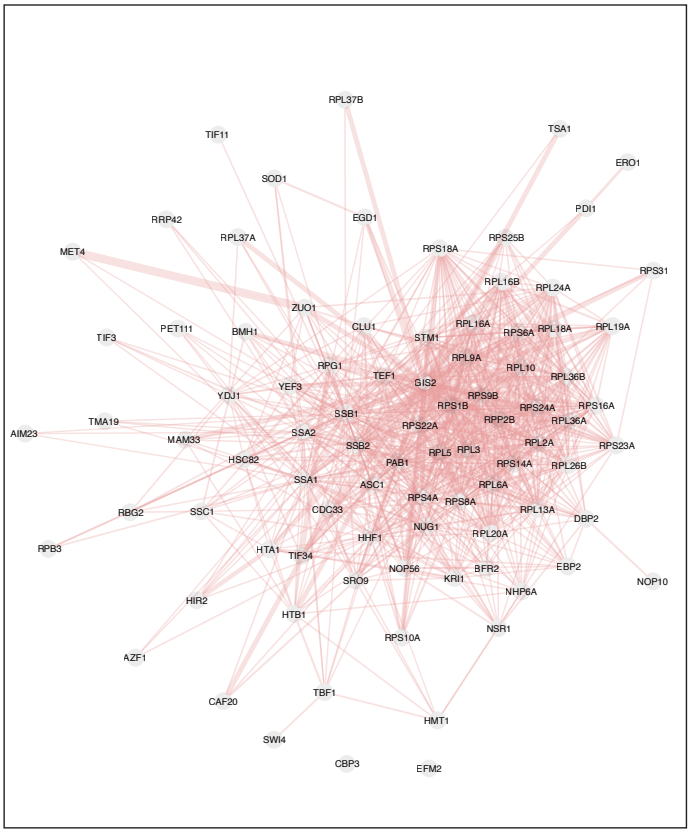

b)

Gene Ontology term	Genes
Cytoplasmic Translation	*SSA1 RPS8A RPG1 RPL19A SRO9 RPS14A RPL13A SSB1 RPP2B RPS18A RPL37B RPS24A RPL2A RPL24A RPL9A RPL26B RBG2 RPL16A RPS22A RPS4A TMA19 RPL10 RPS31 RPL37A RPS25B RPS1B RPL6A CLU1 RPS16A TIF34 RPL36A RPL20A TIF11 RPL16B SSB2 RPL18A RPL3 RPS10A RPS6A RPL5 RPL36B TIF3*
rRNA processing	*RPS8A RPS9B RPS14A RRP42 SSB1 BFR2 RPS18A RPL37B NUG1 RPS24A RPS23A NSR1 ZUO1 NOP10 EBP2 RPS31 RPL37A NOP56 RPS1B RPS16A DBP2 SSB2 KRI1 RPS6A*
Regulation of translation	*RPS9B EFM2 SSB1 PAB1 RPS23A ZUO1 MAM33 STM1 ASC1 PET111 SSB2 GIS2 CAF20 CBP3*
Ribosomal small-subunit biogenesis	*RPS8A RPS9B RPS14A BFR2 RPS18A RPS24A RPS23A NSR1 RPS31 RPS1B RPS16A KRI1 RPS6A*
Transcription from RNA PolII promoter	*HHF1 HMT1 HTB1 HTA1 SWI4 BMH1 RPB3 SOD1 MET4 HIR2 AZF1 TBF1 NHP6A*
Protein Folding	*SSA1 PDI1 SSB1 ZUO1 SSC1 SSA2 TSA1 ERO1 HSC82 YDJ1 SSB2 EGD1*
Translational initiation	*RPG1 PAB1 AIM23 STM1 CLU1 TIF34 TIF11 CDC33 TIF3*
Translational elongation	*RPS9B SSB1 RPS23A ZUO1 STM1 YEF3 ASC1 SSB2 TEF1*

Figure 4.26: **Network analysis of downregulated and translational-related proteins in Adapted refractory cells** - (a) Network of the identified proteins involved in translation. Edges are related to physical interaction between proteins, and their width correlates with consensus number in interaction databases. The network was created with Cytoscape (Cline *et al.* 2007; Saito *et al.* 2012; Shannon *et al.* 2003; Smoot *et al.* 2011), using GeneMANIA plugin (Montojo *et al.* 2010) and only referring to physical interactions among protein. (b) Selection of ribosome and translational proteins in Adapted refractory cells. The list was obtained by performing SGD (Cherry *et al.* 2012) Gene Ontology Slim Mapper (`https://www.yeastgenome.org/cgi-bin/GO/goSlimMapper.pl`) on downregulated proteome of Adapted Cells.

4.3.2 Proteomic Analysis of *tub2-401* Adapted cells

Once we analyzed the proteome of Adapted refractory cells upon Mad2 overexpression, a similar screen was performed for *tub2-401* Adapted cells, whose phenotype was described in Section 4.2. As a control we used *WT* cells, which do not depolymerize microtubules upon semi-restrictive temperature. *WT* and *tub2-401* cells were inoculated in liquid medium at 30°C, and shifted to 21/22°C. After ~20 hours from the shift, cells were collected and processed for LC/MS-MS analysis. In principle, cold-stress response should be the same in both conditions, allowing to appreciate specific up/down-regulations due to the constant SAC activity of *tub2-401* cells.

About 3500 proteins were identified. Unlike the Mad2 overexpression experiment, here we ob-

a)

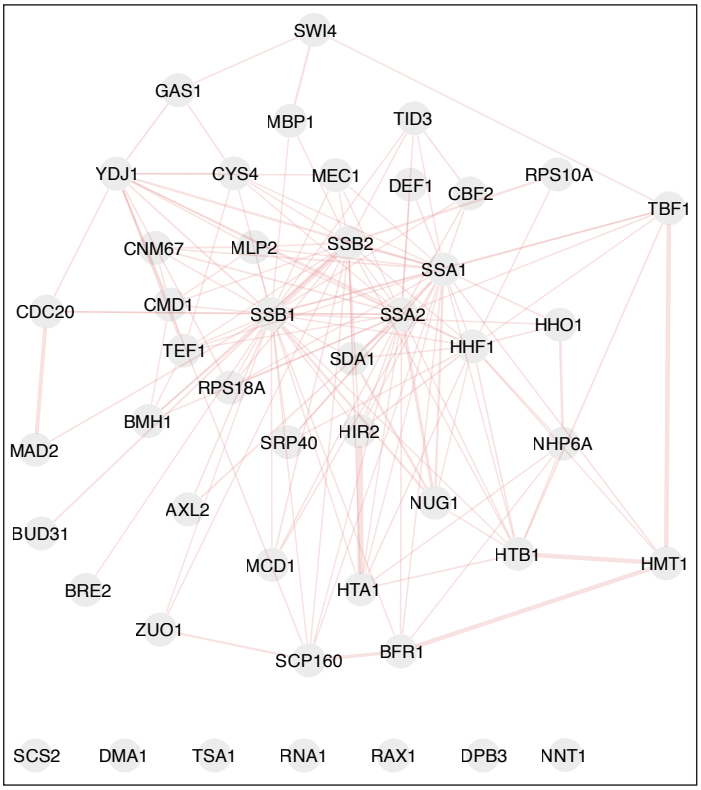

b)

Gene Ontology term	Genes
Nuclear Transport	*SSA1 HMT1 CMD1 SSB1 RPS18A NUG1 SCS2 SDA1 ZUO1 MLP2 SRP40 SSA2 RNA1 YDJ1 SSB2 RPS10A TEF1*
Chromatin organization	*HHF1 MEC1 DPB3 HTB1 HTA1 SCS2 SCP160 BRE2 NNT1 RNA1 GAS1 HIR2 HHO1 TBF1 NHP6A*
Mitotic Cell Cycle	*BUD31 MCD1 MBP1 SWI4 BMH1 CDC20 CBF2 CYS4 SDA1 DMA1 AXL2 MAD2 CNM67 BFR1 RAX1*
Cellular response to DNA damage stimulus	*MEC1 DPB3 MCD1 HTB1 HTA1 BMH1 DEF1 TSA1 NHP6A*
Chromosome segregation	*MCD1 BMH1 CDC20 CBF2 DMA1 NDC80 MAD2 SCP160*
DNA repair	*DPB3 MCD1 HTB1 HTA1 DEF1 NHP6A*

Figure 4.27: **Network analysis of downregulated and cell cycle-related proteins in Adapted refractory cells** - (a) Network of the identified proteins involved in the cell cycle. Edges are related to physical interactions among proteins, and their width correlates with consensus number in interaction databases. The network was created with Cytoscape (Cline *et al.* 2007; Saito *et al.* 2012; Shannon *et al.* 2003; Smoot *et al.* 2011), using GeneMANIA plugin (Montojo *et al.* 2010) and only referring to physical interactions among protein. (b) Selection of cell cycle proteins in Adapted refractory cells. The list was obtained by performing SGD (Cherry *et al.* 2012) Gene Ontology Slim Mapper (`https://www.yeastgenome.org/cgi-bin/GO/goSlimMapper.pl`) on downregulated proteome of Adapted refractory cells.

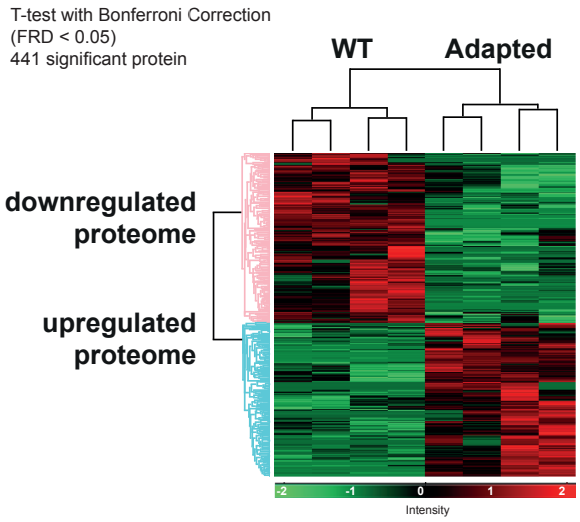

Figure 4.28: **Heatmap of the identified proteome in *tub2-401* Adapted cells** - Out of ~ 3500 proteins, 441 exhibited a significant increase (in red) or decrease (in green) protein abundance in Adapted cells. The analysis was performed on two biological replicates, with two technical replicates, by Vittoria Matafora - Lab of Functional Proteomics (A. Bachi) - IFOM, Milan - IT.

served an increased heterogeneity between different biological replicates, probably reflecting the heterogeneity of spindle depolymerization upon semi-restrictive temperature. Nevertheless, relaxing the False Discovery Rate from 0.01 to 0.05, 441 protein showed significant differences between *WT* and Adapted cells (Figure 4.28). Again, we identified an upregulated and a downregulated proteome.

4.3.2.1 Upregulated proteome of Adapted cells

204 out of 441 detected proteins exhibited an increased protein abundance in Adapted cells as opposed to *WT*. Most of them are involved in metabolic processes (Figure 4.29a), in particular in the TCA cycle and fatty acid biosynthesis (Figure 4.29b). Beyond metabolic effects, we identified proteins involved in the cell cycle (Figure 4.30b). As for *GAL1-MAD2(3x)* Adapted refractory cells, we observed the Gene Ontology terms "mitotic cell cycle", "protein phosphorylation", "DDR". Looking at physical interactions among cell cycle proteins, three of them showed the highest number of interactions: Cdc5, Cdc7, Mcm6 (Figure 4.30a). The first two are kinases, while Mcm6 is a DNA helicase involved in DNA replication. Cdc28, which was detected in Adapted refractory *GAL1-MAD2(3x)* cells, could not be identified here. In general, while the GO categories are similar in both analysis, many individual proteins seem to be typical of the specific approach used to activate the SAC (see Subsection 4.3.3 for details).

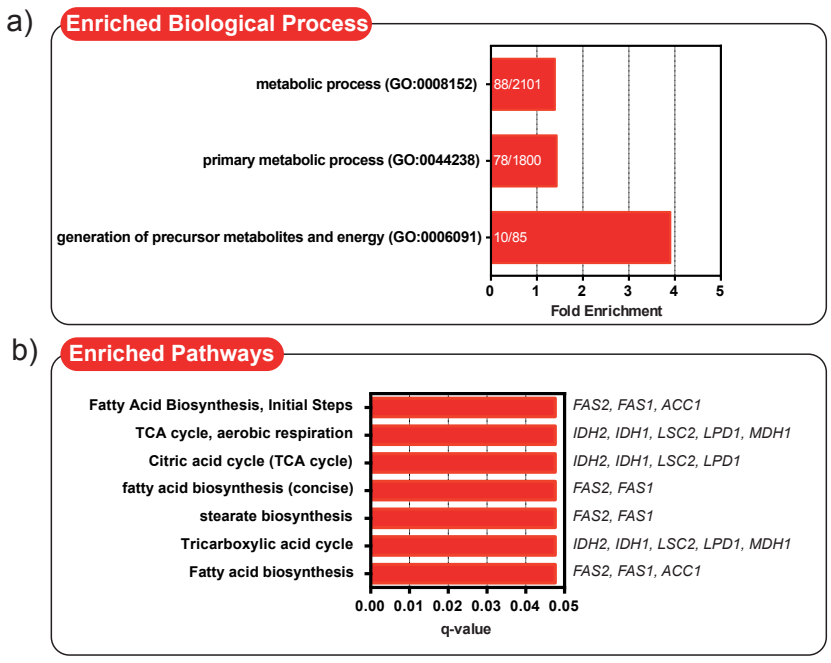

Figure 4.29: **Analysis of Enriched Biological Processes and Pathways in the upregulated proteome of Adapted cells** - (a) Statistical Overrepresentation Test of upregulated proteome in Adapted cells was performed on PANTHER GO-Slim Biological Process entries (Mi *et al.* 2013; Mi *et al.* 2017) (`www.pantherdb.org`). Entries significantly enriched (adjusted p-value < 0.05) are reported, in terms of fold-enrichment compared to the reference list. For each term, the ratio between protein identified in our study and protein in the reference list is reported. (b) - Statistical Overrepresentation Test of upregulated proteome in Adapted cells was performed on ConsensusPathDB-yeast (Herwig *et al.* 2016; Kamburov *et al.* 2013; Kamburov *et al.* 2011; Pentchev *et al.* 2010) Pathway Entries (`cpdb.molgen.mpg.de/YCPDB`). Pathways significantly enriched (q-value < 0.05) are reported, together with the genes obtained from our study.

a)

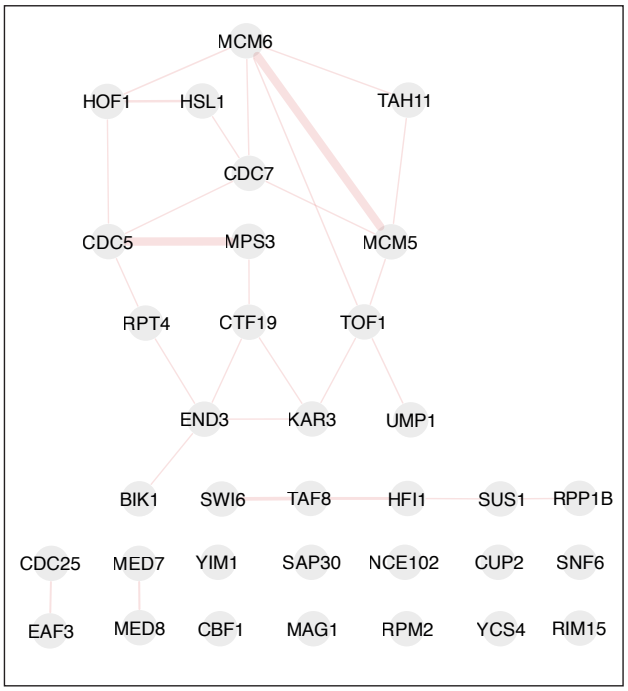

b)

Gene Ontology term	Genes
Transcription from RNA polymerase II promoter	*SUS1 MED8 CUP2 SNF6 CBF1 SWI6 RPM2 TAF8 SAP30 MED7 RPT4 HFI1 EAF3*
Mitotic Cell Cycle	*BIK1 CDC7 MPS3 HSL1 SWI6 YCS4 CDC25 CDC5 HOF1 END3 TOF1 CTF19 KAR3*
Cellular response to DNA damage stimulus	*UMP1 CDC7 MAG1 MCM6 SNF6 TAH11 MCM5 HOF1 YIM1 TOF1 RPT4 EAF3*
Regulation of cell cycle	*CDC7 RIM15 HSL1 SWI6 YCS4 CDC25 CDC5 TOF1 CTF19 KAR3*
DNA repair	*CDC7 MAG1 MCM6 SNF6 TAH11 MCM5 TOF1 RPT4 EAF3*
Protein phosphorylation	*CDC7 RPP1B RIM15 HSL1 CDC5 NCE102*
DNA replication	*CDC7 MCM6 TAH11 MCM5 TOF1 EAF3*
DNA recombination	*CDC7 MCM6 TAH11 SWI6 MCM5 CDC5*

Figure 4.30: **Network analysis of upregulated cell cycle proteins in Adapted cells** - (a) Network of the identified proteins involved in cell cycle processes. Edges are related to physical interaction between proteins, and their width correlates with consensus number in interaction databases. The network was created with Cytoscape (Cline *et al.* 2007; Saito *et al.* 2012; Shannon *et al.* 2003; Smoot *et al.* 2011), using GeneMANIA plugin (Montojo *et al.* 2010) and only referring to physical interactions among protein. (b) Selection of cell cycle protein in Adapted cells. The list was obtained by performing SGD (Cherry *et al.* 2012) Gene Ontology Slim Mapper (`https://www.yeastgenome.org/cgi-bin/GO/goSlimMapper.pl`) on upregulated proteome of Adapted cells.

4.3.2.2 Downregulated proteome of Adapted cells

We also found 237 proteins downregulated in Adapted cells. Despite the absence of significantly enriched pathways, we were able to observe significant enriched GO terms (Figure 4.31). The major enrichments were observed in cellular component biogenesis and, similarly to Mad2 overexpression (Section 4.3.1.2), in RNA metabolic process. Indeed, several proteins were involved in rRNA processing, biogenesis of ribosomal subunits and protein folding (Figure 4.32).

Among cell cycle components, we identified proteins involved in mitosis, protein phosphorylation, DNA damage and DNA replication (Figure 4.33b). In particular, we identified α-tubulin Tub1 and its paralog Tub3, together with β-tubulin Tub2, suggesting a general decrease in tubulin levels upon microtubule depolymerization. Decrease of Tub1 levels was also confirmed by Western Blot analysis (Figure 4.35b). Tub1 and Tub2 were the proteins with the highest number of physical interactions in the network (Figure 4.33a).

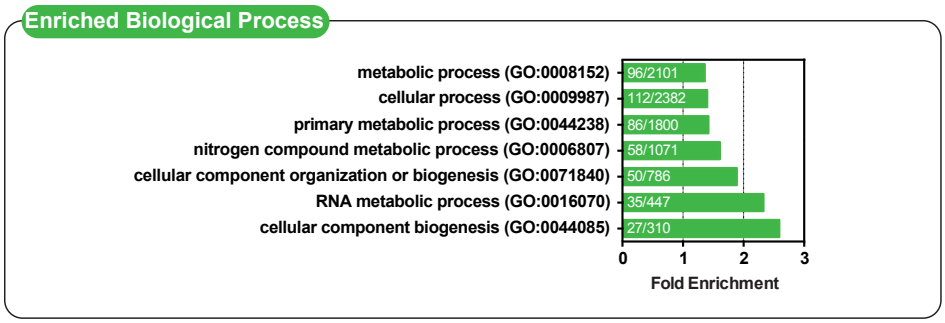

Figure 4.31: **Analysis of Enriched Biological Processes and Pathways in the downregulated proteome of Adapted cells** - Statistical Overrepresentation Test of downregulated proteome in Adapted cells was performed on PANTHER GO-Slim Biological Process entries (Mi *et al.* 2013; Mi *et al.* 2017) (`www.pantherdb.org`). Entries significantly enriched (adjusted p-value < 0.05) are reported, in terms of fold-enrichment compared to the reference list. For each term, the ratio between protein identified in our study and protein in the reference list is reported.

a)

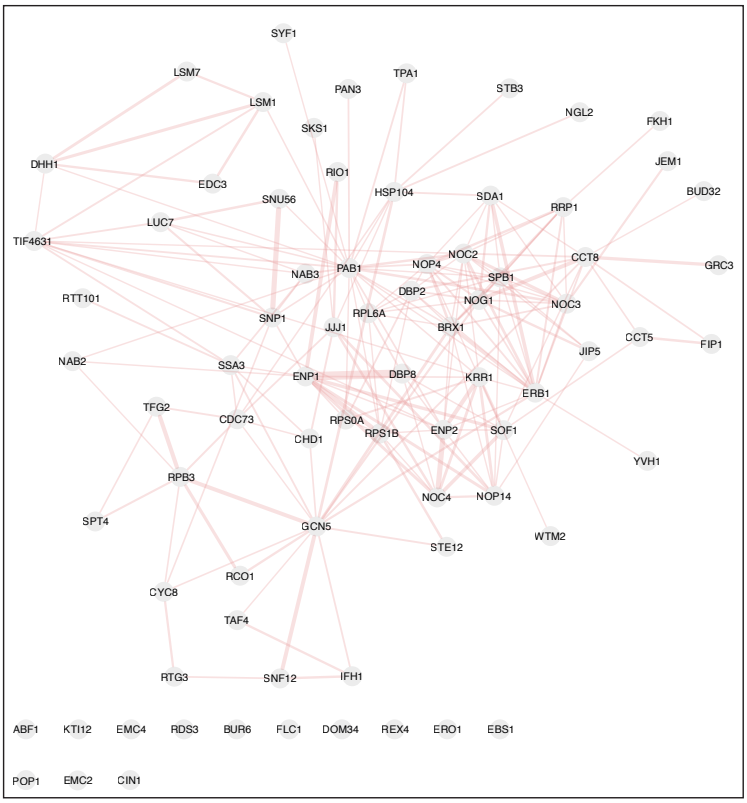

b)

Gene Ontology term	Genes
rRNA processing	*ENP1 SPB1 KRR1 NOP14 RRP1 SPT4 ENP2 RPS0A DBP8 SOF1 GRC3 NOC3 RPS1B ERB1 NGL2 DBP2 LSM7 POP1 JJJ1 REX4 RIO1 NOP4 NOG1 NOC4*
transcription from RNA polymerase II promoter	*RTG3 CYC8 STB3 BUR6 CHD1 TFG2 SPT4 GCN5 BUD32 STE12 RPB3 KTI12 ABF1 IFH1 CDC73 TAF4 RCO1 SNF12 WTM2 SKS1 NAB3 FKH1*
RNA catabolic process	*DHH1 EBS1 EDC3 TPA1 PAB1 NAB2 RTT101 LSM1 PAN3 DOM34 DBP2 LSM7 POP1 NAB3*
Ribosomal large subunit biogenesis	*SPB1 TIF4631 SDA1 YVH1 GRC3 RPL6A ERB1 JJJ1 BRX1 REX4 NOC2 NOP4 NOG1 JIP5*
mRNA processing	*LUC7 SNU56 SYF1 NAB2 SPT4 SNP1 FKH1 FIP1 CDC73 LSM7 NAB3 RDS3*
Ribosomal small subunit biogenesis	*ENP1 KRR1 NOP14 ENP2 RPS0A DBP8 SOF1 RPS1B LSM7 RIO1 NOC4*
Protein folding	*SSA3 EMC4 CCT8 JEM1 CCT5 EMC2 HSP104 ERO1 CIN1 FLC1*

Figure 4.32: **Network analysis of downregulated and translational-related proteins in Adapted cells** - (a) Network of the identified proteins involved in translation. Edges are related to physical interaction between proteins, and their width correlates with consensus number in interaction databases. The network was created with Cytoscape (Cline *et al.* 2007; Saito *et al.* 2012; Shannon *et al.* 2003; Smoot *et al.* 2011), using GeneMANIA plugin (Montojo *et al.* 2010) and only referring to physical interactions among protein. (b) Selection of ribosome and translational proteins in Adapted cells. The list was obtained by performing SGD (Cherry *et al.* 2012) Gene Ontology Slim Mapper (`https://www.yeastgenome.org/cgi-bin/GO/goSlimMapper.pl`) on downregulated proteome of Adapted cells.

a)

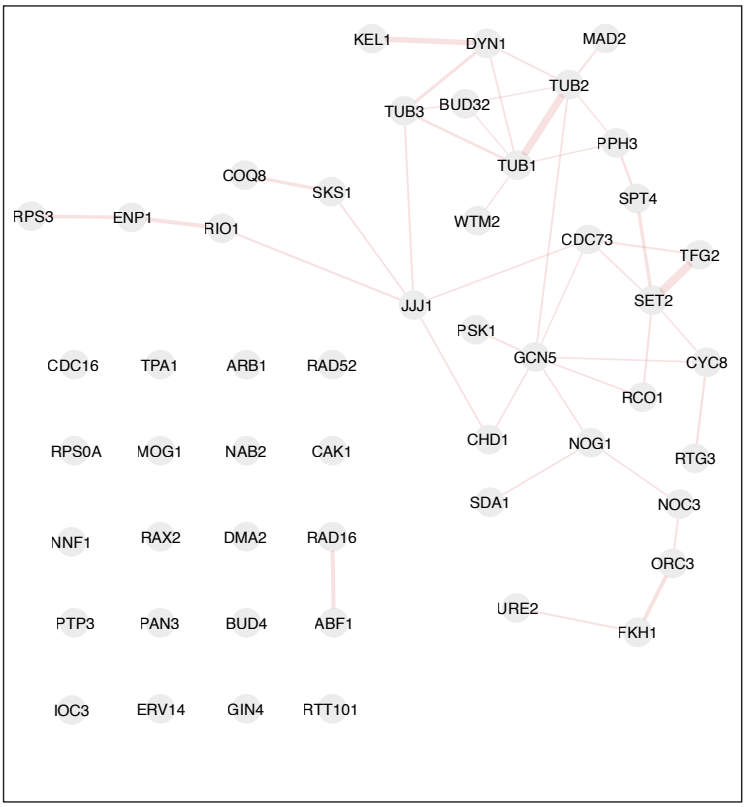

b)

Gene Ontology term	Genes
Mitotic cell cycle	*GIN4 CAK1 TUB2 ERV14 SDA1 BUD32 KEL1 FKH1 MAD2 RTT101 BUD4 DYN1 RAX2 TUB1 TUB3 DMA2 RIO1*
Nuclear transport	*RTG3 ENP1 ARB1 NAB2 RPS0A SDA1 MOG1 RPS3 JJJ1 URE2 NOG1*
Cellular response to DNA damage stimulus	*CYC8 RAD16 PPH3 TPA1 SPT4 PAN3 ABF1 CDC73 RAD52 WTM2*
Regulation of cell cycle	*PPH3 GIN4 SDA1 KEL1 FKH1 MAD2 RTT101 SET2 DMA2 RIO1*
Protein phosphorylation	*PSK1 GIN4 PTP3 CAK1 COQ8 BUD32 CDC73 RIO1 SKS1*
DNA replication	*CHD1 FKH1 RTT101 SET2 CDC16 ABF1 ORC3 NOC3 RCO1*
Chromosome segregation	*TUB2 IOC3 SPT4 MAD2 NNF1 DYN1 TUB1 TUB3 DMA2*
DNA repair	*RAD16 PPH3 TPA1 SPT4 PAN3 ABF1 CDC73 RAD52*
Regulation of DNA metabolic process	*PPH3 CHD1 SPT4 FKH1 SET2 CDC16 CDC73 RCO1*
DNA-templated transcription, elongation	*CHD1 TFG2 SPT4 GCN5 FKH1 SET2 CDC73 RCO1*

Figure 4.33: **Network analysis of downregulated and cell cycle-related proteins in Adapted cells** - (a) Network of the identified proteins involved in cell cycle. Edges are related to physical interaction between proteins, and their width correlates with consensus number in interaction databases. The network was created with Cytoscape (Cline *et al.* 2007; Saito *et al.* 2012; Shannon *et al.* 2003; Smoot *et al.* 2011), using GeneMANIA plugin (Montojo *et al.* 2010) and only referring to physical interactions among protein. (b) Selection of cell cycle proteins in Adapted cells. The list was obtained by performing SGD (Cherry *et al.* 2012) Gene Ontology Slim Mapper (`https://www.yeastgenome.org/cgi-bin/GO/goSlimMapper.pl`) on downregulated proteome of Adapted cells.

4.3.3 Towards general properties of Adapted refractory cells

We asked whether general properties of refractoriness to the checkpoint can be found, independently from the type of SAC-inducing stimulus. To this purpose, we merged the sets of proteins obtained with the two experimental approaches (Figure 4.34). The resulting intersections do not exhibit significant enrichment of GO entries or pathways, maybe due to the low number of proteins for each subset. However, many GO entries and pathways are similar in the two upregulated and the downregulated proteomes. In particular, we saw a decreased protein abundance of protein involved in ribosome biogenesis or translational control in both system. On the other hand, the upregulated proteome was enriched not only in metabolic processes, but also in cell cycle genes, related to DDR or mitosis.

Even if we could not retrieve Cdc28 among the proteins upregulated in both the experimental approaches, by Western Blot we confirmed the increased protein abundance of Cdc28 in *GAL1-MAD2(3x)* Adapted refractory cells (Figure 4.35a), and we confirmed this result on *tub2-401* Adapted cells (Figure 4.35b).

At this stage, there are different aspects of Adapted refractory cells to be characterized. In the next section, we focus our analysis on Cdc28, trying to understand how its activity could promote Refractoriness to the Mitotic Checkpoint.

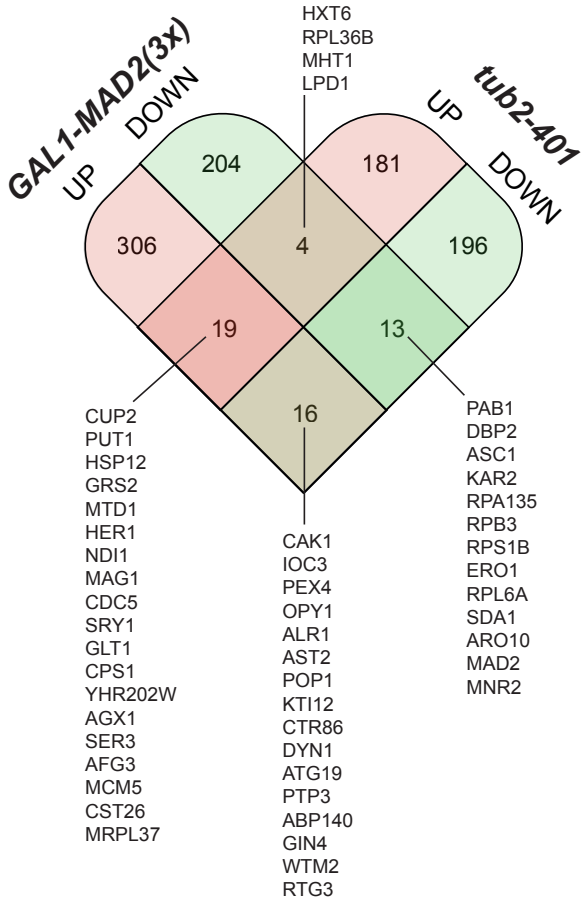

Figure 4.34: **Merging data from *GAL1-MAD2(3x)* and *tub2-401* Adapted cells** - Upregulated (UP) and downregulated (DOWN) proteomes coming from *GAL1-MAD2(3x)* adapted refractory and *tub2-401* adapted cells were merged. For each intersection, number of protein was reported, together with the resulting list.

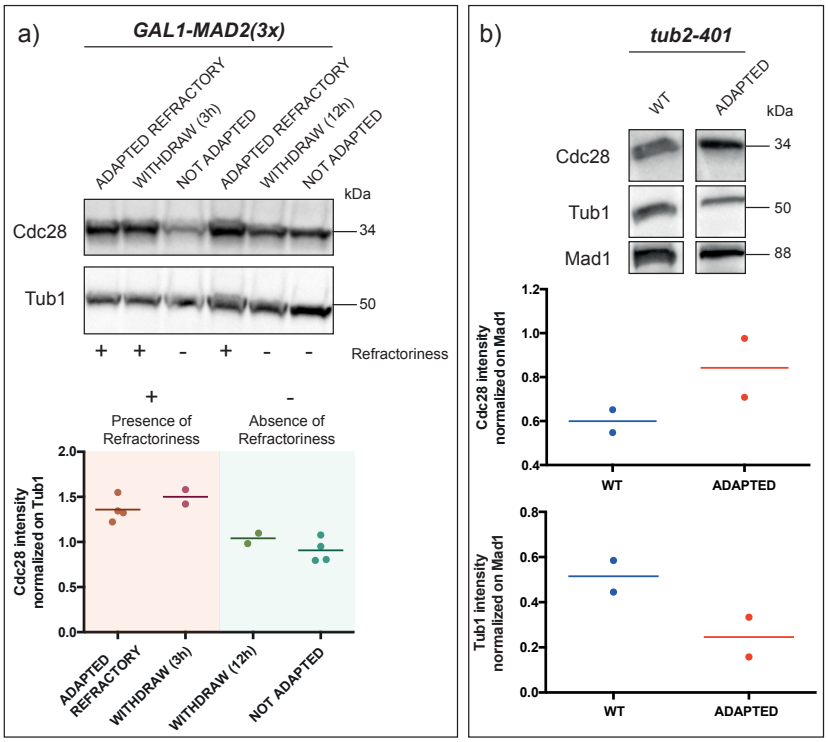

Figure 4.35: **Western Blot analysis on some candidates** - (a) Checking levels of Cdc28 in *GAL1-MAD2(3x)* Adapted refractory cells. *tetO$_2$-CDC20-127(1x), GAL1-MAD2(3x)* (yAC2807) cells were grown as Adapted refractory, not Adapted and Withdraw(3h) and Withdraw(12h), as reported in Section 4.1 (Subsection 4.1.4, Figure 4.8a). Cells were sampled for Western Blot analysis. Cdc28 signal was then normalized to the housekeeping protein Tub1, and compared between the four conditions. (b) Checking levels of Cdc28 and Tub1 in *tub2-401* Adapted cells. *MATa WT* (yAC3717) and *MATa tub2-401* (yAC3220) cells were inoculated in liquid medium at 30°C, and after 9.5h they were shift to 22°C. After 21h, cells were collected for Western Blot analysis. Using Mad1 as housekeeping proteins, levels of Cdc28 and Tub1 were revealed and quantified. For each dot plot of a) and b), each dot correspond to a technical replica, while the line represent the mean value of replicates. These Western Blot were performed by Elena Chiroli.

4.4 Testing the Role of Cdc28 and APC/C activity in Adapted refractory cells

Among the possible candidates emerged in the MS screening (Section 4.3), we were intrigued by the role of Cdc28 in adapted refractory cells. In budding yeast, an active Cdc28 is essential for exit from mitosis (Rudner *et al.* 2000), and in particular Cdc28-mediated phosphorylation of APC/C is required for stimulation of Cdc20-dependent APC/C activity during anaphase onset (Rudner & Murray 2000). Since APC/C phosphorylation is required for adaptation to the SAC (Vernieri *et al.* 2013; Rudner & Murray 2000), we speculate that increased levels of Cdc28 may correlate with a hyper-phosphorylation of APC/C after adaptation, establishing a hyperactive APC/C in adapted refractory cells. This hypothesis would explain the faster mitotic timing of *GAL1-MAD2(3x)* adapted refractory cells. In this section, we report preliminary experiments performed to validate this hypothesis.

a)

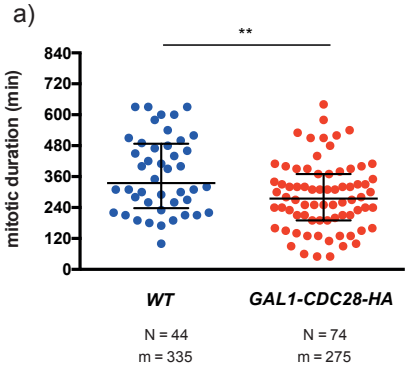

b)

	Adapting Cells	Cell with high levels of Clb2 at the end of the movie	Cells dying with high levels of Clb2	Total Cell Number
GAL1-CDC28-HA	130	1	3	134
GAL1-CDC28-HA cdc16-6A cdc27-5A	66	58	68	192

c)

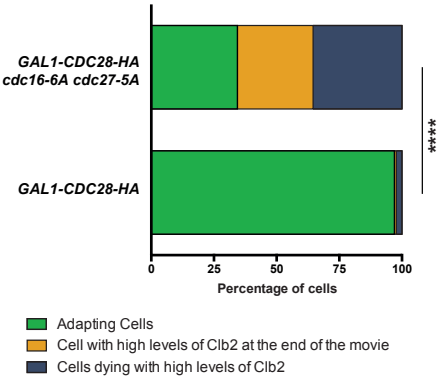

Figure 4.36: **Overexpression of Cdc28 promotes APC/C:Cdc20 activity in nocodazole-arrested cells** - (a) Comparison between mitotic timings. *MATa, MAD2-GFP, CLB2-mCherry* (yAC3538) and *MATa, MAD2-GFP, CLB2-mCherry, GAL1-CDC28-HA* (yAC3723) cells were synchronized in G1 in liquid YEPR, and then released in microfluidic chamber in YEPRG supplemented with nocodazole 15 $\mu g/ml$. After 1.5h from release, α-factor was readded, in order to re-synchronize cells in G1 after their adaptation. Cells were monitored for 18h. For both conditions, timespan between Clb2 increase and decrease was estimated and defined as mitotic duration, in a similar way as described in Section 4.1, but using an automatic procedure in MATLAB® setup by Paolo Bonaiuti (Bonaiuti *et al.* 2017). Statistical analysis was performed with GraphPad Prism ®, using Wilcoxon-Mann-Whitney Test (significance level 0.05). N: number of observation. m: median of population. For each population, median and interquartile range were reported. The significant difference between these two population was observed in two biological replicates. (b) *MATa, MAD2-GFP, CLB2-mCherry, GAL1-CDC28-HA* (yAC3723) and *MATα, MAD2-GFP, CLB2-mCherry, GAL1-CDC28-HA, cdc16-6A, cdc27-5A* (yAC3810) cells were grown in YEPR. Then, from asynchronous conditions they were released in microfluidic chamber in YEPRG supplemented with nocodazole 15 $\mu g/ml$. Cells were monitored for 18h. For each strain, we count the number of cells undergoing these events: adapting cells, cells with high levels of Clb2 after 18h, cells that were dying with high levels of Clb2. In the contingency table, number of these events is reported. (c) Bar plot of the observed phenomenon in b), reported as percentage. Statistical analysis was performed with GraphPad Prism ®, using χ-square Test (significance level 0.05).

4.4.1 Overexpression of Cdc28 anticipates adaptation to the SAC in nocodazole-arrested cells

We reasoned that if increased Cdc28 levels correspond to an increased activity of APC/C^{Cdc20}, then cells with extra-amount of this kinase will anticipate adaptation to the SAC. We thus ectopically induced overexpression of Cdc28 under a galactose-inducible promoter (*GAL1-CDC28-HA* (Rudner *et al.* 2000)) in nocodazole arrested cells, and we tested whether adaptation was anticipated in these cells respect to *WT*. We also proved that overexpression of Cdc28 was not altering an unperturbed cell cycle (see Appendix). *WT* and *GAL1-CDC28-HA* were grown in raffinose, synchronized in G1, and grown in microfluidic chamber under a constant flow of medium supplemented with galactose and nocodazole 15 $\mu g/ml$. We measured in single cells the degradation timing of a tagged version of mitotic cyclin B (Clb2-mCherry) as a readout for APC/C^{Cdc20} activity. We defined adaptation as the condition of Clb2 degradation in the presence of localized Mad2, which we also followed at the single cell level (Bonaiuti *et al.* 2017). We found that adaptation to the SAC is anticipated in the presence of ectopic *CDC28* overexpression (Figure 4.36a). In order to test whether APC/C^{Cdc20} was the target of high levels of Cdc28, we introduced in *GAL1-CDC28-HA* cells a non-phosphorylatable mutant of APC/C (*cdc16-6A cdc27-5A*), which has defects in binding Cdc20 (Rudner & Murray 2000). In these cells, the proportion of cells dying in mitosis with high levels of Clb2 or without performing adaptation after 18h of imaging increased significantly compared to *GAL1-CDC28-HA* cells with a functional APC/C (Figure 4.36b). Taken together, these data suggest a role of high levels of Cdc28 in promoting APC/C phosphorylation and thus APC/C^{Cdc20} activity during a mitotic arrest.

4.4.2 Evaluating APC/C phosphorylation in the presence of high levels of Cdc28

To confirm that high Cdc28 levels facilitate adaptation by phosphorylating APC/C, we looked at APC/C phosphorylation. We expect *GAL1-CDC28-HA* to have APC/C more phosphorylated than *WT* cells in a nocodazole-arrest. Moreover, adapted refractory cells should have already reached a high APC/C phosphorylated levels, and thus in adapted refractory cells APC/C phosphorylation should be higher than adapting cells. In the next subsections, we investigate APC/C phosphorylation, and in particular that of two APC/C subunits, Cdc16 and Cdc27, which play a key role in activating APC/C^{Cdc20} and promoting adaptation to the SAC (Vernieri *et al.* 2013; Rudner *et al.* 2000; Rudner & Murray 2000), as mentioned in the Introduction.

4.4.2.1 Phosphorylation of Cdc16 and Cdc27 in adapted refractory cells

Since our preliminary observation of an active APC/C^{Cdc20} comes from adapted refractory cells upon Mad2 overexpression (Section 4.1), we evaluated phosphorylation of Cdc16 and Cdc27 in these cells, using Phos-Tag Western Blot (Kinoshita *et al.* 2006; Kinoshita *et al.* 2009).

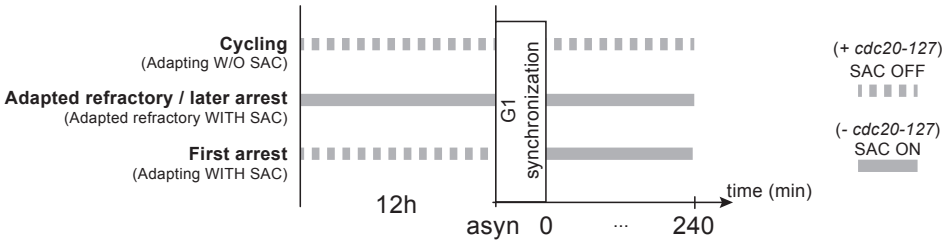

Figure 4.37: **Experimental setup for evaluation of phosphorylated APC/C in adapted refractory cells** - *MATa, $tetO_2$-CDC20-127(1x), GAL1-MAD2(3x), CDC27-MYC* (yAC3754) and *MATa, $tetO_2$-CDC20-127(1x), GAL1-MAD2(3x), CDC16-MYC* (yAC3770) were grown as cycling, adapted refractory and first arrest. For each condition, the corresponding name related to the experimental setup discussed in Section 4.1 is reported (see Subsection 4.1.4 for details). Cells were synchronized in G1 by α-factor and released to galactose-containing medium, supplemented or not with doxycycline 10 $\mu g/ml$ in order to repress or allow cdc20-127 synthesis. After 90' from release, α-factor was readded, in order to resynchronize cells in the subsequent G1. Cells were monitored for 4 hours.

From *$tetO_2$-CDC20-127(1x) GAL1-MAD2(3x) CDC27-MYC* cells, we reproduced three population (Figure 4.37): *Cycling*, corresponding to cells that overexpress Mad2 without arresting in mitosis; *Adapted refractory / later arrest*, representing a population of adapted refractory cells; *First arrest*, in which a first mitotic block was induced. These populations refer to the corresponding conditions of Adapting W/O SAC, Adapted refractory WITH SAC and Adapting WITH SAC cells (Figure 4.37), like described in Section 4.1 (see Subsection 4.1.4).

Cells were synchronized in G1 and released in the continuous Mad2 overexpression. We identified critical timepoints for describing the metaphase-to-anaphase transition, keeping track of the percentage of metaphase and anaphase spindles (Figure 4.38a). In particular, the proportion of anaphase spindles in Adapted refractory cells increased between 1 and 2 hours from G1 release (Figure 4.38a, Adapted refractory/later arrest, green box). These data suggest that APC/C^{Cdc20} activity should take place in this timespan. During a first arrest, instead, cells slowly progressed into anaphase (Figure 4.38a, First Arrest), with about 80% of them being arrested in metaphase after 2h from G1 release. In view of these observations, we expected Cdc27 phosphorylation to be higher in Adapted refractory cells than in First arrest cells, between 1 and 2 hours from G1 release. Phos-Tag Western Blot analysis however showed a different result (Figure 4.38b-c). Cycling cells showed the highest phosphorylation at 60', while Adapted refractory cells 90' after G1 release (Figure 4.38b). This result is in agreement with the fact the Adapted refractory cells have a slower mitosis than Cycling cells, as was previously reported on Section 4.1. When we compared Adapted refractory cells to cells experiencing the arrest for the first time, the minimum amount of mitotic Cdc27 phosphorylation was observed in Adapted re-

fractory cells (Figure 4.38c). Taken together, these data suggest the absence of a hyperphosphorylated Cdc27 in Adapted refractory cells, which rather seem to need to reach a lower APC/C phosphorylated state to trigger adaptation.

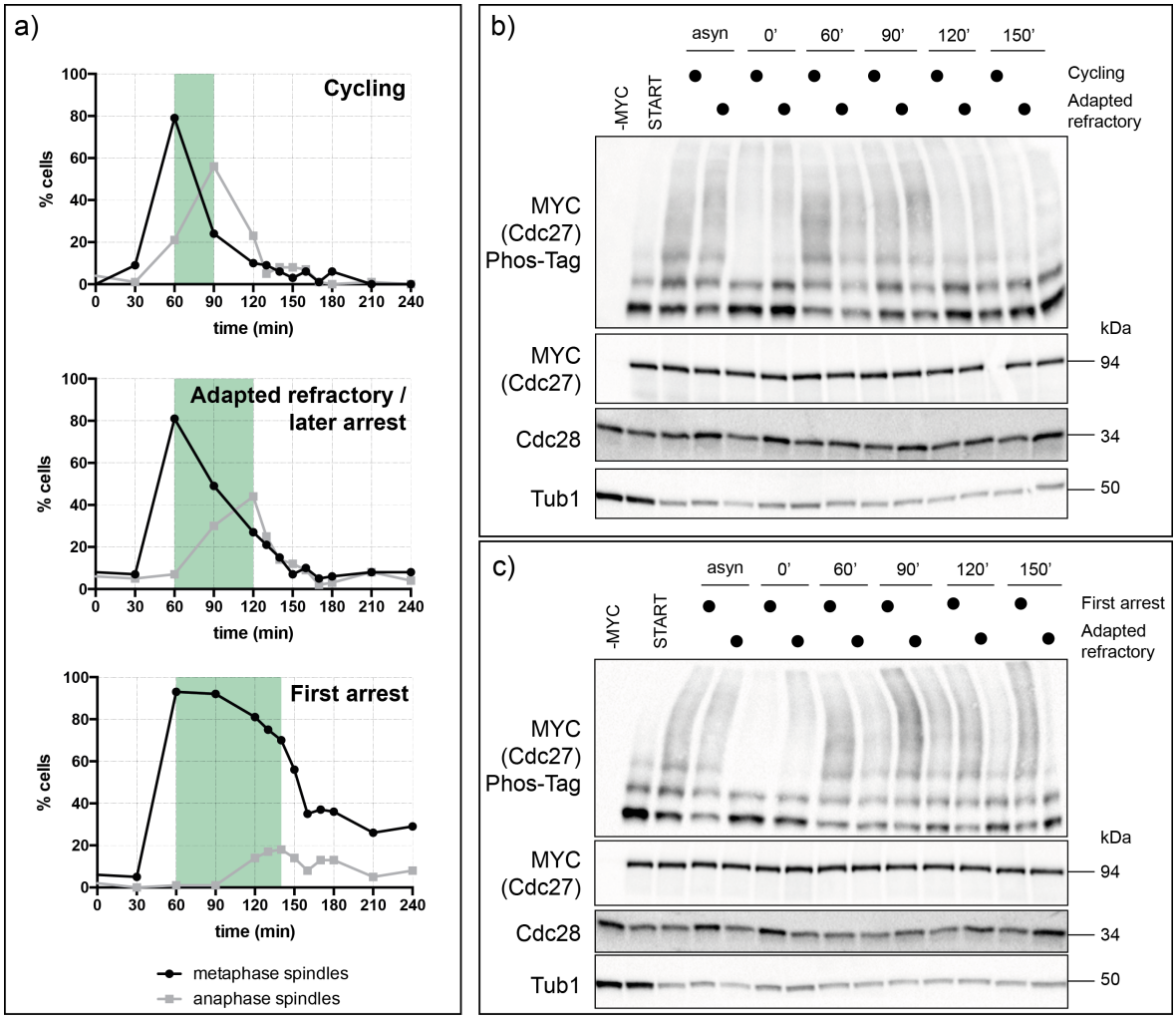

Figure 4.38: **Evaluating Cdc27 phosphorylation in Adapted refractory cells** - *tetO$_2$-CDC20-127(1x), GAL1-MAD2(3x), CDC27-MYC* (yAC3754) cells were grown as indicated in Figure 4.37, and samples were taken for Western Blot analysis (b-c) and for immunofluorescence (IF,a) against α-tubulin. (a) IF analysis. 100 cells were counted for each condition and for each timepoint, evaluating proportion of cells with interphase, metaphase or anaphase spindles. Proportion of metaphase and anaphase spindle is plotted versus time, and the green box represents the timespan between peaks of metaphase and anaphase spindles. (b-c) Western Blot analysis. Regular 10% and Phos-Tag 7.5% Western Blot were run, in order to compare (b) Adapted refractory versus Cycling cells and (c) Adapted refractory versus First Arrest cells.

Next, we performed a similar analysis on Adapted refractory cells for Cdc16. Compared to the previous case, here we encountered more technical difficulties in performing Phos-Tag Western Blot: we could not clearly distinguish different phosphorylated forms like in the previous case. However, a smear can be appreciated in the presence of phosphorylated Cdc16, in particular by adjusting gel composition (see Material and Methods) and modulating chemiluminescence exposure time. Based on the time of metaphase-to-anaphase transition as detected by spindle percentages, we expected to see Cdc16 phosphorylation higher in Adapted refractory than First arrest cells between 90' and 135'

from G1 release (Figure 4.39a). Unfortunately, due to technical reasons, the comparison between Cycling and Adapted refractory cells could not be performed. Nevertheless, Adapted refractory cells reach the highest phosphorylation of Cdc16 at 90', while First arrest cells at 120'/150' (Figure 4.39b). Moreover, at 90' we could appreciate a slight increase of Cdc16 phosphorylation in Adapted refractory cells compared to that of cells during a First arrest, by long exposure time (Figure 4.39b-c) or by increasing the loading volume in Phos-Tag Western Blot (Figure 4.39c). These results suggest that Adapted refractory cells reach a slight increased phosphorylation of Cdc16 in a faster way respect to cells experiencing a first mitotic arrest (Figure 4.39b).

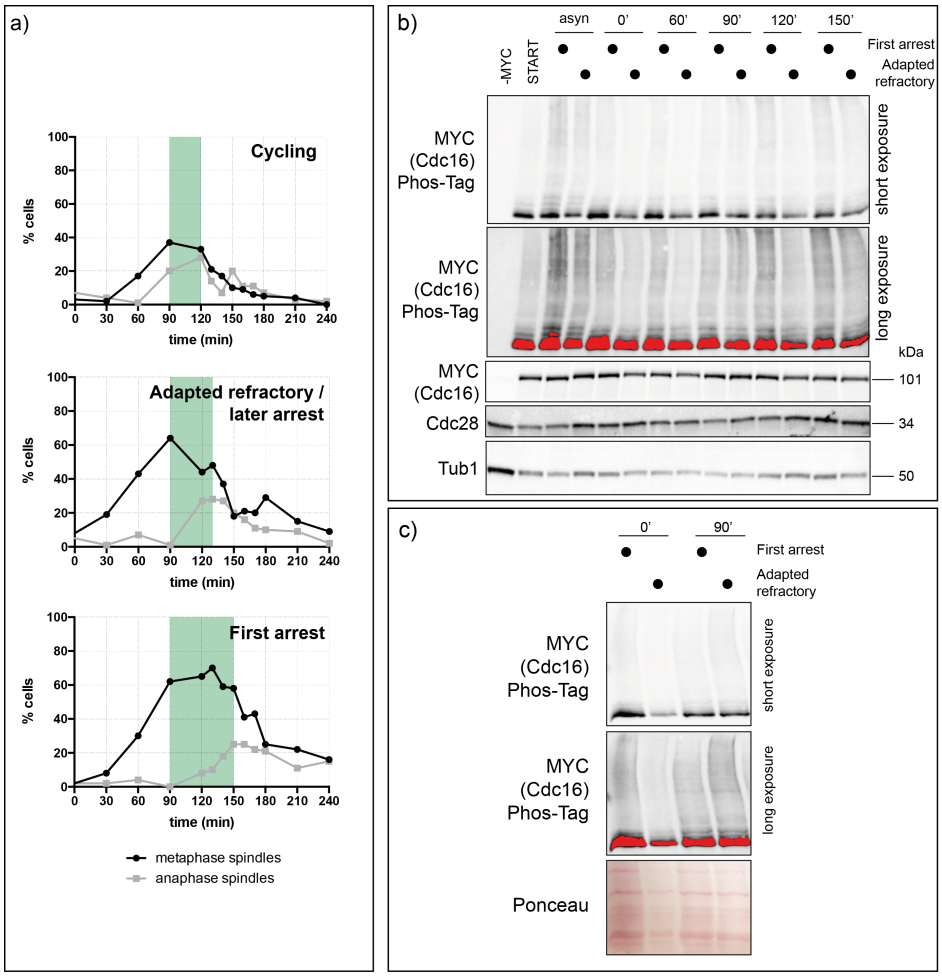

Figure 4.39: **Evaluating Cdc16 phosphorylation in Adapted refractory cells** - *MATa, tetO$_2$-CDC20-127(1x), GAL1-MAD2(3x), CDC16-MYC* (yAC3770) cells were grown as indicated in Figure 4.37, and samples were taken for Western Blot analysis (b-c) and for immunofluorescence (IF,a) against α-tubulin. (a) IF analysis. 100 cells were counted for each condition and for each timepoint, evaluating proportion of cells with interphase, metaphase or anaphase spindles. Proportion of metaphase and anaphase spindle is plotted versus time, and the green box represents the timespan between peaks of metaphase and anaphase spindles. (b-c) Western Blot analysis. Regular 10% and Phos-Tag 7.5% Western Blot were run, in order to compare Adapted refractory versus First arrest cells.

In summary, we could not see any increased phosphorylation for Cdc27, and a slight one for Cdc16.

4.4.2.2 Ectopic overexpression of *CDC28* does not increase the amount of phosphorylated Cdc16

Experimental data suggest the presence of high levels of Cdc28 and slightly increased phosphorylation of APC/C (Cdc16) in Adapted refractory cells upon Mad2 overexpression. These results could explain the shorter mitotic arrest of adapted refractory cells. We thus tested whether high doses of Cdc28 increased Cdc16 phosphorylation. To this purpose, we measured Cdc16 phosphorylation in *GAL1-CDC28-HA* cells arrested in nocodazole (Figure 4.40a). Preliminary data rather show that *WT* cells have a larger amount of phosphorylated Cdc16 than *GAL1-CDC28-HA* cells after 3h of nocodazole arrest.

These results are somehow hard to reconcile with our previous observation. *GAL1-CDC28-HA* may have started to exit from mitosis after 3h of nocodazole, therefore reducing the average mitotic phosphorylation of Cdc16. Otherwise, high levels of Cdc28 per se may not be sufficient to increase mitotic APC/C phosphorylation. We are going to discuss these results in the Discussion.

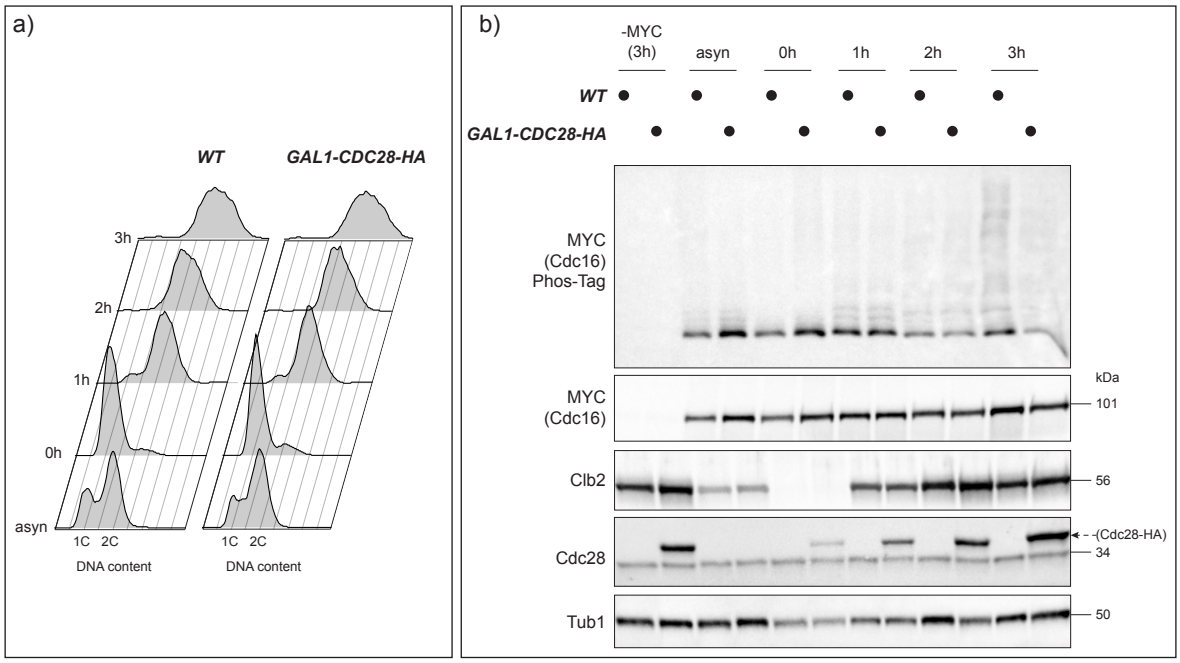

Figure 4.40: **Evaluating Cdc16 phosphorylation in *GAL1-CDC28-HA* cells arrested in nocodazole** - *MATa, CDC16-MYC* (yAC1936) and *MATa, CDC16-MYC, GAL1-CDC28-HA* (yAC3854) cells were grown in raffinose, synchronized in G1 and released in medium containing galactose and nocodazole 15 $\mu g/ml$. Cells were monitored for 3 hours, and every hour sample for FACS analysis (a) and Western Blot (b) were taken. (a) FACS profiles of the experiment (b) Regular 10% and Phos-Tag 7.5% Western Blot related to the experiment.

4.4.3 High levels of Cdc28 and viability of adapted cells: Mitotic Exit Network may play a role

High Cdc28 levels may help cells to perform the metaphase-to-anaphase transition during an active SAC, anticipating the anaphase onset (though we have not demonstrated it). However, they may hinder

mitotic exit. It has been shown that high levels of Cdc28 activity do not allow cells to exit (Cross 2003). Hence, we asked whether the condition of adapted cells would make them sensitive on the mechanisms that control Clb2 degradation after anaphase.

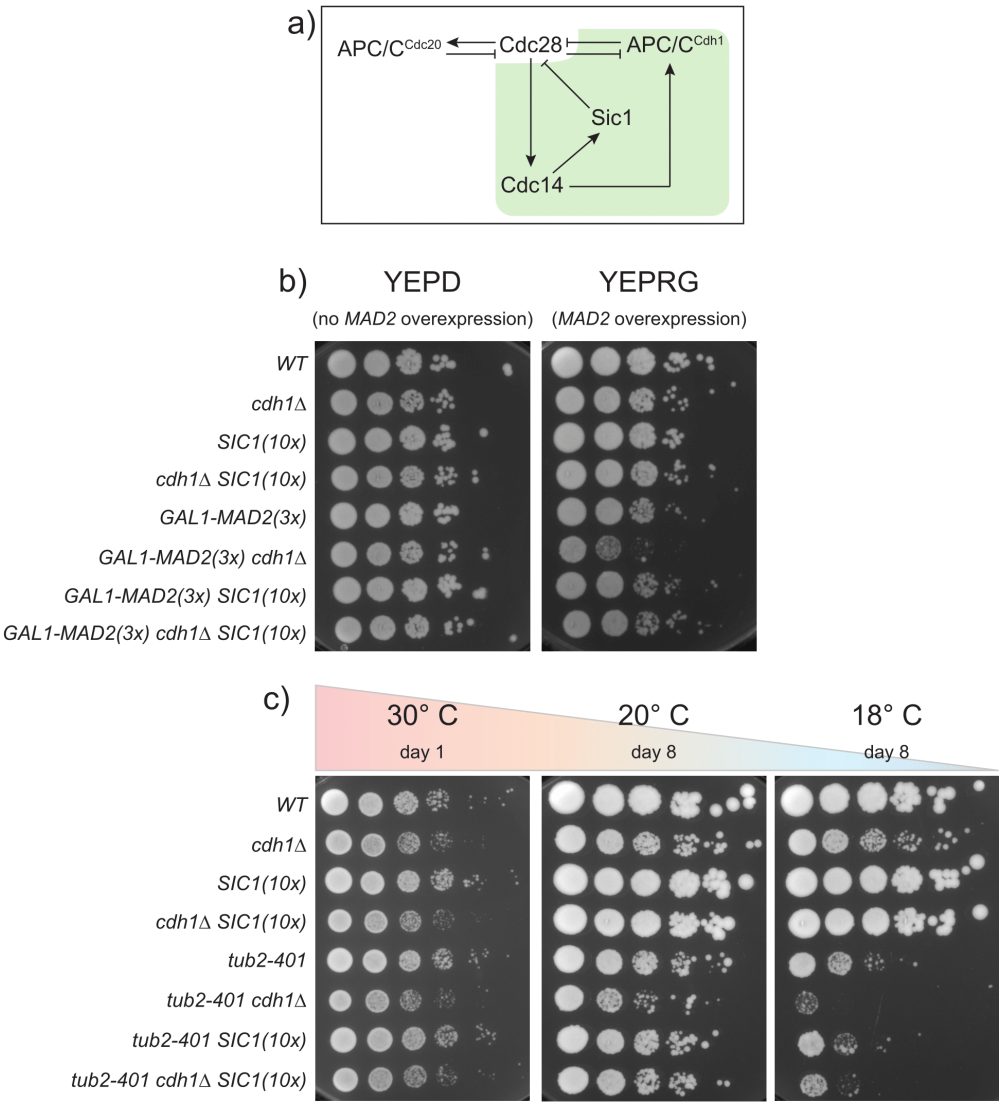

Figure 4.41: **MEN plays a role in ensuring viability of Adapted cells** - (a) A possible working model for Mitotic Exit Network (MEN) in ensuring viability of Adapted cells. While a first inhibition of Clb2:Cdc28 is performed by APC/C^{Cdc20}, a second one is performed by APC/C^{Cdh1} and Sic1 activity. (b) *MATa WT* (yAC3568), *MATa cdh1*Δ (yAC1533), *MATa SIC1(10x)* (yAC3650), *MATa cdh1*Δ *SIC1(10x)* (yAC3683), *MATa GAL1-MAD2(3x)* (yAC2465), *MATa GAL1-MAD2(3x) cdh1*Δ (yAC3582), *MATa GAL1-MAD2(3x) SIC1(10x)* (yAC3654), *MATa GAL1-MAD2(3x) cdh1*Δ *SIC1(10x)* (yAC3659) cells were grown in liquid medium containing raffinose. Then, they were diluted to ∼ 2e+8 cell/ml and serial dilutions and spotting were performed on agar plates, which were incubated at 30°C and monitored. (c) *MATa WT* (yAC3568), *MATa cdh1*Δ (yAC1533), *MATa SIC1(10x)* (yAC3650), *MATa cdh1*Δ *SIC1(10x)* (yAC3683), *MATa tub2-401* (yAC3220), *MATa tub2-401 cdh1*Δ (yAC3686), *MATa tub2-401 SIC1(10x)* (yAC3685), *MATa tub2-401 cdh1*Δ *SIC1(10x)* (yAC3694) cells were grown in liquid medium. Then, they were diluted to ∼ 2e+8 cell/ml and serial dilutions and spotting were performed on agar plates, which were incubated at 30, 20 and 18°C and monitored.

Cdh1 is a co-factor of APC/C that plays a key role in the process. When we deleted it, viability of *GAL1-MAD2(3x)* adapted refractory cells was reduced (Figure 4.41b), even if they adapt similarly to *GAL1-MAD2(3x) CDH1* (Vernieri *et al.* 2013) . Viability of adapted refractory cells was rescued by

the overexpression of the cyclin-dependent kinase inhibitor Sic1 - *SIC1(10x)* (Thornton & Toczyski 2003) - (Figure 4.41b), suggesting that proliferation of Adapted refractory cells is affected when high levels of Clb2:Cdc28 are present after the anaphase onset. This result is also reproduced by activating SAC in *tub2-401* mutants at restrictive temperatures (Figure 4.41c), exhibiting a property which seems to be independent from the SAC-inducing stimulus. Data show a role for Mitotic Exit Network (MEN) in the cell cycle of adapted cells (Figure 4.41a).

5 Discussion

Cells resume proliferation after adaptation

Upon prolonged SAC activation, cells perform metaphase-to-anaphase transition in the presence of an active SAC. We call this event *adaptation* (Bonaiuti *et al.* 2017; Vernieri *et al.* 2013), and cells experiencing it as *adapting* (Figure 5.1, red box). Cells arrest in mitosis and adapt after several hours (Bonaiuti *et al.* 2017; Vernieri *et al.* 2013; Rossio *et al.* 2010b), thanks to APC/C^{Cdc20} activation.

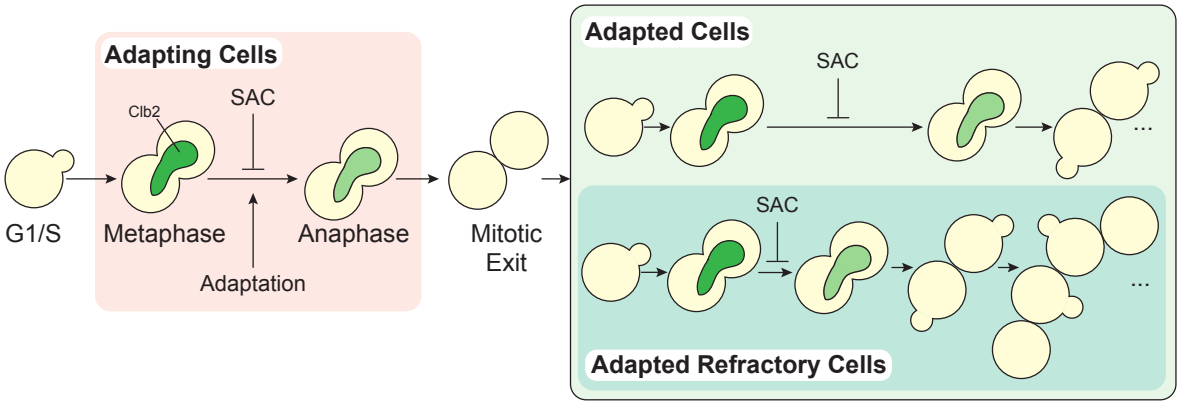

Figure 5.1: **Cells resume proliferation after adaptation** - When cells sense the SAC stimulus for the first time, a mitotic arrest is introduced, after which cells eventually adapt (red box), inducing degradation of key mitotic substrates (for instance, Clb2 in green). We call these cells "adapting". Then, adapting cells perform mitotic exit and resume proliferation in the continuous presence of the SAC stimulus. This population of cells is called "adapted". Within this progeny, some cells may proliferate with a decreased mitotic timing: we call them "Adapted refractory cells".

If cells perform a successful mitotic exit, they could enter in the subsequent G1 and resume cellular division, establishing a progeny of proliferating cells in the continuous presence of an operational SAC. We call these cells *adapted* (Figure 5.1, light green box).

Mitotic duration of adapted cells could vary, according to the type of the SAC-inducing stimulus. In cells adapted to microtubules depolymerization induced by the *tub2-401* mutations, mitotic length is similar or even higher than that of adapting cells. In this case, missegregation events are likely to occur. An incorrect inheritance of DNA is likely to influence the proliferative capacity and the viability of adapted cells (Sullivan & Huffaker 1992), as was also suggested by a preliminary live-cell

imaging experiment (Figure 4.20). Here, 56% of the monitored adapting cells resumed proliferation after adaptation within the 40 hours of imaging. However, cellular viability seemed to decrease after 20/30 hours from the beginning of the experiment, probably because of the deleterious effects introduced by missegregation events (Santaguida & Amon 2015). At the present stage, however, we cannot absolutely conclude that cell death was due to missegregation.

Upon Mad2 overexpression, on the contrary, adapted cells spend less time in mitosis compared to adapting cells, suggesting that they entry into a refractory state. These cells are defined as *adapted refractory* (Figure 5.1, dark green box). In this thesis we followed a population of adapted refractory cells for 24 hours from *GAL1pr* induction. These cells do not missegregates chromosomes and live without alteration of viability. This property is quite peculiar for budding yeast, since Mad2 overexpression has wider effects in mammals, where it introduces chromosomes misalignment, lagging chromosomes and micronuclei (Rowald *et al.* 2016). If the SAC stimulus is transiently removed and reintroduced after a certain timespan, adapted cells may remain refractory. If so, we say that adapted refractory cells keep a *memory* of their adaptation to the SAC.

In this thesis we characterized adapted and adapted refractory progenies in *S. cerevisiae*, in response to *tub2-401* and Mad2 overexpression, respectively.

Metabolic alterations occur in adapted cells

Our analysis suggests that adapted cells rewire their metabolic processes. These alterations are due to adaptation, and not to galactose (for *GAL1-MAD2(3x)*) or cold-stress response (for *tub2-401*). Our results could reflect the energy demand of adapted cells for proliferating under a constant SAC stimulus. In line with this hypothesis, alterations in TCA cycle and glycolysis/gluconeogenesis could be associated to a rewiring in the carbon source uptake and processing; fatty acid biosynthesis and chitin biosynthesis could be required for supporting the increased cellular volume of adapted cells. Finally, upregulation of metabolic processes involving phosphate-containing compounds takes place in adapted refractory cells upon Mad2 overexpression. This may suggest a high requirement of phosphate groups for several phosphorylation reactions.

Refractoriness in adaptation to the SAC induced by Mad2 overexpression

When the SAC is induced by Mad2 overexpression, cells develop a refractoriness to the SAC. Adapted refractory cells spend less time in mitosis in the following cycles, despite the continuous SAC activity. This refractory state is imperfect, since the mitotic duration of adapted refractory cells is significantly delayed compared to wild-type cells (Figure 4.2). This could be due to a persistent partial inhibitory effect of MCC, of which we expect a continuous production. Indeed, we proved that adapted refrac-

tory cells, although less prone to arrest, produce enough MCC to induce a mitotic arrest, both under continuous Mad2 overexpression (Figure 4.4) and under nocodazole treatment (Figure 4.5). Adapted refractory cells retained memory in adaptation to the SAC for 3h, but not for 12h. This implies that the molecular mechanism underlying refractoriness is lost between 3h and 12h, discarding the possibility that memory is due to genetic alterations, and favoring the hypothesis that adapted refractory cells have rewired their cell cycle network to become less responsive to the SAC. In support of this hypothesis, proteome analysis shows extensive alterations of protein abundances in adapted refractory cells compared to not adapted.

Is refractoriness explained by a decrease of SAC stimulus?

If there is a refractory state, we would expect a molecular mechanism that elaborates a response (Lyon 2015) towards a prolonged SAC activity. One simple possibility is that, despite the continuous MCC assembly, adapted refractory cells could reduce the SAC signal, favoring cell survival (Weaver & Cleveland 2005).

Transcriptional/translational defects of the SAC genes One of the possible scenarios could include decreasing levels of SAC proteins with time. In the case of Mad2 overexpression, adapted refractory cells exhibit a slight decrease in Mad2 levels compared to adapting cells (Figure 4.3, western blot analysis). A downregulation of Mad2 levels would imply a defective activity of *GAL1pr* in adapted refractory cells. Although we proved that the time of *GAL1pr* activation cannot explain the difference between adapting and adapted refractory cells (Figure 4.4), we cannot exclude that a reduction in transcriptional/translational activity is taking place during a prolonged mitotic arrest. Indeed, several proteins involved in transcription and translation were identified in the downregulated proteome of adapted refractory cells (see Results, Section 4.3). We have not thoroughly explored this possibility yet, but it is clear that a detailed investigation of the SAC protein levels and their synthesis is required: not only for Mad2, but also for the other MCC components, Bub3 and Mad3.

Cellular size does not trigger refractoriness to the SAC We also investigated whether cellular size is involved in reducing the effectiveness of the SAC signal in adapted cells, by diluting MCC when a critical size is reached. In *GAL1-MAD2(3x)* cells, occurrence of refractoriness to the SAC positively correlates with an increased cellular size. Here, cells adapt to the SAC and undergo anaphase with a median volume that is twice that of cycling cells. This volume is then constantly maintained during the anaphase onset of adapted refractory cells, suggesting a size homeostasis during the refractory state. A positive correlation between adaptation time and size exclude the presence of a critical vol-

ume of refractoriness. Adapted refractory cells, instead, resume a peculiar growth with an increased growth rate. In these cells, the prominent growth is given by daughter cells, which exhibit a hyperpolarization in most of the cases. A pronounced apical growth could be explained by a higher activity of Clns:Cdc28 complex (Lew & Reed 1993), which could correlate with the observed increase of Cdc28 levels in refractory adapted cells.

Also in the case of spindle depolymerization, size and mitotic duration positively correlates during a nocodazole arrest (Paolo Bonaiuti, data not shown), suggesting the absence of a critical size of refractoriness during spindle depolymerization. To test this hypothesis more thoroughly, a detailed analysis on cellular size of *tub2-401* cells has to be performed.

In conclusion, our data show that size is not responsible for the refractory period, and in general our (incomplete) data also suggest that silencing of the SAC is also unlikely. We thus investigated other molecular mechanisms to explain the presence of memory.

Increase of Cdc28 may explain refractoriness to the SAC

Our proteomic analysis of adapted cells reveals several alterations of cell cycle proteins, which usually represent the low-abundant portion of the *S. cerevisiae* proteome (Matafora *et al.* 2014). Label-free shotgun proteomics provides an increased proteome coverage respect to the labelling approaches (Patel *et al.* 2009; Bantscheff *et al.* 2007), allowing the detection of low-abundant proteins. However, accuracy of the quantification is reduced, and the data coming from the analysis have to be validated, for instance by Western Blot. We identified several key mitotic regulators upon Mad2 overexpression and/or spindle depolymerization. Among these proteins, the increased abundance of kinases could correlate with the upregulation of metabolic processes concerning phosphates, suggesting a high kinase activity in adapted cells. In particular, levels of Cyclin-dependent Kinase 1 Cdc28 - the master regulator of the budding yeast cell cycle - increase in adapted cells both induced by *GAL1-MAD2(3x)* and *tub2-401*. Cdc28 is required for APC/C^{Cdc20} activity in adaptation to the SAC (Rudner & Murray 2000; Vernieri *et al.* 2013), and according to this notion we showed that overexpression of Cdc28 in nocodazole-arrested cells (*GAL1-CDC28-HA*) anticipates the anaphase onset (Figure 4.36).

Both *GAL1-CDC28-HA* and adapted refractory cells have in common two properties: high levels of Cdc28 and presumably high activity of APC/C^{Cdc20} in promoting the anaphase onset. If the former has an effect on the latter, then we should observe an increased phosphorylation of APC/C (Vernieri *et al.* 2013; Rudner & Murray 2000). Indeed, the phosphorylation of the APC/C subunit Cdc16 slightly increases in adapted refractory cells upon Mad2 overexpression (Figure 4.39), but not in *GAL1-CDC28-HA* cells arrested in nocodazole (Figure 4.40). In the second case, cells might exit from mitosis after 3h of nocodazole, reversing Cdc28-mediated phosphorylations. This result may

imply that high Cdc28 levels are necessary but not sufficient for increasing APC/C phosphorylation in adapted refractory cells. In discordance with this hypothesis, Cdc28 overexpression is sufficient to anticipate the anaphase onset during a nocodazole arrest (Figure 4.36a), even if the range of mitotic duration of these cells quite overlaps to that of wild-type. Moreover, we observed that cells overexpressing Cdc28 still need a functional APC/C in order to adapt (Figure 4.36b). We know for sure that overexpression of Cdc28 is not entirely recapitulating adapted refractory cells from a molecular point of view, since many other alterations take place. Thus, Cdc28 may cooperate with other kinase(s) in APC/C phosphorylation. For instance, Cdc5 is upregulated in adapted cells and it could be one of the possible candidates (Rudner & Murray 2000).

Finally, for a complete comprehension of APC/C^{Cdc20} regulation, we need to explore other mechanisms. Phosphorylation of Apc1 and Cdc20 play key roles in the activation of APC/C^{Cdc20} in mammals (Qiao *et al.* 2016; Zhang *et al.* 2016; Hein & Nilsson 2016; Hein *et al.* 2017) (see Introduction, Section 1.1). Cdc28 may also strongly inhibit the transcriptional repressor Yox1 (Liang *et al.* 2012), therefore bursting Cdc20 synthesis in adapted cells.

In conclusion, Cdc28 overexpression (confirmed in both *tub2-401* and *GAL1-MAD2(3x)*) could explain the refractoriness to the SAC, possibly via hyper activation of APC/C. The final molecular mechanism, however, needs to be fully understood. Our preliminary data do not totally reconcile with the hypothesis of Cdc28 as a driver of refractoriness, and further experiments are required.

SAC stimuli and refractoriness: an open question

Mad2 overexpression is quite artificial, and suffers from the obvious problem of overexpressing one protein that is part of the same network we propose to analyze. For this reason, we have tested whether the refractory state would be maintained with stimuli that prevent microtubule polymerization (i.e., proper activators of the SAC). Unfortunately, we could not confirm the refractory state when adapted cells upon Mad2 overexpression were treated with high dosage of nocodazole. Knowing that the spontaneous Mad2:Cdc20 binding is slow (Simonetta *et al.* 2009; Faesen *et al.* 2017), the mere Mad2 overexpression requires approximately 60 times the endogenous Mad2 levels in order to induce a mitotic arrest via MCC assembly (Mariani *et al.* 2012). Instead, the presence of unattached kinetochores via nocodazole treatment supports the conversion of O-Mad2 in C-Mad2 conformation (De Antoni *et al.* 2005; Simonetta *et al.* 2009), which can easily bind Cdc20 and therefore assembly MCC in a faster way. When nocodazole was given to *GAL1-MAD2(3x)* adapted refractory cells, the conformational switch of the overexpressed Mad2 could provide a better MCC assembly, therefore arresting cells in mitosis and masking the acquired refractoriness to the SAC.

We then used *tub2-401* cold-sensitive mutants (Huffaker *et al.* 1988; Sullivan & Huffaker 1992) to

induce a "physiological" activation of the SAC. These cells arrest for several hours in prometaphase, after which they adapt and establish a viable population of adapted cells on agar plates and liquid medium, with decreased doubling time after 22h from the temperature shift (Figure 4.19b-c). These results support the presence of a refractory state also in this setting. When proliferation was monitored in a microfluidic chamber, however, only 50% of the adapted cells spent less time in mitosis when compared to their ancestral adapting cells (Figure 4.20c). Moreover, the difference between the distributions of mitotic arrest in adapting (first arrest) and adapted (later arrests) cells was not significant (Figure 4.20b). One possible explanation is that, although there is a refractoriness to the SAC, cells are delayed here in metaphase by the large genetic errors caused by missegregation. Indeed, adapted cells also exhibit wide alterations in proteins related to DNA repair, replication, recombination and damage response (see Results, Chapter 4.3). We did not investigate whether adapted cells also show a rewiring of these enriched pathways, but this is something we propose to do. Interestingly, the proteome of *tub2-401* adapted cells exhibits changes which are similar to Mad2 overexpression, in terms of Gene Ontology entries and pathways. This last evidence suggests a quite comparable rewiring of the cell cycle under both inducing SAC stimuli. Thus, it may be worth repeating the experiment with *tub2-401* cells with an increased semi-permissive temperature, and monitoring viability on liquid medium (for instance by staining with methylene blue). Finally, investigating the extent of DNA damage in M phase of *tub2-401* adapted cells is also something worth following.

Cdh1 and MEN are required for viability of adapted cells

While an increased kinase activity could facilitate the metaphase-to-anaphase transition, it may be deleterious for cellular viability. In adapted cells, inhibition of APC/C^{Cdc20} by MCC introduces an accumulation of mitotic cyclin Clb2, making Cdh1 essential for viability (Figure 4.41). Even if *CDH1* deletion does not impair the anaphase onset in *GAL1-MAD2(3x)* adapting cells (Vernieri *et al.* 2013), it leads to the accumulation of Clb2 in the subsequent G1 phase, altering the cell cycle progression and the viability of adapted refractory cells (Claudio Vernieri, data not shown). Overexpression of Sic1 - the functional homolog of mammalian $p27^{Kip1}$ - rescues the viability (Figure 4.41), by inhibiting the residual Clb2:Cdc28. Therefore, adapted cells need a functional Cdh1 in order to abolish kinase activity in anaphase (Cross 2003).

Cdh1 is phosphorylated and inhibited by Cdc28, and a reversal of its phosphorylation state allows its binding with APC/C (Höckner *et al.* 2016). Here, FEAR and MEN pathways could play an important role, by mediating Cfi1/Net1 phosphorylation and releasing Cdc14 phosphatase. In this framework, several players could be evaluated. For instance, Cdc28 kinase activity could be required for Net1 phosphorylation (Azzam *et al.* 2004; Queralt *et al.* 2006), as well as Polo like kinase

Cdc5 (Visintin *et al.* 2003; Rodriguez-Rodriguez *et al.* 2016), which has been identified upregulated in adapted cells. On the other hand, activation of APC/C^{Cdc20} during adaptation may inhibit phosphatase $PP2A^{Cdc55}$, a repressor of Cdc14 release (Queralt *et al.* 2006). In agreement with a role of MEN in promoting viability of adapted cells, we noticed in a SGA screening for synthetic lethality with Mad2 overexpression (in collaboration with Marco Foiani, IFOM - Milan, IT) that deletion of MEN-inhibiting genes - such as *BUB2, BFA1* - enhances viability of adapted refractory cells, while deletion of MEN-promoting genes - such as *CLA4, LTE1* - strongly reduces viability (data not shown).

Refractoriness to the SAC and missegregations: the Ying and Yang of adapted cells

In summary, our data support the existence of a global cellular response upon a prolonged SAC activity (Figure 5.2). During a mitotic arrest, cells experience a stressful condition. If they do not die, they will learn how to deal with the stress, adapting to the SAC and becoming refractory to it. Adaptation may also lead to missegregation events (C. Rieder & Maiato 2004), which could introduce genetic alterations. The balance between refractoriness and missegregation will dictate the cellular fate after adaptation: proliferation or death (Figure 5.2). Differently from *tub2-401*, *GAL1-MAD2(3x)* cells do not experience missegregation defects, a fortunate case that allows us to evaluate the properties of the refractory state in a viable and not genetically-altered context (Figure 5.2, yellow box). In this framework, adapted refractory cells modify their cell cycle, metabolism, translation and cellular size and growth. Among these properties, we would expect some of them being driver of the refractory state, while others as supporters/enhancers. Here, we proposed Cdc28 as a candidate driver, whose levels correlate with the presence of memory (Figure 4.35). We discared cellular size as the source of refractoriness.

Genetic alterations are likely to occur during adaptation of *tub2-401* cells. In this case, cells could experience DNA damage, which would increase mitotic duration and the proportion of not viable cells after adaptation (Figure 5.2). Proteome analysis on *tub2-401* adapted cells showed rewirings similar to that of *GAL1-MAD2(3x)* cells, supporting the idea that the refractory state is present and masked by genetic alterations.

Our working model is based on short-term effects of adaptation to the SAC, since we observed no more than 3/4 generations of adapted cells. We still do not know the long-term consequences of adaptation, which are currently under study in our lab. Preliminary data on *tub2-401* adapted cells grown at 18°C for $\sim$ 100 generations shows a significant enrichment of single nucleotide variants in genes involved in cytoskeleton organization and cell cycle (Federica Natali, Elena Chiroli - data not shown), maybe due to the missegregation events that could favor genetic alterations.

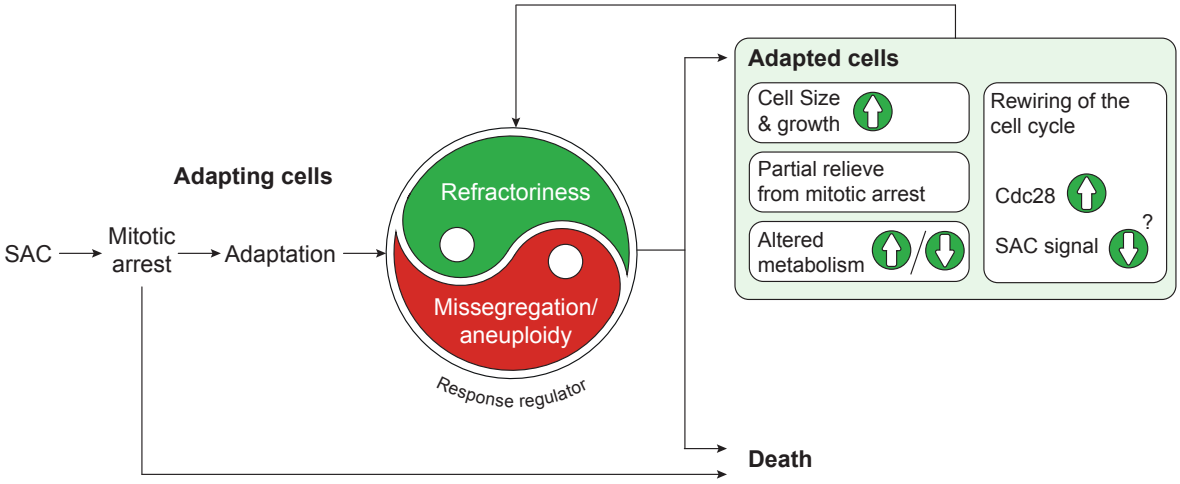

Figure 5.2: **A possible working model for proliferating cells after adaptation** - When SAC is activated, cells arrest in mitosis and eventually adapt to the mitotic checkpoint. In this case, cells learn how to manage with the experienced stressful conditions and become refractory to the SAC, allowing cells to live and proliferate in the presence of the SAC stimulus, with certain properties (green box). Any missegregation event coming from adaptation will negatively influence proliferation, and cellular death would be one of the outcomes. The interplay between refractoriness and missegregations provides the response regulator in adaptation to the SAC.

Clinical perspectives: how to inhibit proliferation after adaptation?

"Differentiation" of adapted cells may establish a variety of features, whose activity could be essential for the maintenance of viability. In particular, cellular refractoriness promotes cellular division even in the presence of genetic alterations. As such, it might introduce irreversible and deleterious effects in the progeny. From the point of view of cancer evolution, thus, inhibition of "differentiation" may abolish proliferation and prevent the inheritance of genetic defects. In this view, our results could suggests possible targets for inhibiting the relapse of cellular proliferation under a constant treatment with antimitotic drugs.

Cdk1 In this thesis we proposed Cdk1 as a driver for refractoriness. If so, we would expect to abolish the refractory state and viability of adapted cells via Cdk1 inhibition. This idea could also be relevant from a clinical point of view. Indeed, high levels of Cdk1 were identified in several cancers with unfavorable prognosis (Uhlen *et al.* 2017). Among them, lung cancer which is treated with taxanes and vinca alkaloids (Chabner & Longo 2014). We do not know whether the proliferative capacity of these cancer cells correlates with high levels of Cdk1; if it is true, Cdk1 inhibition would suppress cellular memory, restoring an efficient activity of the chemotherapeutic agents. However, Cdk1 could cover an important role in SAC activity of mammalian cells (Vincenzo *et al.* 2003; Vázquez-Novelle *et al.* 2014), and its downregulation could alleviate the APC/C^{Cdc20} inhibition, therefore allowing cellular proliferation.

Mitotic exit / Cdh1 The progeny of adapted refractory cells we analyzed shows synthetic lethality with genes involved in the mitotic exit. Deletion of these genes is not lethal in cycling cells, suggesting that they are strongly required only for continued growth in adapted cells. Among these genes, Cdh1 could be one possible target. However, it has been shown that inhibition of Cdh1 might not induce cell death in mammals. After a defective mitotic exit, cells might resume proliferation with a precocious entry in S-phase, introducing defects in chromosome separation and cytokinesis, and facilitating genomic instability (Greil *et al.* 2015; Engelbert *et al.* 2008).

APC/C Finally, APC/C inhibition could prevent proliferation of adapted cells. To this purpose, it has been shown that the drug proTAME (Zeng *et al.* 2010) induces a SAC-dependent mitotic arrest, by preventing binding between Cdc20/Cdh1 and APC/C. Indeed, proTAME administration to hTERT RPE-1 cells during a nocodazole arrest increases mitotic duration and cell death (Tiziana Lischetti - preliminary data not shown).

Completing the decoding of proliferating cells after adaptation to the SAC: future plans

Several experiments have to be performed in order to confirm and strengthen the hypothesis of refractoriness in adaptation to the SAC.

- Proteomic analysis reveals several rewirings in *tub2-401* cells, suggesting the presence of a refractory state. However, its effect on the mitotic duration of adapted cells may be hidden by the deleterious effects introduced by missegregation. To this purpose, we will monitor *tub2-401* cells in semi-permissive conditions, reducing missegregation events and monitoring cellular viability.

- Measurements of SAC protein levels would be useful for understanding the MCC strength in adapted cells. Here, a single-cell analysis would clarify the presence of a correlation between mitotic duration and SAC protein levels. To this purpose, we will monitor Mad2, Bub3 and Mad3 tagged with fluorescent reporter. Moreover, a qPCR analysis of their transcript levels could clarify the existence of transcriptional/translational defects.

- The correlation between the high activity of APC/C^{Cdc20} and high levels of Clb2:Cdc28 of adapted cells is still incomplete, and it needs to be further investigated. As reported above, phosphorylation of Cdc20 and/or Apc1 could represent two additional regulators of the anaphase onset to be taken into account. Moreover, polo like kinase Cdc5 could have a role in promoting APC/C activity, by phosphorylating APC/C (Rudner & Murray 2000) and/or by promoting release of Cdc14 in FEAR/MEN pathways (Visintin *et al.* 2003; Rodriguez-Rodriguez *et al.*

2016). Indeed, Cdc5 is upregulated in adapted cells upon Mad2 overexpression or spindle depolymerization (*tub2-401*), and overexpression of the kinase anticipates Cdc14 release during metaphase (Visintin *et al.* 2003).

- We will re-examine the results coming from the SGA screen for synthetic lethality with Mad2 overexpression. The gene list we obtained might be useful for detection of additional targets for inhibiting proliferation after adaptation to the SAC. By examining the list with the same tools used for the proteomic analysis (see Results, Section 4.3), we noticed a significant enrichment of genes involved in the regulation of catalytic activity, regulation of phosphate metabolic processes and cell cycle.

6 Appendix

6.1 Expression of *cdc20-127* bypasses the mitotic arrest induced by Mad2 overexpression

As described in the Results (see Section 4.1), the expression of *cdc20-127* was used in order to uncouple the SAC activity from Mad2 overexpression. Before using this tool for the evaluation of *GAL1pr* activity and memory in adaptation, we evaluated its ability to overcome the checkpoint arrest in *GAL1-MAD2(3x)* cells. To this purpose, *tetO$_2$-CDC20-127(1x) GAL1-MAD2(3x)* cells were grown in two conditions. Both of them grew overnight without Mad2 overexpression and, after G1 synchronization, they were released in galactose containing medium. However, one condition was experiencing Mad2 overexpression in the presence of *cdc20-127* (Figure 6.1a, Cycling), while the other did not (Figure 6.1a, Adapting). As control, *GAL1-MAD2(3x)* and *GAL1-MAD2(3x) mad3*Δ were grown in parallel, without doxycycline treatment.

Expression of *cdc20-127* in Cycling cells triggered a synchronous mitotic exit after 2h from the release, behaving like the checkpoint-deficient condition (Figure 6.1b, Cycling vs *GAL1-MAD2(3x) mad3*Δ). Adapting cells entered asynchronously in the subsequent G1, with a delay of 1h compared to Cycling condition (Figure 6.1b, Cycling vs Adapting), due to the absence of cdc20-127. We noticed that Adapted cells were slightly faster than *GAL1-MAD2(3x)* cells, in which the expression of *cdc20-127* was totally absent, suggesting the presence of a slight leakage on *tetO$_2$pr* upon doxycycline treatment.

We conclude that the expression of *cdc20-127* allows to bypass the mitotic arrest induced by Mad2 overexpression.

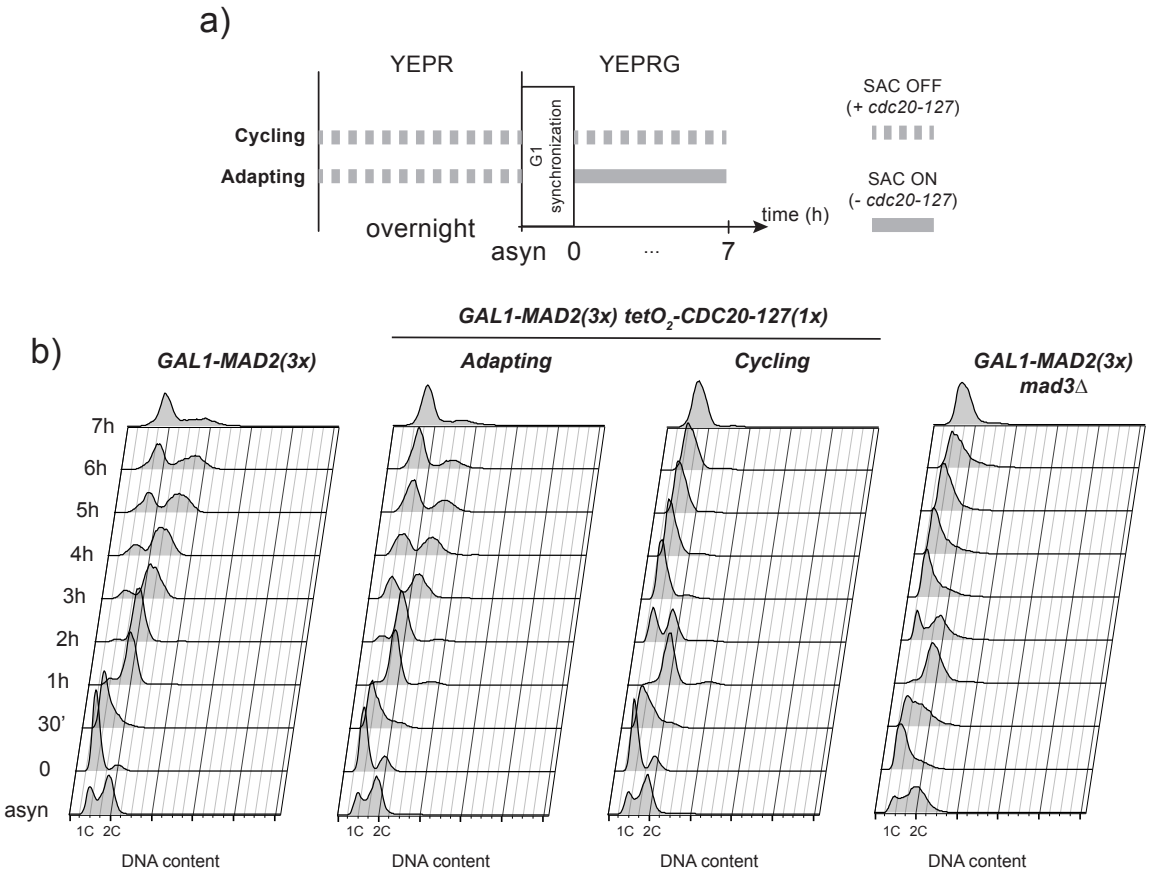

Figure 6.1: **Expression of *cdc20-127* bypasses the SAC induced by Mad2 overexpression** - *MATa GAL1-MAD2(3x)* (yAC2465), *MATa tetO$_2$-CDC20-127(1x) GAL1-MAD2(3x)* (yAC2807) and *MATa GAL1-MAD2(3x) mad3*Δ (yAC436) were grown overnight in raffinose, synchronized in G1 and released in galactose containing medium. After 1h30min from the release, α-factor was readded in order to resynchronize cells in the subsequent G1. Cells were monitored until 7h from G1 release. (a) yAC2807 cells were grown in two different conditions. They were identical during the overnight, but during the YEPRG phase (i.e., during Mad2 overexpression) one strain was expressing *cdc20-127* (cycling), while the other did not (adapting). Repression of *cdc20-127* synthesis was achieved by treating cells with doxycycline hyclate 10 $\mu g/ml$ (Barnhart *et al.* 2011). (b) FACS analysis of the experiment.

6.2 Overexpression of Cdc28 does not alter an unperturbed cell cycle

Before studying the effects of high levels of Cdc28 during a nocodazole arrest (see Results, Section 4.4), we aimed to evaluate whether these levels influenced an unperturbed cell cycle. To this purpose, *WT* and *GAL1-CDC28-HA* were synchronized in G1 and released in galactose containing medium, without activating the SAC. Both strains assumed a similar cellular progression, in terms of DNA replication and segregation (Figure 6.2a) and in terms of metaphase and anaphase onset (Figure 6.2b). Maximum levels of mitotic cyclin Clb2 were observed after 60' from release (Figure 6.2c), in correspondence to the maximum proportion of metaphase cells. Our results suggest the absence of a cell cycle perturbation due to the mere overexpression of Cdc28.

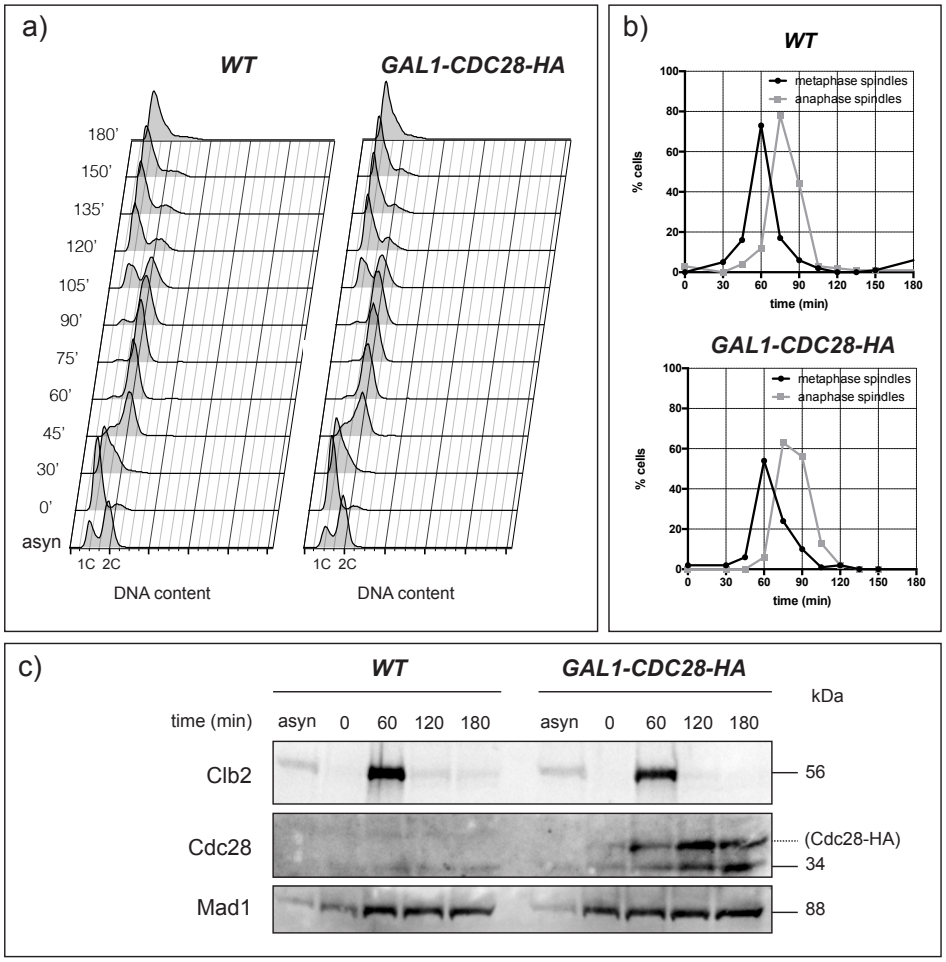

Figure 6.2: **Overexpression of Cdc28 does not alter an unperturbed cell cycle** - *MATa, WT* (yAC3568) and *MATa, GAL1-CDC28-HA* (3716) cells were grown in YEPR, synchronized in G1 and released in YEPRG. After 1h10min from the release, α-factor was readded in order to resynchronize cells in the subsequent G1. Cells were monitored until 3h from the release, collecting samples for FACS, IF and Western Blot analysis. (a) FACS profiles of the experiment. (b) IF analysis. 100 cells were counted for each condition and for each timepoint, evaluating proportion of cells with interphase, metaphase or anaphase spindles. Proportion of metaphase and anaphase spindle is plotted versus time. (c) Regular 10% Western Blot related to the experiment.

6.3 Proteome of Adapted Cells

We report the screened proteome of Adapted Cells, which was obtained by Shotgun Label-Free LC/MS-MS (see Results, Section 4.3).

Upregulated proteome of *GAL1-MAD2(3x)* adapted refractory cells

3-dehydroquinate synthase, 3-hydroxyacyl-[acyl-carrier-protein] dehydratase, 4-alpha-glucanotransferase, AAP1, ABP140, ABZ1, ACF2, ACO2, ADE1, ADE12, ADR1, AFG3, AGX1, AIM14, AIM17, AIM24, ALD2, ALG9, ALK1, ALR1, ALY1, AMD1, AMS1, Anthranilate synthase component 2, APD1, ARA2, ARE1, ARE2, ARG1, ARG2, ARG4, ARI1, ARO7, ARO8, ARP2, AST2, ATG19, ATG3, ATP-dependent (S)-NAD(P)H-hydrate dehydratase, AVT7, BAT1, BBC1, BCD1, BET3, BNA2, BUD3, CAB4, CAK1, CAT2, CDC28, CDC5, CDC53, CEP3, CHC1, CHS1, CHS2, CHS5, CLA4, CMK2, COP1, COQ3, CPA2, CPS1, CRG1, CRM1, CST26, CTK3, CTP1, CTR86, CUP2, CYC3, CYC7, DAM1, DAP1, DBF2, DBP10, DBP9, DBR1, DCS1, DOA1, DOP1, DPB2, DRS2, DSS1, DYN1, ECM22, ELM1, ELP6, EPL1, ERG24, ERG26, ERG7, ERJ5, ESS1, ETR1, FAT1, FIS1, FKS1, FMP27, FPR1, FRD1, FSH3, GAD1, GCD1, GCN1, GCN3, GCV1, GDE1, GDH2, GDI1, GEP4, GGC1, GID7, GID8, GIN4, GLC3, GLT1, Glutamate N-acetyltransferase, Glutamine-dependent carbamoyl-phosphate synthase, GNA1, GPB1, GPM2, GRS2, GSC2, GSY2, GYP7, HBT1, HER1, HIS1, HIS5, HOM3, HRD3, HSH155, HSM3, HSP12, ICL1, IDP2, ILV3, ILV5, IMA1, IMG1, IML2, INM1, IOC3, ISM1, KAP95, KOG1, KSP1, KTI12, KTR4, LEU9, LPX1, LSM6, LST8, LYS1, LYS2, LYS9, MAE1, MAG1, MAG2, MAK3, MAP2, MCM2, MCM5, MDN1, MDR1, MET10, MET5, Methylenetetrahydrofolate dehydrogenase, MEX67, MGM101, MIP1, MKT1, MON2, MRP1, MRPL15, MRPL37, MSC1, MSC2, MTC3, MTD1, MYO4, NADPH-dependent alpha-keto amide reductase, NBP35, NDI1, NMA111, NPL4, NQM1, NRK1, NTF2, NTH1, NUP157, NUP159, NUP170, NUP192, NVJ1, ODC2, OPY1, Orotate phosphoribosyltransferase 1, OXP1, DSF1, SNZ3, COS5, PAC10, PAN6, PCK1, PDC2, PDC5, PDH1, PDR1, PDR12, PEF1, PEX4, PHB1, PHO3, PHO86, Phosphoribosyl-AMP cyclohydrolase, PIH1, PIN3, PLP1, PMC1, PMR1, POL1, POL3, POP1, PRR1, PRS2, PTA1, PTP3, PUF4, PUT1, PXL1, IMA2, QRI1, REG1, RER2, RFC2, RIA1, RIM13, RLI1, RLM1, RNA15, ROD1, RPA14, RPD3, RPL33A, RPN2, RPN6, RPO21, RSM18, RSM26, RTG2, RTG3, RVB1, SAC7, SAM50, SBA1, SDS22, SEC18, SED4, SER3, SER33, SIT4, SLM5, SMM1, SNZ1, SOV1, SPS19, SPT16, SRB8, SRY1, SSA4, SSE2, STE23, STT4, STV1, SUB1, SUV3, SWA2, SWI5, TEL1, TEL2, TFC7, THI80, TPK1, TPS2, TPS3, TRM3, TRP1, TRP5, TRS130, TRX3, TSL1, TTI2, TYW1, UBP15, UBP2, UBP3, UBR2, UFD2, Urea carboxylase, UTP10, VAN1, VAR1, VPS13, VPS28, VPS30, VPS35, VPS62, WTM2, YAK1, YAT2, YBR225W, YCF1, YDR391C, YFL042C, YGP1, YGR126W, YHR202W, YIL108W, YIR024C, YJL016W, YJL132W, YJL218W, YJR011C, YJR111C, YJR142W, YLR149C, YLR446W, YML087W, YMR111C, YMR196W, YNR065C, YOL098C, YPK2, YPL088W, YPL150W, YPL260W, YUR1, ZRG17, ZRT3

Downregulated proteome of *GAL1-MAD2(3x)* adapted refractory cells

ABF2, ACP1, AIM23, AIM25, AIM32, ARO10, ARO2, ASC1, AXL2, AZF1, BFR1, BFR2, BMH1, BRE2, BRF1, BTS1, BUD31, CAF20, CAR2, CBF2, CBP3, CCC2, CDC20, CDC33, CFT2, CIT3, CLU1, CMD1, CNM67, CTR1, CTS2, CUL3, CYS3, CYS4, DBP2, DEF1, DLD1, DMA1, DPB3, DYS1, EBP2, EGD1, EMP24, ENO2, ERO1, FAR3, FET3, FRS1, FSH2, FUI1, FZO1, GAL1, GAL2, GAL7, GAS1, GDA1, GIS2, GIT1, GLR1, GND1, GRS1, GUT1, HHF1, HHO1, HIR2, HMT1, HSC82, HXT6, IES5, KAR2, KRI1, LIA1, LPD1, MAD2, MAK10, MAL33, MAM33, MBP1, MCD1, MEC1, MET4, MHT1, MIC27, MLP2, MNR2, NDE1, NHP6A, NMT1, NNT1, NOP10, NOP13, NOP56, NSR1, NTH2, NUG1, OLA1, OLE1, HTB1, HTA1, RPS25B, RPS22A, RPL20A, RPS23A, RPS24A, RPS4A, RPS6A, RPS8A, RPL2A, RPL18A, RPS16A, RPS18A, RPL19A, PMA2, HXT13, PAB1, PDI1, PET111, PEX8, PHO90, PKH1, PMU1, POP8, PRO2, PRP46, PSA1, PUS9, RAS2, RAX1, RBG2, RGI1, RNA1, RPA135, RPB3, RPG1, RPL10, RPL13A, RPL16A, RPL16B, RPL24A, RPL26B, RPL3, RPL36A, RPL36B, RPL37A, RPL37B, RPL5, RPL6A, RPL9A, RPP2B, RPS10A, RPS14A, RPS1B, RPS9B, RRP42, RUD3, SAF1, SCP160, SCS2, SDA1, SDH4, SEC53, SEC9, SES1, SKG6, SLM2, SOD1, SPC3, SPL2, SRO9, SRP40, SSA1, SSA2, SSB1, SSB2, SSC1, SSK1, STM1, STU1, SUP35, SWI4, SWS2, TAL1, TBF1, TCD2, TDA10, TDA11, TDH2, TEF1, TID3, TIF11, TIF3, TIF34, TMA19, TPI1, TPM1, TPM2, TRR1, TRX1, TSA1, TYR1, Ubiquitin-40S ribosomal protein S31, VAS1, VFA1, VPS52, YBL010C, YBR271W, YCP4, YCR015C, YDJ1, YDL109C, YDL121C, YEF3, YEH2, YGL041W, YIF1, YIP5, YJU2, YNL010W, YNL050C, ZEO1, ZUO1

Upregulated proteome of *tub2-401* adapted cells

ACC1, ACK1, ADP1, AFG3, AGP1, AGX1, AIM19, AIM45, ALE1, ALG6, ALT2, ART5, ATG7, ATP11, ATP2, ATP3, ATP4, ATP7, BAR1, BCS1, "bI2, COB, bI3, bI4", BIK1, BRE5, BRO1, BUL1, CBF1, CCW14, CDC25, CDC5, CDC7, COA3, COQ2, COR1, CPS1, CST26, CTF19, CUE1, CUP2, CWC2, CWC27, CYC1, CYT2, DIA4, DNF1, DOS2, DPP1, DSK2, DUR1,2, EAF3, ECM2, ECM38, EDC1, END3, ENV7, EXG1, FAA1, FAS1, FAS2, FMP25, GAP1, GCV2, GDH1, GEF1, GEM1, GGA2, GLT1, GRS2, GRX2, GRX5, GTT1, GYP6, HEH2, HER1, HER2, HFI1, HOF1, HSE1, HSH49, HSL1, HSP12, HXT6, HYM1, HYP2, HYR1, IDH1, IDH2, IES6, ILV2, IRA2, ISN1, KAR3, LAC1, LDB19, LPD1, LSC2, MAG1, MCM5, MCM6, MDH1, MDM35, MDV1, MED7, MED8, MEF1, MEH1, MHT1, MIC60, MMR1, MPM1, MPS3, MRP21, MRP8, MRPL10, MRPL20, MRPL37, MRPS16, MRPS17, MRPS18, MTD1, NCE102, NDE2, NDI1, NHP2, NKP1, NNF2, NPC2, NUP49, OMA1, PAH1, PBI2, PET10, PET112, PET54, PEX13, PHB2, PHM8, PHO12, PHO5, PHO84, PHO89, PMT7, PRE3, PRP40, PSD1, PSP2, PSR2, PUT1, RAF1, RAV2, RCF1, RHB1, RIM15, RKM2, "RPL12B, RPL12A", RPL15B, RPL36B, RPL9B, RPM2, RPP1B, RPT4, RSM19, RSM28, RTN2, RUB1, SAM35, SAM37, SAP30, SBE22, SER3, SFH5, SNF6, SNX3, SNX41, SPO71, SRY1, SST2, SUS1, SWI6, TAF8, TAH11, TGL1, TMA10, TOF1, TOM71, TPO3, UBC12, UGO1, UMP1, URA2, VPS27, VPS54, VPS60, VTC2, VTC3, VTC4, WHI4, YCS4, YDR109C, YHR202W, YIL161W, YIM1, YOR1, YRB2

Downregulated proteome of *tub2-401* adapted cells

AAT1, ABF1, ABP140, ADI1, AGC1, ALG1, ALG11, ALG12, ALG5, ALR1, ARB1, ARO10, ARO9, ASC1, AST2, ATG11, ATG19, BEM1, BET4, BNA4, BOI1, BOI2, BRX1, BUD32, BUD4, BUR6, CAK1, CCA1, CCT5, CCT8, CDC16, CDC73, CFD1, CHA1, CHD1, CHS3, CHS6, CIC1, CIN1, COQ8, CTR86, CWH41, CYC8, DBP2, DBP8, DHH1, DMA2, DOM34, DYN1, EBS1, ECT1, EDC3, EMC2, EMC4, ENP1, ENP2, ERB1, ERG1, ERG11, ERG27, ERO1, ERV14, FES1, FIP1, FKH1, FLC1, FLC3, FMP30, GCN5, GEA1, GIN4, GLN4, GLY1, GRC3, GYP1, HAT2, HNT2, HSP104, HUA1, ICT1, IFH1, IOC3, IRA1, IRC5, IRC6, JEM1, JIP5, JJJ1, KAR2, KEL1, KEX1, KRE6, KRR1, KTI12, KTR6, LIP2, LPP1, LRO1, LSM1, LSM7, LTP1, LUC7, MAD2, MCT1, MDM20, MMF1, MNN5, MNN9, MNR2, MOG1, MRPL16, MSW1, MVP1, NAB2, NAB3, NGL2, NHA1, NNF1, NOC2, NOC3, NOC4, NOG1, NOP14, NOP4, NRP1, OPY1, ORC3, OSH3, PAB1, PAN3, PCT1, PEX4, PHO87, PMT2, PMT5, PNT1, POP1, PPH3, PPZ1, "PRM8, PRM9", PSK1, PTP3, RAD16, RAD52, RAX2, RBG1, RCO1, RDS3, REX4, RFS1, RIO1, RNR3, RPA135, RPB3, RPL22B, RPL6A, RPS0A, RPS12, RPS1B, RPS3, RRP1, RTG3, RTT101, SAH1, SAN1, SAR1, SCW11, SDA1, SDO1, SEC4, SEC63, SET2, SET5, SIA1, SKS1, SNF12, SNP1, SNU56, SOF1, SPB1, SPC42, SPE4, SPT4, SRL2, SRP72, SSA3, SSO1, SSO2, STB3, STE12, STE6, SYF1, SYN8, TAF4, TDA2, TFC3, TFG2, TGL3, THR4, TIF4631, TNA1, TPA1, TSC10, TUB1, TUB2, TUB3, TVP23, UIP3, URE2, VID24, VMA8, VPS5, WTM2, YAP1801, YDR415C, YER156C, YGL036W, YGL101W, YHR112C, YLL007C, YLR225C, YOL019W, YOR289W, YPS7, YVH1

Table 6.1: Yeast Strains used in this study

strain	genotype	source
yAC39	*MATa, mad2::TRP1*	our lab
yAC41	*MATa, leu2-3::LEU2::GAL1-MAD2(3x)*	our lab
yAC309	*MATalpha, leu2-3::LEU2::GAL1-MAD2(3x)*	our lab
yAC436	*MATa, leu2-3::LEU2::GAL1-MAD2(3x), mad3::TRP1*	our lab
yAC783	*MATalpha, CFIII (CEN3.L.YPH278) URA3SUP11*	our lab
yAC792	*MATalpha, MAD2-3GFP-KanMX6*	our lab
yAC802	*MATa, trp1::tetO2-CDC20-127::TRP1*	our lab
yAC1001	*MATa*	our lab
yAC1011	*MATalpha*	our lab
yAC1013	*MATa, TUB2-mCherry::URA3*	R. Visintin
yAC1156	*MATalpha, mad2::TRP1*	our lab
yAC1513	*MATa, MAD2-3GFP-KanMX6*	T. Tanaka
yAC1533	*MATa, cdh1::HIS3*	our lab
yAC1546	*MATa, cdc16::CDC16-6A-TRP1, bar1:HISG*	A. Murray
yAC1571	*MATa, cdc27::CDC27-5A-KAN*	A. Murray
yAC1619	*MATalpha, cdc16:CDC16-6A-TRP1, cdc27::CDC27-5A-KAN*	our lab
yAC1700	*MATa, CLB2-GFP::LEU2 (isogenic to S288C)*	P.A. Silver
yAC1749	*MATa, CFIII (CEN3.L.YPH278) URA3SUP11*	P. D. Wulf
yAC1863	*MATa, CDC27-myc9::TRP1*	J.M. Peters
yAC1864	*MATalpha, CDC16-myc6::URA3*	J.M. Peters
yAC1906	*MATa, leu2-3::LEU2::GAL1-MAD2(3x), CDC27-myc9::TRP1*	our lab
yAC1933	*MATa, leu2-3::LEU2::GAL1-MAD2(3x), CDC16-myc6:URA3*	our lab
yAC1936	*MATa, CDC16-myc6::URA3*	our lab
yAC2006	*MATa, TUB2-mCherry::URA3, CLB2-GFP::LEU2*	our lab
yAC2465	*MATa, leu2-3::LEU2::GAL1-MAD2(3x)*	our lab
yAC2671	*MATa, TUB2-mCherry::URA3, leu2-3::LEU2::GAL1-MAD2(3x), CLB2-GFP::LEU2*	our lab
yAC2782	*MATalpha, leu2-3::LEU2::GAL1-MAD2(3x)*	our lab
yAC2807	*MATa, leu2-3::LEU2::GAL1-MAD2(3x), tetO2-CDC20-127::TRP1 (single copy)*	our lab
yAC2809	*MATalpha, trp1::tetO2-CDC20-127::TRP1*	our lab
yAC2926	*MATa, tub2-401*	our lab
yAC2946	*MATa, tub2-401, mad2::TRP1*	our lab
yAC2970	*MATa, CLB2-GFP::LEU2, tub2-401*	our lab
yAC3021	*MATa*	our lab
yAC3034	*MATa, mad2::TRP1, CLB2-GFP::LEU2, tub2-401*	our lab
yAC3041	*MATa, mad2::TRP1, CLB2-GFP::LEU2*	our lab
yAC3202	*MATa*	our lab
yAC3220	*MATa, tub2-401*	our lab
yAC3228	*MATa, tub2-401, CFIII (CEN3.L.YPH278) URA3SUP11*	our lab
yAC3251	*MATa, tub2-401, mad2::TRP1, CFIII (CEN3.L.YPH278) URA3SUP11*	our lab
yAC3252	*MATa, mad2::TRP1, CFIII (CEN3.L.YPH278) URA3SUP11*	our lab
yAC3372	*MATa, mad2::TRP1*	our lab
yAC3491	*MATa, CLB2-GFP::LEU2*	our lab
yAC3509	*MATa clb2::CLB2-3mCherry-dcu-hphNT1*	our lab
yAC3538	*MATa MAD2-3GFP-KanMX6, clb2::CLB2-3mCherry-dcu-hphNT1*	our lab
yAC3539	*MATalpha MAD2-3GFP-KanMX6, clb2::CLB2-3mCherry-dcu-hphNT1*	our lab
yAC3568	*MATa*	our lab
yAC3582	*MATa, leu2-3::LEU2::GAL1-MAD2(3x), cdh1::HIS3*	our lab
yAC3650	*MATa, (TRP1::SIC1)10x*	D. P. Toczyski
yAC3651	*MATalpha, SIC1(10x)*	our lab
yAC3654	*MATa, leu2-3::LEU2::GAL1-MAD2(3x), (TRP1::SIC1)10x*	our lab
yAC3659	*MATa, leu2-3::LEU2::GAL1-MAD2(3x), cdh1::HIS3, (TRP1::SIC1)10x*	our lab
yAC3682	*MATalpha, cdh1::HIS3, (TRP1::SIC1)10x*	our lab
yAC3683	*MATa, cdh1::HIS3, (TRP1::SIC1)10x*	our lab
yAC3685	*MATa, tub2-401, (TRP1::SIC1)10x*	our lab
yAC3686	*MATa, tub2-401, cdh1::HIS3*	our lab
yAC3694	*MATa, tub2-401, cdh1::HIS3, (TRP1::SIC1)10x*	our lab
yAC3699	*MATa, ura3::pGAL-MPS1-myc::URA3, trp1::pGAL-CDC28-HA::TRP1*	A. Murray
yAC3716	*MATa, trp1::pGAL-CDC28-HA::TRP1*	our lab
yAC3717	*MATa*	our lab
yAC3723	*MATa, trp1::pGAL-CDC28-HA::TRP1, MAD2-3GFP-KanMX6, clb2::CLB2-3mCherry-dcu-hphNT1*	our lab
yAC3754	*MATa, leu2-3::LEU2::GAL1-MAD2(3x), tetO2-CDC20-127::TRP1 (single copy), CDC27-myc9::TRP1*	our lab
yAC3770	*MATa, leu2-3::LEU2::GAL1-MAD2(3x), CDC16-myc6::URA3, tetO2-CDC20-127::TRP1 (single copy)*	our lab
yAC3810	*MATalpha, trp1::pGAL-CDC28-HA::TRP1, cdc16:CDC16-6A-TRP1, cdc27::CDC27-5A-KAN, MAD2-3GFP-KanMX6, clb2::CLB2-3mCherry-dcu-hphNT1*	our lab
yAC3854	*MATa, CDC16-myc6::URA3, trp1::pGAL-CDC28-HA::TRP1*	our lab

References

1. Alberts, B. *et al. Essential Cell Biology - 3rd edition* (Garland Science - Taylor & Francis Group, 2010).

2. Alberts, B. *et al. Molecular Biology of the Cell* (Garland Science - Taylor & Francis Group, 2002-2008).

3. Alfieri, C., Zhang, S. & Barford, D. Visualizing the complex functions and mechanisms of the anaphase promoting complex/cyclosome (APC/C). *Open Biology* **7.** doi:10.1098/rsob.170204 (2017).

4. Azzam, R. *et al.* Phosphorylation by cyclin B-Cdk underlies release of mitotic exit activator Cdc14 from the nucleolus. *Science* **305,** 516–9. ISSN: 0036-8075 (2004).

5. Bantscheff, M., Schirle, M., Sweetman, G., Rick, J. & Kuster, B. Quantitative mass spectrometry in proteomics: a critical review. *Anal Bioanal Chem* **389,** 1017–31. ISSN: 1618-2642 (2007).

6. Bardin, A., Visintin, R. & Amon, A. A mechanism for coupling exit from mitosis to partitioning of the nucleus. *Cell* **102,** 21–31. ISSN: 0092-8674 (2000).

7. Barkai, N. & Leibler, S. Robustness in simple biochemical networks. *Nature* **387,** 913–7. ISSN: 0028-0836 (1997).

8. Barnhart, E. L., Dorer, R. K., Murray, A. W. & Schuyler, S. C. Reduced Mad2 expression keeps relaxed kinetochores from arresting budding yeast in mitosis. *Molecular Biology of the Cell* **22,** 2448–2457 (2011).

9. Bonaiuti, P. *et al.* Cells Escape an Operational Mitotic Checkpoint through a Stochastic Process. *Curr. Biol.* ISSN: 0960-9822. doi:10.1016/j.cub.2017.11.031 (2017).

10. Brito, D. A. & Rieder, C. L. Mitotic Checkpoint Slippage in Humans Occurs via Cyclin B Destruction in the Presence of an Active Checkpoint. *Curr. Biol.* **16,** 1194–200. ISSN: 0960-9822 (2006).

11. Caudron, F. & Barral, Y. A Super-Assembly of Whi3 Encodes Memory of Deceptive Encounters by Single Cells during Yeast Courtship. *Cell* **155,** 1244–1257. ISSN: 0092-8674 (2013).

12. Chabner, B. A. & Longo, D. L. *Harrison's™ Manual of Oncology - 2nd Edition* (Mc Graw Hill Education - Medical, 2014).

13. Charvin, G., Cross, F. R. & Siggia, E. D. A Microfluidic Device for Temporally Controlled Gene Expression and Long-Term Fluorescent Imaging in Unperturbed Dividing Yeast Cells. *PLOS ONE* **3,** 1–12 (Jan. 2008).

14. Cherry, J. M. *et al.* Saccharomyces Genome Database: the genomics resource of budding yeast. *Nucleic Acids Research* **40,** D700–D705 (2012).

15. Cline, M. S. *et al.* Integration of biological networks and gene expression data using Cytoscape. *Nature Protocols* **2,** 2366 EP - (Sept. 2007).

16. Cox, J. & Mann, M. MaxQuant enables high peptide identification rates, individualized p.p.b.-range mass accuracies and proteome-wide protein quantification. *Nature Biotechnology* **26,** 1367 EP - (Nov. 2008).

17. Cox, J. *et al.* Andromeda: A Peptide Search Engine Integrated into the MaxQuant Environment. *Journal of Proteome Research* **10.** PMID: 21254760, 1794–1805 (2011).

18. Cross, F. R. Two Redundant Oscillatory Mechanisms in the Yeast Cell Cycle. *Developmental Cell* **4,** 741–752. ISSN: 1534-5807 (2003).

19. Davey, N. E. & Morgan, D. O. Building a Regulatory Network with Short Linear Sequence Motifs: Lessons from the Degrons of the Anaphase-Promoting Complex. *Mol. Cell* **64,** 12–23. ISSN: 1097-2765 (2016).

20. De Antoni, A. *et al.* The Mad1/Mad2 complex as a template for Mad2 activation in the spindle assembly checkpoint. *Curr. Biol.* **15,** 214–25. ISSN: 0960-9822 (2005).

21. Di Talia, S., Skotheim, J. M., Bean, J. M., Siggia, E. D. & Cross, F. R. The effects of molecular noise and size control on variability in the budding yeast cell cycle. *Nature* **448,** 947 EP - (2007).

22. Dick, A. E. & Gerlich, D. W. Kinetic framework of spindle assembly checkpoint signalling. *Nat. Cell Biol.* **15,** 1370–7. ISSN: 1465-7392 (2013).

23. Engelbert, D., Schnerch, D., Baumgarten, A. & Wäsch, R. The ubiquitin ligase APC(Cdh1) is required to maintain genome integrity in primary human cells. *Oncogene* **27,** 907–17. ISSN: 0950-9232 (2008).

24. Faesen, A. C. *et al.* Basis of catalytic assembly of the mitotic checkpoint complex. *Nature* **542,** 498–502. ISSN: 0028-0836 (2017).

25. Fitch, I. *et al.* Characterization of four B-type cyclin genes of the budding yeast Saccharomyces cerevisiae. *Molecular Biology of the Cell* **3,** 805–818 (1992).

26. Foe, I. T. *et al.* Ubiquitination of Cdc20 by the APC occurs through an intramolecular mechanism. *Curr. Biol.* **21,** 1870–7 (2011).

27. Foster, S. A. & Morgan, D. O. The APC/C subunit Mnd2/Apc15 promotes Cdc20 autoubiquitination and spindle assembly checkpoint inactivation. *Mol. Cell* **47,** 921–32. ISSN: 1097-2765 (2012).

28. Fraschini, R., Formenti, E., Lucchini, G. & Piatti, S. Budding Yeast Bub2 Is Localized at Spindle Pole Bodies and Activates the Mitotic Checkpoint via a Different Pathway from Mad2. *The Journal of Cell Biology* **145,** 979–991. ISSN: 0021-9525 (1999).

29. Galli, M. & Morgan, D. O. Cell Size Determines the Strength of the Spindle Assembly Checkpoint during Embryonic Development. *Developmental Cell* **36,** 344–352. ISSN: 1534-5807 (2016).

30. Gerhold, A. R., Labbé, J. C. & Maddox, P. S. Bigger Isn't Always Better: Cell Size and the Spindle Assembly Checkpoint. *Dev. Cell* **36,** 244–6. ISSN: 1534-5807 (2016).

31. Goranov, A. *et al.* The rate of cell growth is governed by cell cycle stage. *Genes Dev* **23,** 1408–1422. ISSN: 0890-9369 (2009).

32. Greil, C. *et al.* The role of APC/CCdh1 in replication stress and origin of genomic instability. *Oncogene* **35,** 3062–3070. ISSN: 0950-9232 (2015).

33. Hannah, S. & Barkai, N. Loss of growth homeostasis by genetic decoupling of cell division from biomass growth: implication for size control mechanisms. *Mol Syst Biol* **10,** 769–769. ISSN: 1744-4292 (2014).

34. Hardwick, K. G. *et al.* Lesions in Many Different Spindle Components Activate the Spindle Checkpoint in the Budding Yeast Saccharomyces cerevisiae. *Genetics* **152,** 509–518. ISSN: 0016-6731 (1999).

35. Hardwick, K., Weiss, E., Luca, F. C., Winey, M. & Murray, A. W. Activation of the budding yeast spindle assembly checkpoint without mitotic spindle disruption. **273,** 953 (1996).

36. Heasley, L. & of the . . ., M.-. S. "Wait anaphase" signals are not confined to the mitotic spindle. *Molecular Biology of the . . .* ISSN: 1059-1524. doi:10.1091/mbc.E17-01-0036 (2017).

37. Hein, J. B., Hertz, E. P. T. P., Garvanska, D. H., Kruse, T. & Nilsson, J. Distinct kinetics of serine and threonine dephosphorylation are essential for mitosis. *Nat. Cell Biol.* **19,** 1433–1440. ISSN: 1465-7392 (2017).

38. Hein, J. B. & Nilsson, J. Interphase APC/C-Cdc20 inhibition by cyclin A2-Cdk2 ensures efficient mitotic entry. *Nat Commun* **7,** 10975. ISSN: 2041-1723 (2016).

39. Herwig, R., Hardt, C., Lienhard, M. & Kamburov, A. Analyzing and interpreting genome data at the network level with ConsensusPathDB. *Nature Protocols* **11,** 1889 EP - (Sept. 2016).

40. Höckner, S., Lea, N. & Seufert, W. Dual control by Cdk1 phosphorylation of the budding yeast APC/C ubiquitin ligase activator Cdh1. *Mol Biol Cell* **27,** 2198–2212. ISSN: 1059-1524 (2016).

41. Hood, J., Hwang, W. & Silver, P. The Saccharomyces cerevisiae cyclin Clb2p is targeted to multiple subcellular locations by cis- and trans-acting determinants. *J. Cell. Sci.* **114,** 589–97. ISSN: 0021-9533 (2001).

42. Hoyt, M., Totis, L. & Roberts, B. S. cerevisiae genes required for cell cycle arrest in response to loss of microtubule function. *Cell* **66,** 507–517. ISSN: 0092-8674 (1991).

43. Hu, F. & Elledge, S. Bub2 is a cell cycle regulated phospho-protein controlled by multiple checkpoints. **1,** 351–5 (Sept. 2002).

44. Hu, F. *et al.* Regulation of the Bub2/Bfa1 GAP Complex by Cdc5 and Cell Cycle Checkpoints. *Cell* **107,** 655–665. ISSN: 0092-8674 (2001).

45. Huffaker, T. C., Thomas, J. H. & Botstein, D. Diverse effects of beta-tubulin mutations on microtubule formation and function. *The Journal of Cell Biology* **106,** 1997–2010. ISSN: 0021-9525 (1988).

46. Hwang, L. H. *et al.* Budding Yeast Cdc20: A Target of the Spindle Checkpoint. *Science* **279,** 1041–1044. ISSN: 00368075, 10959203 (1998).

47. Izawa, D. & Pines, J. The mitotic checkpoint complex binds a second CDC20 to inhibit active APC/C. *Nature* **517,** 631–634. ISSN: 0028-0836 (2015).

48. Kamburov, A., Stelzl, U., Lehrach, H. & Herwig, R. The ConsensusPathDB interaction database: 2013 update. *Nucleic Acids Research* **41,** D793–D800 (2013).

49. Kamburov, A. *et al.* ConsensusPathDB: toward a more complete picture of cell biology. *Nucleic Acids Research* **39,** D712–D717 (2011).

50. Kinoshita, E., Kinoshita-Kikuta, E. & Koike, T. Separation and detection of large phosphoproteins using Phos-tag SDS-PAGE. *Nature Protocols* **4,** 1513 EP - (Sept. 2009).

51. Kinoshita, E., Kinoshita-Kikuta, E., Takiyama, K. & Koike, T. Phosphate-binding Tag, a New Tool to Visualize Phosphorylated Proteins. *Molecular & Cellular Proteomics* **5,** 749–757 (2006).

52. Kundu, S., Horn, P. J. & Peterson, C. L. SWI/SNF is required for transcriptional memory at the yeast GAL gene cluster. *Genes & Development* **21,** 997–1004 (2007).

53. Lane, S. I. R. I. & Jones, K. T. Chromosome biorientation and APC activity remain uncoupled in oocytes with reduced volume. *J. Cell Biol.* **216,** 3949–3957. ISSN: 0021-9525 (2017).

54. Lee, J., Kim, J. A., Margolis, R. L. & Fotedar, R. Substrate degradation by the anaphase promoting complex occurs during mitotic slippage. *Cell Cycle* **9,** 1792–801. ISSN: 1551-4005 (2010).

55. Leitao, R. M. & Kellogg, D. R. The duration of mitosis and daughter cell size are modulated by nutrients in budding yeast. *J. Cell Biol.* **216,** 3463–3470. ISSN: 0021-9525 (2017).

56. Lew, D. J. & Reed, S. I. Morphogenesis in the yeast cell cycle: regulation by Cdc28 and cyclins. *The Journal of Cell Biology* **120,** 1305–1320 (Mar. 1993).

57. Liang, H., Lim, H. H., Venkitaraman, A. & Surana, U. Cdk1 promotes kinetochore bi-orientation and regulates Cdc20 expression during recovery from spindle checkpoint arrest. *EMBO J.* **31,** 403–16. ISSN: 0261-4189 (2012).

58. London, N. & Biggins, S. Mad1 kinetochore recruitment by Mps1-mediated phosphorylation of Bub1 signals the spindle checkpoint. *Genes Dev.* **28,** 140–52. ISSN: 0890-9369 (2014).

59. Lyon, P. The cognitive cell: bacterial behavior reconsidered. *Front Microbiol* **6,** 264. ISSN: 1664-302X (2015).

60. MacLean, B. *et al.* Skyline: an open source document editor for creating and analyzing targeted proteomics experiments. *Bioinformatics* **26,** 966–968 (2010).

61. Mariani, L. *et al.* Role of the Mad2 Dimerization Interface in the Spindle Assembly Checkpoint Independent of Kinetochores. *Current Biology* **22,** 1900–1908. ISSN: 0960-9822 (2012).

62. Matafora, V., Corno, A., Ciliberto, A. & Bachi, A. Missing Value Monitoring Enhances the Robustness in Proteomics Quantitation. *Journal of Proteome Research* **16.** PMID: 28282139, 1719–1727 (2017).

63. Matafora, V. *et al.* Quantitative proteomics reveals novel therapeutic and diagnostic markers in hypertension. *BBA Clinical* **2,** 79–87. ISSN: 2214-6474 (2014).

64. May, K. M., Paldi, F. & Hardwick, K. G. Fission Yeast Apc15 Stabilizes MCC-Cdc20-APC/C Complexes, Ensuring Efficient Cdc20 Ubiquitination and Checkpoint Arrest. *Curr. Biol.* **27,** 1221–1228. ISSN: 0960-9822 (2017).

65. Mi, H., Muruganujan, A., Casagrande, J. T. & Thomas, P. D. Large-scale gene function analysis with the PANTHER classification system. *Nature Protocols* **8,** 1551 EP - (July 2013).

66. Mi, H. *et al.* PANTHER version 11: expanded annotation data from Gene Ontology and Reactome pathways, and data analysis tool enhancements. *Nucleic Acids Research* **45,** D183–D189 (2017).

67. Montojo, J. *et al.* GeneMANIA Cytoscape plugin: fast gene function predictions on the desktop. *Bioinformatics* **26,** 2927–2928 (2010).

68. Morgan, D. O. *The Cell Cycle: Principles of Control* (New Science Press, 1999-2007).

69. Morimoto, B. & Koshland, D. Short-term and long-term memory in single cells. *FASEB J.* **5,** 2061–7. ISSN: 0892-6638 (1991).

70. Moseley, J. B. & Nurse, P. Cdk1 and cell morphology: connections and directions. *Curr. Opin. Cell Biol.* **21,** 82–8. ISSN: 0955-0674 (2009).

71. Nasmyth, K. & Haering, C. H. Cohesin: its roles and mechanisms. *Annu. Rev. Genet.* **43,** 525–58. ISSN: 0066-4197 (2009).

72. Osella, M., Nugent, E. & Lagomarsino, M. C. Concerted control of Escherichia coli cell division. *Proc National Acad Sci* **111,** 3431–3435. ISSN: 0027-8424 (2014).

73. Pan, J. & Chen, R.-H. Spindle checkpoint regulates Cdc20p stability in Saccharomyces cerevisiae. *Genes & Development* **18,** 1439–1451 (2004).

74. Patel, V. *et al.* A Comparison of Labeling and Label-Free Mass Spectrometry-Based Proteomics Approaches. *J Proteome Res* **8,** 3752–3759. ISSN: 1535-3893 (2009).

75. Paulo, J. A., O'Connell, J. D., Gaun, A. & Gygi, S. P. Proteome-wide quantitative multiplexed profiling of protein expression: carbon-source dependency in Saccharomyces cerevisiae. *Molecular Biology of the Cell* **26,** 4063–4074 (2015).

76. Pentchev, K., Ono, K., Herwig, R., Ideker, T. & Kamburov, A. Evidence mining and novelty assessment of protein–protein interactions with the ConsensusPathDB plugin for Cytoscape. *Bioinformatics* **26,** 2796–2797 (2010).

77. Primorac, I. *et al.* Bub3 reads phosphorylated MELT repeats to promote spindle assembly checkpoint signaling. *eLife* **2** (ed Pines, J.) e01030. ISSN: 2050-084X (Sept. 2013).

78. Qiao, R. *et al.* Mechanism of APC/CCDC20 activation by mitotic phosphorylation. *Proc. Natl. Acad. Sci. U.S.A.* **113,** E2570–8. ISSN: 0027-8424 (2016).

79. Queralt, E., Lehane, C., Novak, B. & Uhlmann, F. Downregulation of PP2A(Cdc55) phosphatase by separase initiates mitotic exit in budding yeast. *Cell* **125,** 719–32. ISSN: 0092-8674 (2006).

80. Rahal, R. & Amon, A. Mitotic CDKs control the metaphase–anaphase transition and trigger spindle elongation. *Genes & Development* **22,** 1534–1548 (2008).

81. Rieder, C. & Maiato, H. Stuck in Division or Passing through What Happens When Cells Cannot Satisfy the Spindle Assembly Checkpoint. *Dev Cell* **7,** 637–651. ISSN: 1534-5807 (2004).

82. Rodriguez-Rodriguez, J.-A., Moyano, Y., Játiva, S. & Queralt, E. Mitotic Exit Function of Polo-like Kinase Cdc5 Is Dependent on Sequential Activation by Cdk1. *Cell Rep* **15,** 2050–62. ISSN: 2211-1247 (2016).

83. Rossio, V., Galati, E. & Piatti, S. Adapt or die: how eukaryotic cells respond to prolonged activation of the spindle assembly checkpoint. *Biochem Soc T* **38,** 1645–1649. ISSN: 0300-5127 (2010).

84. Rossio, V. *et al.* The RSC chromatin-remodeling complex influences mitotic exit and adaptation to the spindle assembly checkpoint by controlling the Cdc14 phosphatase. *The Journal of Cell Biology* **191,** 981–997. ISSN: 0021-9525 (2010).

85. Rowald, K. *et al.* Negative Selection and Chromosome Instability Induced by Mad2 Overexpression Delay Breast Cancer but Facilitate Oncogene-Independent Outgrowth. *Cell Rep* **15,** 2679–91. ISSN: 2211-1247 (2016).

86. Rudner, A. D., Hardwick, K. G. & Murray, A. W. Cdc28 Activates Exit from Mitosis in Budding Yeast. *The Journal of Cell Biology* **149,** 1361–1376. ISSN: 0021-9525 (2000).

87. Rudner, A. D. & Murray, A. W. Phosphorylation by Cdc28 Activates the Cdc20-Dependent Activity of the Anaphase-Promoting Complex. *The Journal of Cell Biology* **149,** 1377–1390. ISSN: 0021-9525 (2000).

88. Saito, R. *et al.* A travel guide to Cytoscape plugins. *Nature Methods* **9,** 1069 EP - (Nov. 2012).

89. Santaguida, S. & Amon, A. Short- and long-term effects of chromosome mis-segregation and aneuploidy. *Nature Reviews Molecular Cell Biology* **16,** 473 EP - (July 2015).

90. Santaguida, S. *et al.* Chromosome Mis-segregation Generates Cell-Cycle-Arrested Cells with Complex Karyotypes that Are Eliminated by the Immune System. *Dev. Cell* **41,** 638–651.e5. ISSN: 1534-5807 (2017).

91. Schmoller, K. M., Turner, J., Kõivomägi, M. & Skotheim, J. M. Dilution of the cell cycle inhibitor Whi5 controls budding-yeast cell size. *Nature* **526,** 268–72. ISSN: 0028-0836 (2015).

92. Schwab, M., Neutzner, M., Möcker, D. & Seufert, W. Yeast Hct1 recognizes the mitotic cyclin Clb2 and other substrates of the ubiquitin ligase APC. *EMBO J.* **20,** 5165–75. ISSN: 0261-4189 (2001).

93. Sewart, K. & Hauf, S. Different Functionality of Cdc20 Binding Sites within the Mitotic Checkpoint Complex. *Curr. Biol.* **27,** 1213–1220. ISSN: 0960-9822 (2017).

94. Shannon, P. *et al.* Cytoscape: A Software Environment for Integrated Models of Biomolecular Interaction Networks. *Genome Research* **13,** 2498–2504 (2003).

95. Shirayama, M., Zachariae, W., Ciosk, R. & Nasmyth, K. The Polo-like kinase Cdc5p and the WD-repeat protein Cdc20p/fizzy are regulators and substrates of the anaphase promoting complex in Saccharomyces cerevisiae. *EMBO J.* **17,** 1336–49. ISSN: 0261-4189 (1998).

96. Simonetta, M. *et al.* The influence of catalysis on mad2 activation dynamics. *PLoS Biol.* **7,** e10. ISSN: 1544-9173 (2009).

97. Sivakumar, S. & Gorbsky, G. J. Spatiotemporal regulation of the anaphase-promoting complex in mitosis. *Nat. Rev. Mol. Cell Biol.* **16,** 82–94. ISSN: 1471-0072 (2015).

98. Smoot, M. E., Ono, K., Ruscheinski, J., Wang, P.-L. & Ideker, T. Cytoscape 2.8: new features for data integration and network visualization. *Bioinformatics* **27,** 431–432 (2011).

99. Spencer, F., Gerring, S. L., Connelly, C. & Hieter, P. Mitotic chromosome transmission fidelity mutants in Saccharomyces cerevisiae. *Genetics* **124,** 237–249. ISSN: 0016-6731 (1990).

100. Stegmeier, F., Visintin, R. & Amon, A. Separase, polo kinase, the kinetochore protein Slk19, and Spo12 function in a network that controls Cdc14 localization during early anaphase. *Cell* **108,** 207–20. ISSN: 0092-8674 (2002).

101. Stockwell, S. R., Landry, C. R. & Rifkin, S. A. The yeast galactose network as a quantitative model for cellular memory. *Mol. BioSyst.* **11,** 28–37 (1 2015).

102. Sullivan, D. S. & Huffaker, T. C. Astral microtubules are not required for anaphase B in Saccharomyces cerevisiae. *The Journal of Cell Biology* **119,** 379–388. ISSN: 0021-9525 (1992).

103. Thornton, B. R. & Toczyski, D. P. Securin and B-cyclin/CDK are the only essential targets of the APC. *Nature Cell Biology* **5,** 1090 EP - (Nov. 2003).

104. Thornton, B. R. *et al.* An architectural map of the anaphase-promoting complex. *Genes Dev.* **20,** 449–60. ISSN: 0890-9369 (2006).

105. Toda, K. *et al.* APC/C-Cdh1-dependent anaphase and telophase progression during mitotic slippage. *Cell Div* **7,** 4. ISSN: 1747-1028 (2012).

106. Topham, C. H. & Taylor, S. S. Mitosis and apoptosis: how is the balance set? *Curr. Opin. Cell Biol.* **25,** 780–5. ISSN: 0955-0674 (2013).

107. Turner, J. J., Ewald, J. C. & Skotheim, J. M. Cell size control in yeast. *Curr. Biol.* **22,** R350–9. ISSN: 0960-9822 (2012).

108. Tyanova, S. *et al.* The Perseus computational platform for comprehensive analysis of (prote)omics data. *Nature Methods* **13,** 731 EP - (June 2016).

109. Uhlen, M. *et al.* A pathology atlas of the human cancer transcriptome. *Science* **357,** eaan2507. ISSN: 0036-8075 (2017).

110. Vadia, S. *et al.* Fatty Acid Availability Sets Cell Envelope Capacity and Dictates Microbial Cell Size. *Curr. Biol.* **27,** 1757–1767.e5. ISSN: 0960-9822 (2017).

111. Vági, P. *et al. Structure of Plants and Fungi - Edited by Zoltan Kristof* `http://elte.prompt.hu/sites/default/files/tananyagok/StructureOfPlantsAndFungi/` (ELTE, Department of Plant Anatomy - Budapest, Hungary, 2012).

112. Vázquez-Novelle, M. D. *et al.* Cdk1 Inactivation Terminates Mitotic Checkpoint Surveillance and Stabilizes Kinetochore Attachments in Anaphase. *Current Biology* **24,** 638–645. ISSN: 0960-9822 (2014).

113. Vernieri, C., Chiroli, E., Francia, V., Gross, F. & Ciliberto, A. Adaptation to the spindle checkpoint is regulated by the interplay between Cdc28/Clbs and PP2ACdc55. *The Journal of Cell Biology* **202,** 765–778. ISSN: 0021-9525 (2013).

114. Vincenzo, D., Mari, C., Nocera, D., Rametti, L. & Grieco, D. The spindle checkpoint requires cyclin-dependent kinase activity. *Genes Dev.* **17,** 2520–5. ISSN: 0890-9369 (2003).

115. Visintin, R. & Amon, A. Regulation of the mitotic exit protein kinases Cdc15 and Dbf2. *Mol. Biol. Cell* **12,** 2961–74. ISSN: 1059-1524 (2001).

116. Visintin, R., Stegmeier, F. & Amon, A. The role of the polo kinase Cdc5 in controlling Cdc14 localization. *Mol. Biol. Cell* **14,** 4486–98. ISSN: 1059-1524 (2003).

117. Visintin, R. *et al.* The Phosphatase Cdc14 Triggers Mitotic Exit by Reversal of Cdk-Dependent Phosphorylation. *Molecular Cell* **2,** 709–718. ISSN: 1097-2765 (1998).

118. Vodermaier, H. C., Gieffers, C., Sebastian, M., Eisenhaber, F. & Peters, J. M. TPR subunits of the anaphase-promoting complex mediate binding to the activator protein CDH1. *Curr. Biol.* **13,** 1459–68. ISSN: 0960-9822 (2003).

119. Warren, C. D. *et al.* Distinct chromosome segregation roles for spindle checkpoint proteins. *Mol. Biol. Cell* **13,** 3029–41. ISSN: 1059-1524 (2002).

120. Weaver, B. & Cleveland, D. Decoding the links between mitosis, cancer, and chemotherapy: The mitotic checkpoint, adaptation, and cell death. *Cancer Cell* **8,** 7–12. ISSN: 1535-6108 (2005).

121. Webre, D. J., Wolanin, P. M. & Stock, J. B. Bacterial chemotaxis. *Curr. Biol.* **13,** R47–9. ISSN: 0960-9822 (2003).

122. Yamamoto, A., Guacci, V. & Koshland, D. Pds1p, an inhibitor of anaphase in budding yeast, plays a critical role in the APC and checkpoint pathway(s). *J. Cell Biol.* **133,** 99–110. ISSN: 0021-9525 (1996).

123. Yang, H. W., Chung, M., Kudo, T. & Meyer, T. Competing memories of mitogen and p53 signalling control cell-cycle entry. *Nature* **549,** 404–408. ISSN: 0028-0836 (2017).

124. Zeng, X. *et al.* Pharmacologic inhibition of the anaphase-promoting complex induces a spindle checkpoint-dependent mitotic arrest in the absence of spindle damage. *Cancer Cell* **18,** 382–95. ISSN: 1535-6108 (2010).

125. Zhang, S. *et al.* Molecular mechanism of APC/C activation by mitotic phosphorylation. *Nature* **533,** 260–264. ISSN: 0028-0836 (2016).

Declaration of Contributions

The experiments reported in the Results were produced and analyzed by myself, except where otherwise stated.

Elena Chiroli performed the Western Blot analysis reported in Figures 4.35 and 6.2. She also helped me in tetrads dissection - for obtaining some of the strains reported in Section 4.4 - and in yeast transformation for *tub2-401* mutant. Mattia Pavani helped me in preliminary analysis of Cdc28 levels in adapted cells, and in preliminary evaluation of *tub2-401* growth. Paolo Bonaiuti developed the image analysis of Mad2-GFP and Clb2-mCherry signals during a nocodazole arrest.

Acknowledgements

This work would have been impossible without the support of many people. First, I would like to thank my boss Andrea Ciliberto: he covered an important role in my scientific and personal growth, giving me the possibility to approach a challenging biological problem in a multidisciplinary way.

Another person that was important for my scientific growth and for teaching me the wet lab approach is Claudio. After 4 years I am not holding the breath anymore during the inoculum of yeast strains, but he taught me the importance of scientific rigor and to be updated about the scientific literature. Thank you!

I would also like to thank my colleagues Elena, Tiziana, Paolo, Fridolin, Mattia and Federica: for precious help and suggestions at several stages of my project, for useful scientific discussions, for part of the scripts I used for image analysis, for the daily life inside and outside the lab.

I would like to acknowledge several people from IFOM. First, former and present members of Vaccari's Lab (Elena, Valeria, Francesca, Marco, Miriam, Francis, Victor) for their support and for the beautiful moments we spent together. A special thanks goes to the members of Foiani's Lab (Daniele, Arta, Elisa, Chiara, Sophie) for reagents and useful suggestions about protocols and about my project. I would like to thank Angela Bachi and Vittoria Matafora, for their important work in the proteomic screening of adapted cells. A very warm thanks goes to the members of the Imaging TDU: Dario, Amanda and Sara for the technical and motivational support during live-cell imaging experiments with low temperatures; I would also like to thank my "twin brother" Emanuele from the Imaging TDU, for improving our software of image analysis and for the daily life inside and outside the lab.

I want to thank my precious family, my friends here in Milan and my flatmates, for supporting me during these 4 years. A special thanks goes to Nicola and my friends from Pescara, which are close to me even while we are 600 km apart.